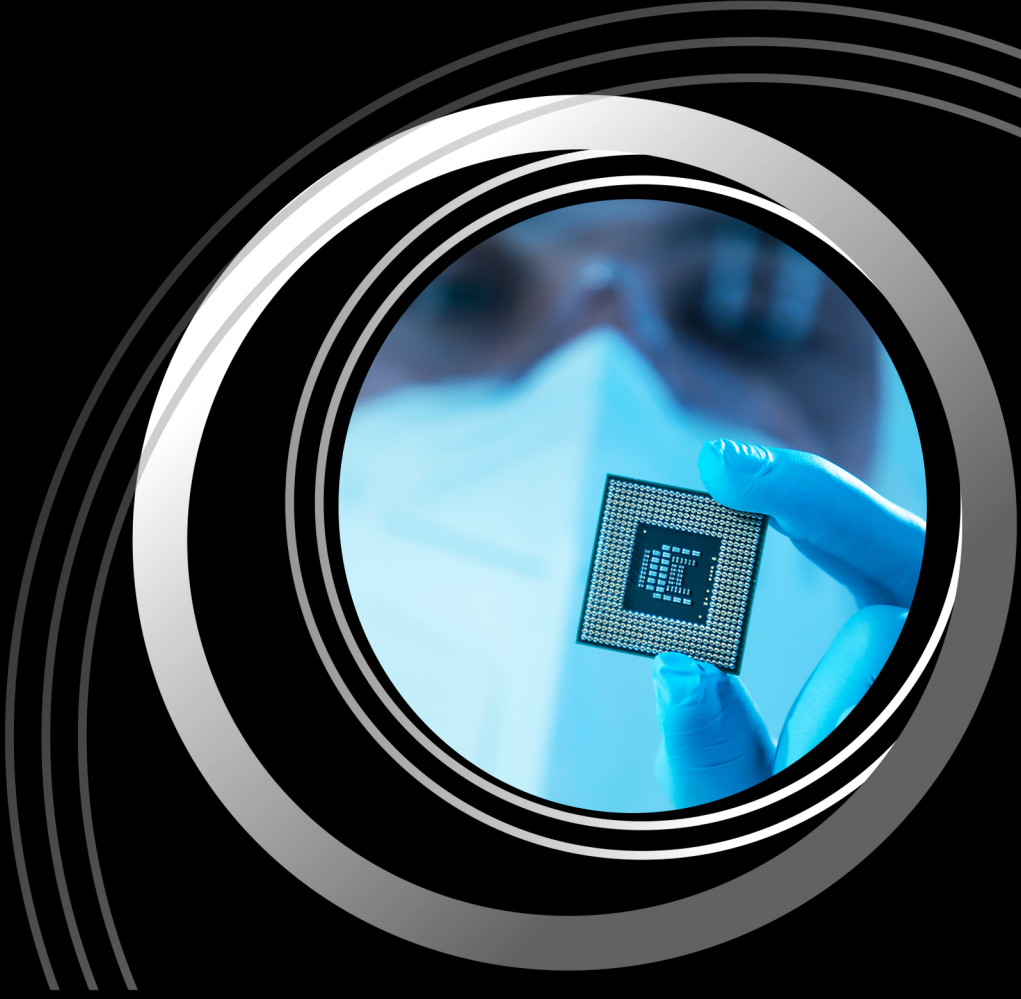

THEORY, CONTEXT, AND PRACTICE IN ENGINEERING

Editor: Asst. Prof. Dr. Sercan KÜLCÜ

DUVAR

THEORY, CONTEXT, AND PRACTICE IN ENGINEERING

Editor

Asst. Prof. Dr. Sercan KÜLCÜ [1]

[1] Giresun Üniversitesi Mühendislik Fakültesi Bilgisayar Mühendisliği Bölümü
https://orcid.org/0000-0002-4871-709X, sercan.kulcu@giresun.edu.tr

Theory, Context, and Practice in Engineering

Editor: Asst. Prof. Dr. Sercan KÜLCÜ

Editor in chief: Berkan Balpetek

Cover and Page Design: Duvar Design

Printing : August -2025

Publisher Certificate No: 49837

ISBN: 978-625-5698-27-8

853 Sokak No:13 P.10 Kemeraltı-Konak/İzmir Tel: 0 232 484 88 68

www.duvaryayinlari.com

duvarkitabevi@gmail.com

TABLE OF CONTENTS

Chapter 1

Designing Intelligent Workflows: A Practical Guide to Agentic AI with LangGraph

Ali ŞENTÜRK[1]

Abstract

This chapter explores the principles and practical implementation of Agentic AI systems, which enable large language models (LLMs) to act autonomously through structured workflows. Beginning with the foundational concepts of AI agents and agentic reasoning, we continue to building real-world applications using the LangGraph framework. The main components of the LangGraph library and the programming structures required for a workflow were addressed. This provided the programming infrastructure necessary to program an AI agent. In the next section, important Agentic AI architectures such as prompt chaining, parallelization, orchestrator-worker models, and evaluator-optimizer were explained. The objective is to understand the programming structures that enable complex operations through their interaction with large language models. As these systems are expected to be used much more extensively in the near future for many tasks routinely performed by humans, understanding these programming structures is considered very valuable.

Keywords: Agentic AI, Large Language Models, LangGraph Framework, Autonomous Agents, AI Workflows.

[1] Isparta University of Applied Sciences, Faculty of Technology, Department of Electrical and Electronics Engineering, Isparta, Turkiye. alisenturk@isparta.edu.tr, ORCID: 0000-0002-5868-7365.

INTRODUCTION

Since the publication of the “Attention Is All You Need” paper in 2017 [1], the field of artificial intelligence has witnessed unprecedented advancements. The introduction of the Transformer architecture paved the way for machines to effectively understand and respond to natural human language. Initially applied to translating texts from one language to another with great success , this approach laid the foundation for today's Large Language Models (LLMs) [2], which have now become a part of our daily lives.

What makes this architecture particularly powerful is not just its ability to translate between different languages, but also its capacity to enable human-like interaction with computers. As a result, users can now pose natural language queries to machines and receive comprehensive, relevant, and often accurate responses in return also in natural language [3].

Building on these capabilities, AI agents were developed, autonomous systems that not only generate the desired content but also carry out complex tasks on behalf of users, independently, by leveraging the power of LLMs. As the next step, systems were introduced in which multiple AI agents, each working toward a specific goal, could operate independently yet in a coordinated manner. These systems are referred to as Agentic AI [4].

Although the terms are often used interchangeably, AI agents and Agentic AI represent fundamentally different design philosophies, system capabilities, and operational goals. In this unit, both concepts are examined in detail, with explanations of their unique roles, architectural frameworks, and practical applications [5].

AI Agents

AI agents are AI-based autonomous programs designed to perform a specific and clearly defined task without human intervention. They generally perform their tasks by following predefined rules or using decision trees. They are used in various fields such as customer service, banking services, or special-purpose bots [6].

An AI agent typically focuses on a single task. For example, consider a customer service bot that answers questions related to orders. This AI agent receives the user's query, searches a database and provides an appropriate response based on the results found [7]. It does not have the ability to go beyond the defined limits and learn or adapt. There is not a situation where multiple AI agents communicate with each other. Although it has a certain degree of autonomy, this is limited to the scope of the task and the system [5].

Agentic AI

In contrast, Agentic AI refers to a broader, more adaptive system composed of multiple AI agents that collaborate reason, and make decisions independently to accomplish complex workflows or goals [5]. Unlike isolated AI agents, an Agentic AI system exhibits characteristics such as [8]:

- Perception: The ability to sense or gather data from the environment.
- Reasoning: The capacity to interpret that data in context.
- Action: The execution of tasks based on analysis.
- Learning: The continual improvement of performance based on feedback and evolving conditions.

A compelling example is a smart home system designed to optimize energy consumption. Within this system, multiple agents can be utilized to manage lighting, climate control etc. These agents communicate with each other, adapt to user behaviors, and make collective decisions, like turning off unused devices or adjusting the thermostat based on presence detection, all without direct human commands. The overarching goal (e.g., minimizing electricity usage) is achieved by a coordinated, intelligent network of agents operating with shared purpose and dynamic responses.

The distinction between AI agents and Agentic AI shapes how we design, build, and deploy AI-powered systems. As applications become increasingly sophisticated, the need for multi-agent coordination, understanding, and system wide adaptability becomes necessary. Whether automating a chatbot or operating a smart city infrastructure, understanding these paradigms is key to use the full potential of AI [9].

In this chapter, we will explore how to construct both kinds of systems, beginning with simple agent architectures to advanced Agentic AI designs. The programming examples throughout are based on official tutorials provided on the LangGraph website [10].

BUILDING AGENTIC WORKFLOWS with LangGraph

Modern Agentic AI systems rely on the decomposition of complex goals into modular tasks executed by coordinated agents. LangGraph provides a powerful way to build such stateful, graph-based workflows in Python, enabling flexible and scalable agent orchestration.

In this section, we will combine theory and practical implementation to guide the reader through the process of creating your first agentic workflow. The reader will learn about defining state, creating nodes and edges and constructing a complete execution graph.

Understanding the Main Components of LangGraph

LangGraph library provides a graph-based workflow and consists of the following basic components:

- State is a shared structure that holds context as data flows through the graph.
- Nodes are individual simple Python functions.
- Edges are transitions or connections between nodes, optionally conditioned on logic.
- State Graph is the composition of all nodes, edges, and state transitions representing the full workflow.

Defining the State

LangGraph workflow begins by defining a State schema. This schema represents the structure of the data shared between nodes and is critical to maintaining a consistent flow of information. Such structured data can be constructed using `TypedDict` class. The `TypedDict` class, allows to define a dictionary with a specific set of keys and expected value types. It is primarily useful for static type checking in programming environments but does not enforce any behavior at runtime.

```
1. from typing_extensions import TypedDict
2. class State(TypedDict):
3.     message: str
```

The `State` class is expected to have a key `message` with a string type value. At runtime, Python will treat this as a normal dictionary and no validation is done.

Defining Nodes

In LangGraph, each Node is just a standard Python function that performs a relatively simple work. The first argument of every node function is the current state. The node can read values from the state, perform processing, and then return the modified state.

```
1. def message_node(state: State) -> dict:
2.     message = state["message"]
3.     return {"message": f"You typed: {message}"}
```

This simple node reads the message from the `state` and returns the message with prepending the text “You typed:”.

Each node returns a new version of the `state`. By default, LangGraph merges this returned dictionary into the shared state, overwriting previous values of the same keys.

Constructing the Graph

After defining the state and node(s), the full graph can be constructed using LangGraph's `StateGraph` class. This class allows defining nodes as individual processing steps, edges as connections between nodes, and Start and End points.

```
from langgraph.graph import StateGraph, START, END
# Initialize the graph with state schema
builder = StateGraph(State)
# Add the node to the graph
builder.add_node(message_node)
# Define the graph edges: START -> node(s) -> END
builder.add_edge(START, "message_node")
builder.add_edge("message_node", END)
# Compile the graph
graph = builder.compile()
```

LangGraph also supports visualizing the workflows. We can run the code below to visualize the graph. The resulting graph is displayed in Figure 1.

```
from IPython.display import Image, display
display(Image(graph.get_graph().draw_mermaid_png()))
```

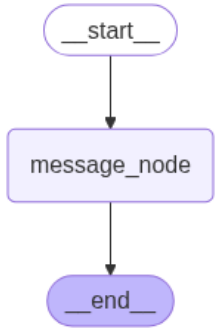

Figure 1. The generated graph image.

Finally, the graph can be invoked as `graph.invoke({"message": "Hello"})`, and the resulting value is `{'message': 'You typed: Hello'}`.

Integrating LLM in the LangGraph

In LangGraph, messages are typically structured pieces of data passed between nodes via the shared `State` as explained in the previous section. These

include represent system prompts, user inputs, LLM responses. Messages are used to represent different roles within a conversation.

LangChain provides several message types, such as `HumanMessage`, `AIMessage`, `SystemMessage` and `ToolMessage`. These types respectively represent input from the user, responses generated by the language model, system level instructions for the model and outputs resulting from specific purpose functions named as tools.

To support message accumulation across turns or graph steps, LangGraph provides utility methods like `add_messages`, which appends one or more messages to the current state under a key which is commonly named as `messages`.

In the previous example, we created a simple graph with a single node that processed a static message. However, real world AI workflows often require interaction with an LLM to generate responses dynamically based on input messages. To enable this, we extended our LangGraph implementation by integrating an LLM into one of the nodes.

Choosing the Language Model

In agentic workflows or conversational systems, the core logic is usually driven by a language model which responds to user inputs, processes intermediate state or acts based on tool outputs.

LangGraph is well-suited for such designs because it supports passing state across nodes and accumulating messages over time. Integrating an LLM makes the graph reactive to dynamic input rather than operating as a static or rule-based flow. We can use a locally hosted LLM through Ollama application.

```
1. from langchain_ollama import ChatOllama
2. llm = ChatOllama(model="mistral:latest")
```

Alternatively, a commercial model such as OpenAI's GPT-4o can be used by setting the appropriate environment variable:

```
1. import os
2. from langchain_openai import ChatOpenAI
3. os.environ["OPENAI_API_KEY"] = "openai-api-key..."
4. llm = ChatOpenAI(model="gpt-4o")
```

Updating the `State` Definition for LLM

In the initial version of the graph, the state was defined as a simple dictionary holding a single string message. This was sufficient for a basic flow where we passed a single message through the graph. However, when working with

LLMs, especially in multi-turn conversations or agentic workflows, we often need to keep track of a list of messages rather than a single input. This allows the system to maintain context and simulate a full conversation. To support this, we updated the state schema as follows:

```
1. from typing_extensions import TypedDict
2. from typing import Annotated
3. from langchain_core.messages import AnyMessage
4. from langgraph.graph.message import add_messages
5. class State(TypedDict):
6.     messages:Annotated[list[AnyMessage],add_messages]
```

`messages` key now holds a list of messages instead of a single string. Each item in the list is an `AnyMessage` which is a general type that can represent `HumanMessage`, `AIMessage`, `SystemMessage` or `ToolMessage`. These are are message types in LangChain for representing different roles in a conversation.

`Annotated[..., add_messages]` tells LangGraph to automatically accumulate (append) messages to this key across graph steps. When a node returns a new message or list of messages, it will be added to the existing state rather than replacing it. This behavior is critical for maintaining full conversation history. `add_messages` omes from `langgraph.graph.message`, and it enables this accumulation behavior behind the scenes.

Updating the Graph Structure

```
1. from langgraph.graph import StateGraph, START, END
2. builder = StateGraph(State)
3. builder.add_node(messages_node)
4. builder.add_edge(START, "messages_node")
5. builder.add_edge("messages_node", END)
6. graph = builder.compile()
7. graph.invoke({"messages": "Hello"})
```

After integrating the LLM into the graph and updating the `State` to accumulate messages, invoking the graph with an initial input like "Hello" produces the following output (some parameters are omitted):

```
{'messages':[
HumanMessage(content='Hello', id='f2d28f88-6016-4e9c..'),
```

```
AIMessage(content='How can I assist you today?', id='run-
-3d7d71b4-02ee-41e4-aae6..',
usage_metadata={'input_tokens': 26, 'output_tokens': 8,
'total_tokens': 34})]}
```

As shown in the program output, this structure enables LangGraph to accumulate a complete conversation history in the messages list by storing various additional metadata.

Interacting with External Systems

In LangGraph's architecture, the tool node serves as a critical bridge between the LLM and external systems. This node enables the LLM to extend its capabilities beyond static knowledge by interacting with functions, APIs, databases and other external resources.

The tool node operates on a simple but powerful principle: when the LLM encounters a query it cannot answer with its internal knowledge, it can route the request to an appropriate external tool, execute the necessary operation, and return the enhanced response to the user.

Let's explore an implementation using simple mathematical functions:

```
 1. def add(a: int, b: int) -> int:
 2.     """Add two integers together.
 3.     Args:
 4.         a: First integer to add
 5.         b: Second integer to add
 6.     Returns:
 7.         The sum of a and b
 8.     """
 9.     return a + b
10.
11. def subtract(a: int, b: int) -> int:
12.     """Subtract the second integer from the first.
13.     Args:
14.         a: The integer to subtract from
15.         b: The integer to subtract
16.     Returns:
17.           The result of the second operand subtracted from the
first operand.
18.     """
19.     return a - b
20.
21. def multiply(a: int, b: int) -> int:
22.     """Multiply two integers together.
23.     Args:
24.         a: First integer to multiply
```

```
        b: Second integer to multiply
    Returns:
        The product of a and b
    """
    return a * b

# Bind the tools to the LLM
tools = [add, subtract, multiply]
llm_with_tools=llm.bind_tools(tools)
```

When we invoke an arithmetic operation, the LLM recognizes which tool is appropriate to use:

```
response = llm_with_tools.invoke("subtract 9879 from 4224342")
```

The output of the prompt is as follows:

```
AIMessage(content='', tool_calls=[{'name': 'subtract', 'args': {'a': '4224342', 'b': '9879'}}])
```

Building the State Graph with Tool Nodes

In LangGraph, we can construct interactive, stateful workflows where a language model not only handles conversation but also invokes tools dynamically based on user input. This is accomplished by defining a state structure, implementing nodes that represent different processing steps, and connecting these nodes conditionally based on the model's behavior. The following example demonstrates how to build a graph that includes a tool calling language model node and a dedicated tool handling node. The graph routes between these nodes based on whether the model's output includes a tool request.

```
from langgraph.prebuilt import ToolNode
from langgraph.prebuilt import tools_condition
from langgraph.checkpoint.memory import MemorySaver
# Node that invokes the LLM with tools bound
def tool_calling_llm(state: State):
    return {"messages": [llm_with_tools.invoke(state["messages"])]}
# Build the graph
builder = StateGraph(State)
builder.add_node("tool_calling_llm", tool_calling_llm) # Node that runs LLM
builder.add_node("tools", ToolNode(tools)) # Node that executes tool calls
builder.add_edge(START, "tool_calling_llm") # Start -> LLM node
builder.add_conditional_edges(
    "tool_calling_llm",
```

```
    tools_condition # LLM -> tools if tool call exists, else ->
END
)
builder.add_edge("tools", "tool_calling_llm")                #
After tool execution, return to LLM
memory = MemorySaver()
graph = builder.compile(checkpointer=memory)
```

`tool_calling_llm` is a custom node that passes the current conversation to the LLM, which may choose to respond directly or invoke a tool call. `ToolNode` which is named as `tools`, executes tool calls present in the LLM output.

Routing Logic is as follows: The graph starts at the LLM node. If the LLM's output contains a tool call (as determined by `tools_condition`), it routes to the tools node. After the tool is executed, the graph loops back to the LLM node, allowing it to process the tool's result and continue the dialogue. This dynamic routing is achieved using `conditional_edge`, which directs the flow between nodes based on runtime conditions.

The `MemorySaver` checkpointer ensures that the full interaction history is remembered across turns. This enables the graph to maintain context over time. The graph image is displayed in Figure 2. Note that dotted lined arrows represent conditional flows.

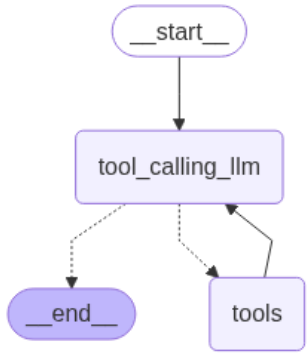

Figure 2. Graph with tool node.

Once the state graph is compiled, we can invoke it with an initial message and a configuration. In this example, we pass a simple arithmetic instruction, which the language model interprets as a tool call. The graph handles this call, routes it to the correct tool, and returns the result.

The config dictionary is used to assign a `thread_id`, which uniquely identifies this execution thread. This is useful when maintaining multiple

conversations or parallel executions with the same graph. The returned output is a dictionary containing updated messages. We can iterate through them and use the `pretty_print` method to display each one clearly.

```
1. config = {"configurable":{"thread_id":"1"}}
2. messages = graph.invoke({"messages":"subtract 90 from 10050"},
config=config)
3. for m in messages["messages"]:
4.     m.pretty_print()
```

The result of the invocation is as follows:

```
==================== Human Message ====================
subtract 90 from 10050
==================== Ai Message ====================
Tool Calls:
  subtract (fdcbfafa-2c10-4397-a74d-d960b6be5556)
 Call ID: fdcbfafa-2c10-4397-a74d-d960b6be5556
  Args:
    a: 10050
    b: 90
==================== Tool Message ====================
Name: subtract
9960
==================== Ai Message ====================
The final answer is: $\boxed{9960}$
```

Because we previously compiled the graph with a memory saver, it can continue and recall conversation history across multiple invocations, as long as the same `thread_id` is used in the configuration. This enables the graph to understand context, remember previous tool calls, and refer to past interactions. For example, after asking the model to "subtract 90 from 10050", we can continue the session with a follow-up like "add 25 to the result." and the model will understand what "the result" refers to using the preserved state.

The tool node represents a powerful paradigm in LangGraph that transforms LLMs from static knowledge systems into dynamic interfaces capable of interacting with the broader digital ecosystem. By properly implementing tool nodes, forming sophisticated workflows is possible that leverage both the language understanding of LLMs and the precise capabilities of external tools and APIs.

Dynamic Workflow Control by Routing

Routing in LangGraph refers to the ability to conditionally determine which node to execute next based on the current state. This powerful feature enables

developers to create dynamic workflows where the execution path adapts to the input or intermediate results. The `Pydantic` library plays a crucial role in enforcing structured outputs from language models, ensuring reliable routing decisions. `Pydantic` based classes are also alternative to `TypedDict` class. However `TypedDict` based classed only provides type hints while `Pydantic` based classed validates data at runtime and can enforce specific output formats. This feature is critical for routing workflows where the system must make deterministic decisions based on model outputs.

Let's constuct a practical implementation of routing. In this implementation a user gives natural language input while an LLM makes a structured decision using a pydantic class. Based on this decision, the input is routed to a different response generator function. Each response function uses system prompts to guide the LLM output. We want to process user input and respond with either a summary or a translation.

We start the program by defining the `pydantic` based class:

```
1. from pydantic import BaseModel, Field
2. from typing import Literal, TypedDict
3. # This schema tells the LLM to output one of these exact strings
4. class Decision(BaseModel):
5.              action:     Literal["summarize",     "translate"]     =
Field(description="User's intended action based on the user input")
```

In this code `BaseModel` is base class in `Pydantic`, which allows you to define data models with validation. It enforces types. `Literal` is a special type hint that limits possible values of a variable to a predefined list of strings, numbers, etc. In the code it means the action field must exactly be `"summarize"` or `"translate"`. `Field` from `pydantic` library adds extra metadata like `description` which helps LLMs to understand the meaning of the field. It also improves clarity.

The following code enforces LLM to output using `Decision` class.

```
1. router_llm = llm.with_structured_output(Decision)
```

We define State class with three attributes: `input_` will be used for user input, `action` will store the type of action and `output` will store the result of the LLM.

```
1. class State(TypedDict):
2.     input_: str
3.     action: str
4.     output: str
```

The node functions in the program are defined as follows:

```
from langchain_core.messages import HumanMessage, SystemMessage
def decide(state: State):
    result = router_llm.invoke([
   SystemMessage(content="Classify the user's input as one of: summarize or translate."),
    HumanMessage(content=state["input_"])
    ])
    return {"action": result.action}

def make_summary(state: State):
    result = llm.invoke([
   SystemMessage(content="Summarize the following text in 2-3 sentences."),
    HumanMessage(content=state["input_"])
    ])
    return {"output": result.content}

make_summary function takes the text and generates 2-3 sentece summary.

def make_translation(state: State):
    result = llm.invoke([
    SystemMessage(content="Translate the following text to Turkish."),
    HumanMessage(content=state["input_"])
    ])
    return {"output": result.content}
```

`decide` is the router function which acts as the decision maker that classifies user intent and returns `summarize` or `translate` strings. `make_summary` function takes the text and invokes the LLM to generate 2-3 sentence summary of the user input where `make_translation` function prompts the LLM to translate the input text to Turkish.

The conditional edge function `route` is given below. This function examines the value of action and returns the name of the next node to execute.

```
def route(state: State):
    if state["action"] == "summarize":
        return "summarize"
    elif state["action"] == "translate":
        return "translate"
```

Finally, the graph is formed as follows:

```
from langgraph.graph import StateGraph, START, END
builder = StateGraph(State)

builder.add_node("decide_node", decide)
builder.add_node("summary_node", make_summary)
builder.add_node("translation_node", make_translation)

builder.add_edge(START, "decide_node")

builder.add_conditional_edges("decide_node", route, {
    "summarize": "summary_node",
    "translate": "translation_node"
})

builder.add_edge("summary_node", END)
builder.add_edge("translation_node", END)
graph = builder.compile()
```

The three functions `decide`, `make_summary`, and `make_translation` are added to the graph as nodes named `decide_node`, `summary_node`, and `translation_node`, respectively. The graph begins at `decide_node`, which processes the user input using a structured LLM which utilizes the `Decision` class, built on the `Pydantic` library.

The `decide_node` branches based on its output, either "`summarize`" or "`translate`", determined by the `route` function. This branching logic is implemented using a conditional edge in the graph. If the route function returns "`summarize`", the graph proceeds to the `summary_node`; if it returns "`translate`", it proceeds to the `translation_node`. Both `summary_node` and `translation_node` ultimately connect to the `END` node. The graph image is displayed in Figure 3.

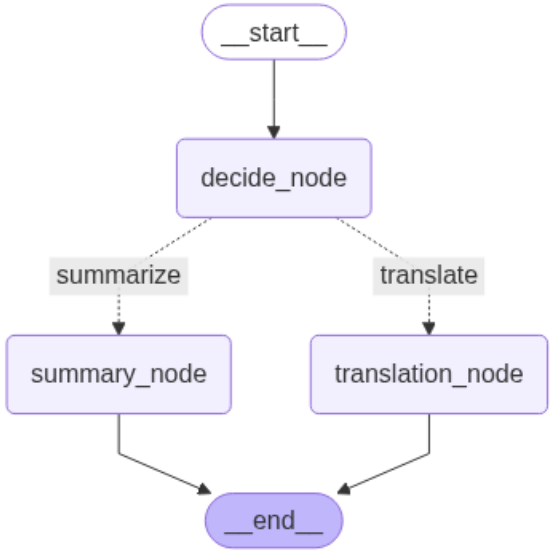

Figure 3. Graph with routing

When the following code is executed:

```
graph.invoke({"input_": "to turkish, hi how are you?"})
```

the obtained result is:

```
{'input_': 'to turkish, hi how are you?',
 'action': 'translate',
 'output': 'Merhaba, nasılsın?'}
```

Another execution of graph is:

```
graph.invoke({"input_": "sum up: LangChain is a software
framework that helps facilitate the integration of large
language models (LLMs) into applications. As a language
model integration framework, LangChain's use-cases largely
overlap with those of language models in general, including
document analysis and summarization, chatbots, and code
analysis."})
```

The result is:

```
{'input_': "sum up:LangChain is a software framework that
helps facilitate the integration of large language models
(LLMs) into applications. As a language model integration
framework, LangChain's use-cases largely overlap with those
of language models in general, including document analysis
and summarization, chatbots, and code analysis.",
 'action': 'summarize',
 'output': 'LangChain is a software framework designed to
integrate large language models into applications. It can
```

```
be used for tasks such as document analysis and
summarization, building chatbots, and analyzing code.'}
```

This example shows how Pydantic's validation ensures reliable routing decisions, while LangGraph's conditional edges enable complex workflow paths.

OTHER IMPORTANR AGENT ARCHITECTURES

LangGraph's official website [11] outlines several important and useful architectures, some of which we will briefly introduce and examine in this section.

Prompt Chaining

Prompt chaining means taking the output of one LLM call and feeding it as the input to the next LLM step. It allows for multi-stage reasoning or refinement, breaking complex tasks into simpler, sequenced subtasks. Each step in the chain can add structure, quality, or depth to the previous result. In the following example, a raw idea is generated first and controlled for a specific condition. If condition passes, then it is improved in chain steps. The resulting graph is shown in Figure 4.

```python
from typing_extensions import TypedDict
from langgraph.graph import StateGraph, START, END
from IPython.display import Image, display

# Graph state
class State(TypedDict):
    subject: str
    improved1: str
    improved2: str

# Nodes
def initial_node(state: State):
    return {"subject": "something generated by llm"}

def check(state: State):
    sth=True
    if sth:
        return "Pass"
    return "Fail"

def chain1(state: State):
    # improve the task
    return {"improved1": "first improvement by llm"}

```

```python
def chain2(state: State):
    return {"improved1": "second improvement by llm"}

# Build workflow
builder = StateGraph(State)

# Add nodes
builder.add_node("initial_node", initial_node)
builder.add_node("chain1", chain1)
builder.add_node("chain2", chain2)

# Add edges to connect nodes
builder.add_edge(START, "initial_node")
builder.add_conditional_edges(
    "initial_node", check, {"Pass": "chain1", "Fail": END}
)
builder.add_edge("chain1", "chain2")
builder.add_edge("chain2", END)

# Compile
graph = builder.compile()
```

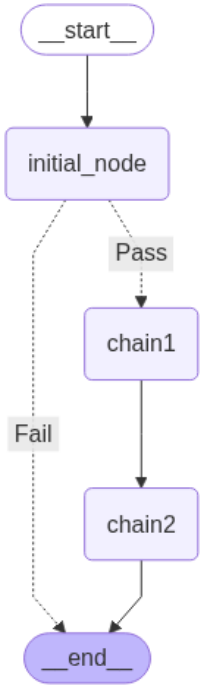

Figure 4. Prompt chaining graph architecture.

Parallelization

Parallelization enables multiple tasks to run simultaneously rather than sequentially, which significantly speeding up execution. In LLM workflows, this means processing independent subtasks (like content sections) concurrently, reducing total runtime. Parallel execution may minimize delays, especially for slow LLM calls, by running tasks in parallel. It is especially used for breaking tasks into smaller, independent units (sectioning) allows flexible scaling for complex projects. In addition, voting mechanisms can be utilized to generate diverse outputs, enhancing creativity and reliability. The following example demonstrates the parallelization of generating multiple sections parallel. The resulting graph image is shown in Figure 5.

```
from typing_extensions import TypedDict
from langgraph.graph import StateGraph, START, END
# Graph state
class State(TypedDict):
    subject: str
    section1: str
    section2: str
    section3: str
    combined: str

# Nodes
def section1(state: State):
  message=llm.invoke(f"Write section 1 about {state['subject']}")
    return {"section1": message.content}
def section2(state: State):
  message=llm.invoke(f"Write section 2 about {state['subject']}")
    return {"section2": message.content}
def section3(state: State):
  message=llm.invoke(f"Write section 3 about {state['subject']}")
    return {"section3": message.content}

def combine(state: State):
   combined = f"SUBJECT:\n{state['subject']}\n\n"
   combined += f"SECTION 1:\n{state['section1']}\n\n"
   combined += f"SECTION 2:\n{state['section2']}\n\n"
   combined += f"SECTION 3:\n{state['section3']}\n\n"
   return {"combined": combined}

# Build workflow
parallel_builder = StateGraph(State)
# Add nodes
parallel_builder.add_node("section1", section1)
parallel_builder.add_node("section2", section2)
```

```
parallel_builder.add_node("section3", section3)
parallel_builder.add_node("combine", combine)
# Add edges to connect nodes
parallel_builder.add_edge(START, "section1")
parallel_builder.add_edge(START, "section2")
parallel_builder.add_edge(START, "section3")
parallel_builder.add_edge("section1", "combine")
parallel_builder.add_edge("section2", "combine")
parallel_builder.add_edge("section3", "combine")
parallel_builder.add_edge("combine", END)
parallel_workflow = parallel_builder.compile()
```

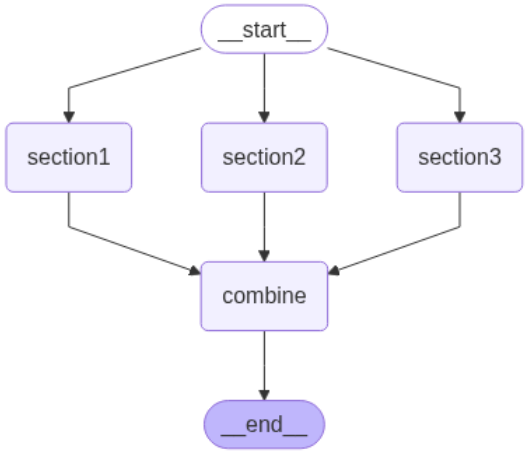

Figure 5. Parallelization graph architecture.

Orchestrator-Worker

Orchestrator-Worker architecture takes a complex input task, dynamically decomposes it into multiple subtasks, executes each one in parallel and then aggregates the individual results into a final combined output. This structure resembles the parallelization architecture but the difference is subtasks are determined dynamically by the orchestrator in this architecture.

```
from typing import List, TypedDict, Annotated
from pydantic import BaseModel, Field
from langchain_core.messages import HumanMessage, SystemMessage
from langgraph.graph import StateGraph, START, END
import operator

# Schema for task decomposition
class Task(BaseModel):
    task_id: str = Field(description="Unique identifier for the
subtask")
```

```
    instructions: str = Field(description="Specific instructions for this subtask")

class TaskList(BaseModel):
    tasks: List[Task] = Field(description="List of subtasks to execute")

class State(TypedDict):
    input_data: str  # Original input
    subtasks: List[Task]  # Decomposed tasks
    worker_outputs: Annotated[List[str], operator.add]  # Parallel results
    final_output: str  # Combined result

# Nodes
def orchestrator(state: State):
    """Break main task into independent subtasks"""
    tasks = llm.with_structured_output(TaskList).invoke([
        SystemMessage(content="Break this task into independent subtasks"),
        HumanMessage(content=state["input_data"])
    ])
    return {"subtasks": tasks.tasks}

def worker(state: Task):
    """Execute one subtask"""
    result = llm.invoke([
        SystemMessage(content="Execute this specific subtask"),
        HumanMessage(content=state.instructions)
    ])
    return {"worker_outputs": [result.content]}

def assembler(state: State):
    """Combine all worker results"""
    return {"final_output": "\n-\n".join(state["worker_outputs"])}

# Parallel task distributor
def distribute_tasks(state: State):
    """Create parallel execution branches"""
    return [Send("worker", {"task_id": t.task_id, "instructions": t.instructions})
            for t in state["subtasks"]]
# Workflow
builder = StateGraph(State)
builder.add_node("orchestrator", orchestrator)
builder.add_node("worker", worker)
builder.add_node("assembler", assembler)
```

```
52.
53. builder.add_edge(START, "orchestrator")
54. builder.add_conditional_edges(
55.     "orchestrator",
56.     distribute_tasks,
57.     {"worker": "worker"}
58. )
59. builder.add_edge("worker", "assembler")
60. builder.add_edge("assembler", END)
61.
62. graph = builder.compile()
```

In the `orchestrator` function, the LLM is forced to split the main task into simpler subtasks using the `Task` and `TaskList` classes. The `distribute_tasks` function sends these subtasks to the `worker` function in parallel, enabling concurrent execution. Once all subtasks are completed, the `assembly` function gathers and combines the results. The resulting graph image is shown in Figure 6. In the graph there will be multiple worker node to process subtasks concurrently.

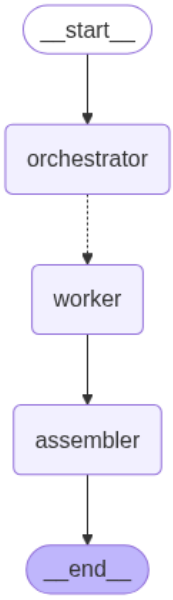

Figure 6. Orchestrator-worker graph architecture.

Evaluator-Optimizer

The evaluator-optimizer workflow is a self-improving loop that enables iterative refinement of outputs generated by a language model. It consists of three main components: a generator that produces an initial response, an evaluator that assesses the quality of that response using structured feedback, and a router that decides whether to accept the result or send it back for revision. This loop continues until the output meets predefined quality standards or a maximum number of iterations is reached. The process mimics human review cycles, where feedback is used to incrementally polish a draft. It's especially effective when tasks have clear evaluation criteria and when improvements can be guided by constructive feedback. This architecture is well-suited for use cases like code refinement, content rewriting, or any scenario requiring output alignment to specific goals. By automating the review and revision cycle, it increases efficiency and reduces the need for manual oversight while ensuring high-quality results.

```
from typing import Annotated, Literal
from pydantic import BaseModel, Field
from langchain_core.messages import HumanMessage, SystemMessage
from typing_extensions import TypedDict
from langgraph.graph import StateGraph, START, END
# Evaluation schema
class Evaluation(BaseModel):
    status: Literal["approved", "needs_revision"] = Field(
      description="Whether the output meets quality standards")
    feedback: str = Field(
     description="Constructive feedback for improvement if needed")
class State(TypedDict):
    input_: str  # Original input/request
    output: str  # Current version of the output
    evaluation: Evaluation  # Quality assessment
    iteration: int  # Track revision cycles
# Nodes
def generator(state: State):
    """Generate initial output or revised version"""
    if state.get("evaluation"):
        # Revision
        prompt = f"""
        Improve this content based on the feedback:
        Current version: {state['output']}
        Feedback: {state['evaluation'].feedback}
        """
    else:
        # First attempt
        prompt = f"Create output for: {state['input_']}"
    result = llm.invoke(prompt)
```

```
    return {
        "output": result.content,
        "iteration": state.get("iteration", 0) + 1}
def evaluator(state: State):
    """Assess output quality"""
    assessment = llm.with_structured_output(Evaluation).invoke(
        f"Evaluate this output:\n{state['output']}")
    return {"evaluation": assessment}
# Conditional routing
def router(state: State):
    """Determine next step based on evaluation"""
    if state["evaluation"].status == "approved":
        return "accept"
    return "revise"
# Build workflow
builder = StateGraph(State)
builder.add_node("generate", generator)
builder.add_node("evaluate", evaluator)

builder.add_edge(START, "generate")
builder.add_edge("generate", "evaluate")
builder.add_conditional_edges(
    "evaluate",
    router, {
        "accept": END,
        "revise": "generate"})
graph = builder.compile()
```

`Evaluation` class defines a structured format for assessing the quality of the generated output. The `evaluator` function uses this schema to generate structured feedback. The conditional routing logic, implemented in the `router` function and the `add_conditional_edges` method, determines what happens after evaluation. If the output is approved, the loop ends. If not, the output is sent back to the `generator` for revision. To prevent infinite loops, a safety condition terminates the workflow after five iterations. This mechanism ensures that the system either converges to a high-quality result or halts after reasonable effort. The resulting graph image is displayed in Figure 7.

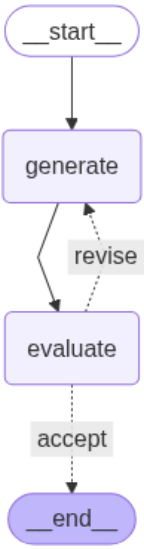

Figure 7. Evaluator-Optimizer architecture.

CONCLUSION

Agentic AI enables the development of intelligent applications that utilize workflows powered by large language models, as opposed to systems built with fixed rules. This chapter describes the components of the LangGraph library, used to develop such systems. The discussion covers the process of setting up AI agents, managing information exchange between functional nodes through state variables, designing adaptive routing mechanisms to create dynamic workflows and communication with external systems to create dynamic workflows. The chapter further examines some important AI architectures, such as prompt chaining, parallelization, orchestral-worker models, and evaluator-optimizer loops. By applying these tools and patterns across various scenarios and adaptations, developers can create artificial intelligence systems capable of reasoning, adapting, and collaborating autonomously.

REFERENCES

[1] A. Vaswani *et al.*, “Attention is all you need,” *Advances in neural information processing systems*, vol. 30, 2017.

[2] J. Devlin, M.-W. Chang, K. Lee, and K. Toutanova, “Bert: Pre-training of deep bidirectional transformers for language understanding,” in *Proceedings of the 2019 conference of the North American chapter of the association for computational linguistics: human language technologies, volume 1 (long and short papers)*, 2019, pp. 4171–4186.

[3] T. Brown *et al.*, “Language models are few-shot learners,” *Advances in neural information processing systems*, vol. 33, pp. 1877–1901, 2020.

[4] L. Hughes *et al.*, “AI Agents and Agentic Systems: A Multi-Expert Analysis,” *Journal of Computer Information Systems*, vol. 65, no. 4, pp. 489–517, Jul. 2025, doi: 10.1080/08874417.2025.2483832.

[5] R. Sapkota, K. I. Roumeliotis, and M. Karkee, “AI Agents vs. Agentic AI: A Conceptual Taxonomy, Applications and Challenges,” May 28, 2025, *arXiv*: arXiv:2505.10468. doi: 10.48550/arXiv.2505.10468.

[6] G. Wang *et al.*, “Voyager: An Open-Ended Embodied Agent with Large Language Models,” Oct. 19, 2023, *arXiv*: arXiv:2305.16291. doi: 10.48550/arXiv.2305.16291.

[7] J. S. Park, J. O’Brien, C. J. Cai, M. R. Morris, P. Liang, and M. S. Bernstein, “Generative agents: Interactive simulacra of human behavior,” in *Proceedings of the 36th annual acm symposium on user interface software and technology*, 2023, pp. 1–22.

[8] S. Murugesan, “The Rise of Agentic AI: Implications, Concerns, and the Path Forward,” *IEEE Intelligent Systems*, vol. 40, no. 2, pp. 8–14, Mar. 2025, doi: 10.1109/MIS.2025.3544940.

[9] D. B. Acharya, K. Kuppan, and B. Divya, “Agentic AI: Autonomous Intelligence for Complex Goals—A Comprehensive Survey,” *IEEE Access*, vol. 13, pp. 18912–18936, 2025, doi: 10.1109/ACCESS.2025.3532853.

[10] “Build a basic chatbot,” LangGraph. Accessed: Aug. 07, 2025. [Online]. Available: https://langchain-ai.github.io/langgraph/tutorials/get-started/1-build-basic-chatbot

[11] “Workflows & agents,” LangGraph. Accessed: Aug. 07, 2025. [Online]. Available: https://langchain-ai.github.io/langgraph/tutorials/workflows/

Chapter 2

Sustainable Geopolymer Mortar Production: A Waste-Based Alternative Approach

Başak ZENGİN[1], Ahmet Hayrullah SEVİNÇ[2], Müslüm Murat MARAŞ[3],

Abstract

The production of Portland cement poses a significant threat to environmental sustainability due t its high carbon emissions and energy-intensive processes. Therefore, the development of alternative binder systems has become a crucial necessity both environmentally and economically. Geopolymer materials have emerged as eco-friendly alternatives to cement-based materials owing to their high strength, chemical resistance, and low carbon emissions. However, the production of geopolymer binders typically relies on commercial alkali activators such as NaOH and KOH, which are expensive and have negative environmental impacts. This study investigates the feasibility of producing geopolymer mortar using only industrial waste materials (hazelnut shell ash and ground granulated blast furnace slag) without any chemical activators. Hazelnut shell ash supports geopolymerization reactions due to its potassium oxide (K_2O) and calcium oxide (CaO) content, enhancing the mechanical strength of the mortar. Moreover, the use of agricultural waste contributes to natural resource conservation and improved waste management, thereby supporting environmental sustainability. Experimental studies show that mortars produced using this waste-based activation method exhibit comparable mechanical performance to systems utilizing commercial activators.

This study aims to evaluate the applicability of waste-based activation in geopolymer mortars, contributing to the development of sustainable, eco-friendly, and cost-effective construction materials.

Keywords: Geopolymer mortar, sustainability, hazelnut shell ash, waste-based activation, eco-friendly materials, blast furnace slag, compressive strength

[1] bKahramanmaraş İstiklal University, Elbistan Vocational School of Higher Education, Construction Program, 46300, Kahramanmaraş / TÜRKİYE, basak.zengin@istiklal.edu.tr
[2] bKahramanmaraş İstiklal University, Elbistan Vocational School of Higher Education, Construction Program, 46300, Kahramanmaraş / TÜRKİYE, ahmethayrullah.sevinc@istiklal.edu.tr
[3] İnönü University, Engineering Faculty, Department of Civil Engineering, 44280, Malatya / TÜRKİYE murat.maras@inonu.edu.tr

1. Introduction

The construction industry is responsible for approximately 8% of global carbon emissions, making the development of sustainable building materials increasingly critical (Mehta & Monteiro, 2014; Pacheco-Torgal et al., 2018). Traditional Portland cement production adversely affects environmental sustainability due to its high energy consumption and carbon dioxide (CO_2) emissions. For every ton of clinker produced, around 0.8 tons of CO_2 are released, contributing significantly to global warming (Davidovits, 2015; Provis & Bernal, 2014).

As the economy grows, the construction sector faces significant challenges due to the vast consumption of raw materials and energy. The increasing demand for raw materials poses a serious environmental threat and highlights the urgent need for resource conservation. In response, researchers are seeking environmentally friendly alternatives that can address the depletion and rising costs of natural resources. Agricultural and industrial waste products, due to their abundance and favourable mechanical properties, have emerged as promising secondary raw materials in the construction sector (Bakhoum et al., 2017). These waste-based materials are gaining momentum as replacements for cement and sand, offering sustainable potential for future applications.

Rapid urbanization and industrialization have exacerbated raw material shortages and increased environmental degradation. The growing volume of hazardous industrial waste presents a serious challenge, as it cannot be easily managed or disposed of, leading to further climate-related concerns. From the perspective of sustainable construction, the integration of hazardous waste into building materials has gained importance. These waste materials, with their good mechanical properties, serve as viable alternatives to conventional cement and sand. Experimental studies have revealed promising results regarding their effects on the mechanical and microstructural properties of mortar under various mix designs.

One significant source of waste is hazelnut shell residue, generated in large quantities annually. Rather than disposing of this biomass through landfilling or incineration, utilizing it as a raw material for construction presents a more sustainable approach. Türkiye, which accounts for approximately 70% of global hazelnut production, generates considerable amounts of husk waste during industrial processing (Tufan et al., 2015). While a small portion of this by-product is used in particleboard manufacturing, the majority remains underutilized. Hazelnuts are not only a key agricultural product of the Black Sea region but also closely tied to the local economy and culture. Given the proximity of processing facilities to agricultural zones, the availability and distribution of hazelnut waste offer strong potential for technological innovation in the development of bio-based materials. This intersection

of agriculture and construction supports both regional agro-economies and sustainable material development.

An alternative to traditional cementitious materials is geopolymer binders, known for their low carbon footprint, high mechanical strength, and chemical resistance (Van Deventer et al., 2012; Duxson et al., 2007). However, the production of geopolymer mortars typically involves commercial chemical activators such as NaOH, KOH, and sodium silicate (Na_2SiO_3), which are costly and carbon intensive. For instance, the production of 1 kg of NaOH releases approximately 1.4 kg of CO_2 into the atmosphere (Passuello et al., 2017). Moreover, the storage, transportation, and handling of these chemicals involve high financial and safety risks (Omur et al., 2024).

Recent studies suggest that agricultural and industrial waste can be used as alternative alkali activators (Pinheiro et al., 2018; Alonso et al., 2019). Utilizing these wastes not only contributes to waste management but also reduces the consumption of natural resources. Hazelnut shell ash exhibits binding properties due to its high potassium oxide (K_2O) and calcium oxide (CaO) content, supporting geopolymerization reactions and enhancing mechanical strength (Omur et al., 2024; Sevinç, 2022). Incorporating this locally available waste into the construction industry presents a significant opportunity for environmental sustainability and regional industrial growth (Baran et al., 2020). In this context, the main objective of this study is to investigate the feasibility of producing geopolymer mortar using a fully waste-based activation system, without any commercial chemical activators. An environmentally friendly and cost-effective binder system was developed using hazelnut shell ash and blast furnace slag. The compressive strength of mortars with varying ratios of these components was examined and compared with systems based on commercial activators. Microstructural analysis revealed that activation with hazelnut ash can reduce porosity and improve compressive strength (Sevinç, 2022; Omur et al., 2024). These findings provide important scientific evidence for the development of a more eco-friendly and economically viable binder system that minimizes dependence on chemical activators. This study aims to evaluate the applicability of waste-based activation in geopolymer mortars, contributing to the advancement of sustainable construction materials.

2. Waste Materials and Their Critical Role in Geopolymer Production

The valorization of waste materials in geopolymer production not only addresses the environmental challenges posed by conventional cementitious systems but also promotes the circular economy by reintroducing industrial and agricultural by-products into the production cycle. The utilization of aluminosilicate-rich waste such as blast furnace slag, fly ash, and biomass-derived ashes significantly reduces the

reliance on virgin raw materials and diminishes carbon emissions associated with traditional Portland cement manufacture (Provis & Bernal, 2014; Davidovits, 2015).

Waste-based geopolymer systems leverage the inherent chemical composition of industrial by-products, such as the calcium, silica, and alumina contents, to initiate geopolymerization reactions without the need for high-temperature calcination processes. This results in lower energy consumption during binder production and contributes to a substantial reduction in the carbon footprint (Van Deventer et al., 2012). Additionally, the incorporation of agricultural residues, such as hazelnut shell ash, not only valorises otherwise discarded biomass but also introduces beneficial oxides like potassium oxide (K_2O) and silica (SiO_2), which are essential for enhancing the geopolymeric network and mechanical performance (Omur et al., 2024; Sevinç, 2022).

From a sustainability perspective, integrating waste materials into geopolymer mortars offers a dual benefit: it alleviates environmental pressures associated with waste disposal and reduces the environmental impact of the construction sector. Moreover, the localized sourcing of agricultural and industrial wastes fosters regional economic development and minimizes the environmental costs associated with long-distance material transportation. Therefore, waste utilization in geopolymer production is not merely a technical alternative but an essential strategy for achieving sustainable construction practices and advancing low-carbon material technologies.

3. Material Characteristics and Mortar Mix Design

The hazelnut shell ash utilized in this study was sourced from a bread oven. This ash does not possess a uniform particle size distribution, which necessitated an initial sieving process to remove larger particles. The remaining ash was then ground to achieve a fine particle structure, yielding ash particles no larger than 2 mm. Using a grinder equipped with steel balls, the ash was subjected to a 45-minute grinding process, resulting in a particle size distribution of less than 45 microns. The specific gravity of the processed ash was determined to be 2.59.

Blast furnace slag was obtained in a finely ground form from a cement factory for use in the mortar mixes. The specific gravity of the slag is 2.87, and it exhibits a fineness value of 5200 (Blaine).

The aggregate employed in this research consists of limestone-based crushed stone with a particle size range of 0 to 4 mm. This aggregate has a specific gravity of 2.71, a water absorption rate of 1.87%, and a fineness modulus of 2.72. The mixing water used in all formulations was potable tap water to ensure the quality of the mortars. Four distinct series of mortar were produced:GH25, GH35, GH45, and GH55. The inclusion rates of hazelnut shell ash were systematically varied to evaluate the impact of this waste material on the properties of the mortar. The mix

proportions of the produced mortar samples were determined in accordance with TS EN 196-1 standards. The specific mix ratios are detailed in Figure 1.

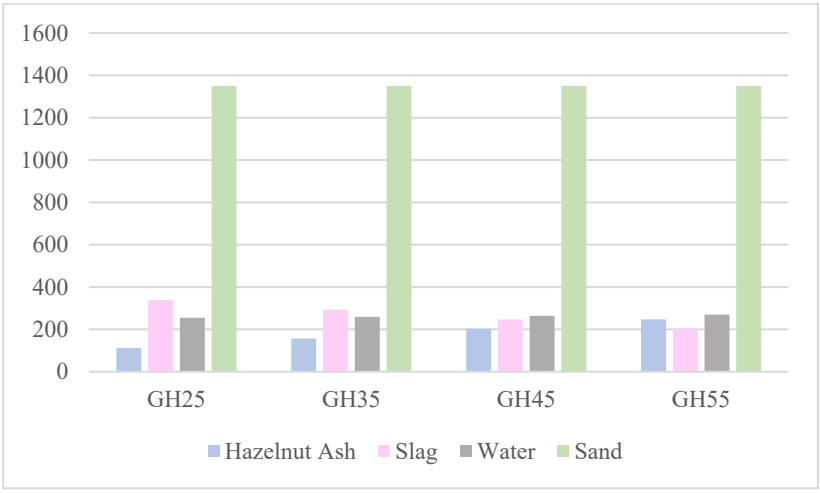

Figure 1. Mortar mixture quantities (Kg/m³)

4. Experimental

4.1. Unit Weight and Flexural Strength

The unit weights of mortar samples incorporating varying amounts of hazelnut shell ash (HSA) were evaluated in accordance with ASTM C138 (Figure 2). The unit weights of the samples were recorded as 2.37 g/cm³ (GH25), 2.34 g/cm³ (GH35), 2.31 g/cm³ (GH45), and 2.29 g/cm³ (GH55).

Figure 2. Measuring the unit volume weights of samples and Flexural Strength

The highest fresh and hardened unit weights were observed in GH25, the sample with the lowest HSA content, whereas GH55, containing the highest amount of HSA, exhibited the lowest unit weights. This decrease in unit weight with increasing HSA can be attributed to the lower specific gravity of hazelnut shell ash compared to blast furnace slag. Despite these reductions, the overall differences among samples remained relatively moderate (approximately 3.4% decrease in unit weight), which indicates a consistent density profile across different mix designs. Similar trends have been reported when using agricultural by-product ashes as partial replacements in cementitious systems (Maddalena et al., 2018; Tashima et al., 2019).

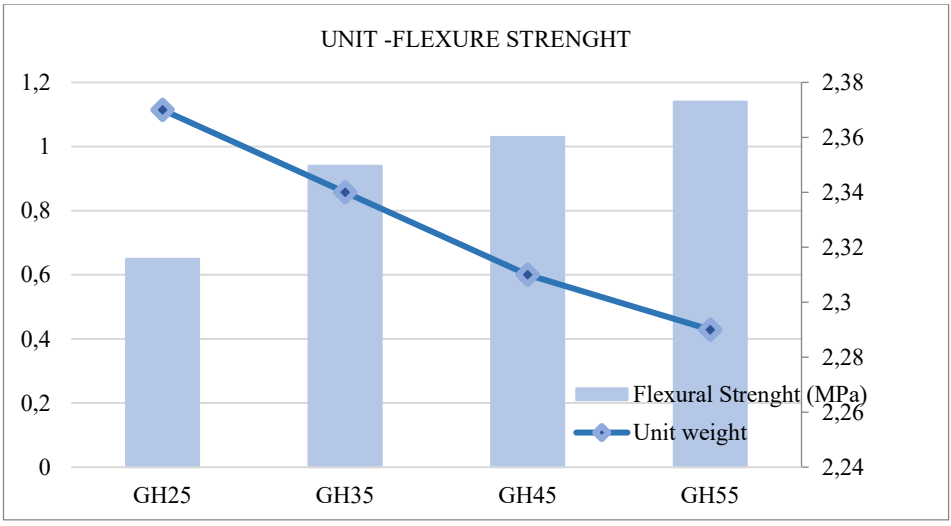

Figure 3 Unit -Flexural Strength

In terms of flexural strength, sample GH55 also exhibits the best performance, while GH25 has the lowest strength values. An increase in flexural strength with age is observed for all samples. However, unlike the distinct and high-percentage increases seen in compressive strength, the age-dependent increase percentages for flexural strength are generally more modest. This might suggest that the material's flexural strength does not develop as rapidly or at the same rate as its compressive strength. The increasing number in the GH series is positively correlated with an increase in flexural strength (Figure 3).

In terms of mechanical performance, the 7-day flexural strength values of the mortar samples were found to be 0.65 MPa (GH25), 0.94 MPa (GH35), 1.03 MPa (GH45), and 1.14 MPa (GH55) (Figure 3). Among these, GH25 demonstrated the lowest flexural strength, while GH55 showed the highest performance. The

increase in flexural strength observed with higher HSA content suggests a positive correlation, indicating that HSA effectively contributes to early-age flexural performance.

This enhancement can be attributed to the pozzolanic activity of hazelnut shell ash, which promotes additional calcium silicate hydrate (C-S-H) formation, strengthening the matrix structure (Islam et al., 2021; Gunasekara et al., 2020). Moreover, the micro-filling effect of fine ash particles reduces the overall porosity and leads to a denser microstructure, further improving flexural resistance (Siddique & Klaus, 2009).

It is important to note that while flexural strength increased with HSA content, the improvement was relatively moderate compared to typical compressive strength gains often reported in similar studies. This may be due to the complex nature of stress distribution under flexural loads and the dependence on the matrix-aggregate interface quality.

In summary, as the amount of hazelnut shell ash increased, the mortar samples exhibited a slight decrease in both fresh and hardened unit weights, accompanied by a clear enhancement in 7-day flexural strength. The findings support the potential use of hazelnut shell ash as a supplementary cementitious material, contributing to the development of more sustainable, lighter, and higher-performing mortar systems.

4.2. Ultrasonic Pulse Velocity and Compressive Strength Test

The compressive strengths and ultrasonic pulse velocity (UPV) values of mortar samples incorporating hazelnut shell ash (HSA) were evaluated after 7 days of curing (Figure 4). The 7-day compressive strength values were recorded as 3.79 MPa (GH25), 5.16 MPa (GH35), 6.77 MPa (GH45), and 8.54 MPa (GH55). Meanwhile, the corresponding UPV values were measured as 1576 m/s, 1683 m/s, 1858 m/s, and 1939 m/s for GH25, GH35, GH45, and GH55, respectively.


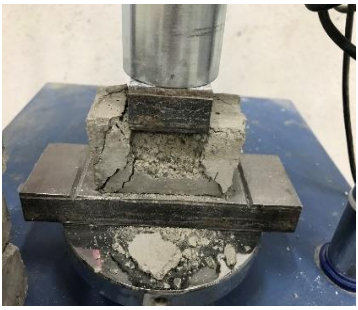

Figure 4. Compressive and UPV tests of samples

Among the samples, GH25 exhibited the lowest compressive strength and UPV value, while GH55 demonstrated the highest results in both parameters (Figure 5). The increase in compressive strength with higher HSA content suggests that hazelnut shell ash effectively contributes to the early-age mechanical performance of the mortar. This enhancement is primarily attributed to the pozzolanic reactivity of HSA, which promotes the formation of additional calcium silicate hydrate (C-S-H) phases, thereby improving the densification and overall integrity of the microstructure (Islam et al., 2021; Gunasekara et al., 2020).In parallel, the progressive increase in UPV values indicates improved material compactness and reduced internal defects or voids. Higher UPV values typically reflect a denser and more homogeneous matrix, implying that the incorporation of HSA enhances the quality and continuity of the hardened mortar body (Siddique & Klaus, 2009). The strong positive correlation between compressive strength and UPV observed across all samples supports the use of UPV as a non-destructive indicator of mechanical performance and internal integrity at early ages.

Overall, these findings demonstrate that mortars with higher contents of hazelnut shell ash achieve both superior early-age compressive strength and improved ultrasonic pulse velocity, emphasizing their potential for producing sustainable, high-quality cementitious materials with enhanced durability and structural performance.

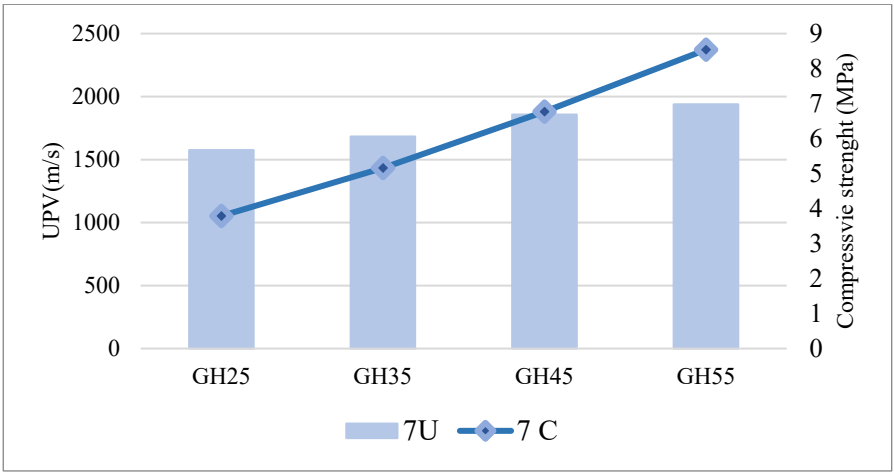

Figure 5. Compressive and flexural strength tests of samples

In terms of compressive strength, sample GH55 demonstrates superior performance, while GH25 shows the lowest. All samples exhibit an increase in strength with age, but GH55's high early-age strength and relatively earlier maturation are noteworthy. These data clearly show a positive correlation between the increasing number in the GH series and the increase in strength.

5. Results and Discus

The experimental findings of this study clearly demonstrate that geopolymer mortars produced with hazelnut shell ash and blast furnace slag, without the need for commercial activators, can achieve comparable early-age performance to traditional chemically activated systems. Various fresh and hardened properties were analysed, providing a holistic view of the material behaviour under different compositions during the crucial initial curing period.

Fresh and hardened unit weights exhibited a decreasing trend with the increase in hazelnut shell ash (HSA) content. The fresh unit weights ranged from 2.37 g/cm³ (GH25) to 2.29 g/cm³ (GH55). Correspondingly, the hardened unit weights, evaluated after 7 days, varied between 2.14 g/cm³ and 2.09 g/cm³. The GH25 sample, with the lowest ash content, showed the highest unit weight, whereas GH55 exhibited the lowest. This trend can be attributed to the lower specific gravity of hazelnut shell ash (2.59) compared to blast furnace slag (2.87) and aggregate (2.71). Similar observations have been reported by Özkoçak and Şişman (2020), who noted that the incorporation of biomass ashes increases the porosity and reduces the overall density of cementitious systems. This slight reduction in unit weight is favourable from a structural engineering perspective, as it may allow for lighter construction and reduced seismic loads.

Setting times were significantly affected by the ash content. The GH25 mixture exhibited an exceptionally prolonged initial setting time (750 minutes), which is considerably longer than that of conventional cements. Conversely, mixtures with higher ash content, such as GH45 and GH55, demonstrated much shorter setting times, reaching the initial set within 15 to 18 minutes. This acceleration in setting behavior can be explained by the high K_2O content of hazelnut shell ash, which enhances the alkalinity of the system and promotes rapid geopolymerization reactions (Sevinç, 2022; Omur et al., 2024). Nonetheless, extremely short setting times may challenge the workability of fresh mortar, necessitating careful adjustment of mixture proportions or the use of retarders in practical applications.

Compressive strength measurements revealed that the increase in hazelnut shell ash content substantially improved early-age mechanical performance. At 7 days, compressive strength values increased from 3.79 MPa (GH25) to 8.54 MPa (GH55). Similarly, flexural strength improved with ash content, rising from 0.65 MPa (GH25) to 1.14 MPa (GH55) at 7 days. These results are consistent with the findings of Samsudin and Ban (2015) and Cheah et al. (2021), who highlighted that potassium-rich biomass ashes enhance the solubility of aluminosilicate materials, thereby increasing the production of geopolymeric gel phases and improving mechanical properties. Moreover, the presence of K_2O facilitates a higher pH environment compared to sodium-based systems, further accelerating the geopolymerization process and contributing to denser microstructures.

During the 7-day curing period, compared to the GH25 sample, the GH35, GH45, and GH55 samples exhibited substantial increases in mechanical strength. For compressive strength, these samples showed increases of 36% (GH35), 79% (GH45), and 125% (GH55), respectively. In terms of flexural strength, these samples achieved increases of 45% (GH35), 58% (GH45), and 75% (GH55), respectively. The general trend across all mechanical tests at 7 days indicates that hazelnut shell ash effectively acts as an activator when combined with blast furnace slag, supporting the rapid development of high-strength binders without the need for commercial alkali chemicals. This approach not only reduces the carbon footprint but also leverages agricultural waste products, promoting sustainability and resource efficiency. The increased strength of mortars produced with biomass ashes containing high K_2O is attributed to the increased solubility of aluminosilicate raw materials in a highly alkaline environment due to the elevated K_2O content (Samsudin and Ban, 2015). Potassium compounds have significantly higher pH levels than sodium-based solutions, further enhancing the solubility of ground granulated blast furnace slag (GGBFS),

leading to greater hydration products and a denser microstructure, consequently improving early-age strength and durability characteristics (Cheah et al., 2021).

When comparing the results to previous studies, such as those by Alonso et al. (2019) and Pinheiro et al. (2018), it becomes evident that agricultural residues can successfully replace synthetic activators, provided that their chemical composition is appropriate. The outcomes of this study reinforce the viability of hazelnut shell ash as a sustainable and effective raw material for geopolymer production. Overall, the experimental results substantiate that a complete waste-based activation system can yield geopolymer mortars with satisfactory mechanical strength, suitable setting times, and reduced densities, all while contributing significantly to environmental sustainability. These findings align with the broader objectives outlined by Davidovits (2015) and Van Deventer et al. (2012) regarding the use of geopolymers as low-carbon alternatives to Portland cement-based materials.

6. Conclusions

This study demonstrates that it is possible to produce geopolymer mortar solely using industrial waste materials (hazelnut shell ash and blast furnace slag) without the use of chemical activators. Experimental results indicate that the potassium oxide (K_2O) and calcium oxide (CaO) content of hazelnut shell ash supports geopolymer reactions, thereby enhancing mechanical strength. This study successfully demonstrated the potential of hazelnut shell ash (HSA) as a valuable supplementary cementitious material in mortar production. The systematic variation of HSA inclusion rates yielded several key findings:

The incorporation of hazelnut shell ash led to a slight but consistent decrease in both fresh and hardened unit weights of the mortar samples. This reduction is attributed to the lower specific gravity of HSA compared to other mix constituents.

A clear and positive correlation was observed between increasing HSA content and improved 7-day flexural strength. The highest HSA content (GH55) resulted in the best flexural performance, primarily due to HSA's pozzolanic activity and micro-filling effects. A slight decrease in unit weight was observed as the proportion of hazelnut shell ash increased. Furthermore, flexural and compressive strength tests demonstrated that the strength values significantly increased with higher proportions of hazelnut shell ash, with the GH55 sample exhibiting the highest mechanical strength.

Hazelnut shell ash significantly enhanced the early-age compressive strength of the mortar. Higher HSA contents (e.g., GH55) consistently produced superior

compressive strengths, again linked to the pozzolanic reactivity of HSA and the resulting formation of additional C-S-H phases.

Ultrasonic pulse velocity (UPV) values increased with higher HSA content, indicating improved material compactness, reduced internal defects, and a denser, more homogeneous mortar matrix. The strong correlation between UPV and compressive strength validates UPV as a non-destructive tool for evaluating mortar quality.

In summary, mortars with higher hazelnut shell ash content not only exhibited slightly lower unit weights but also achieved superior early-age mechanical properties, including enhanced flexural and compressive strengths, and improved internal quality as indicated by higher UPV values. These findings strongly support the effective utilization of hazelnut shell ash as a sustainable and high-performing supplementary cementitious material, contributing to the development of lighter and more durable mortar systems.

Overall, the GH55 sample demonstrated the best performance in terms of mechanical and physical properties, showing that these mortars produced through a completely waste-based activation method are competitive with traditional commercial activator-based systems. This study highlights a significant alternative for developing sustainable building materials.

These findings indicate that waste-based activation can be successfully applied in geopolymer mortars and contribute to the development of an environmentally friendly, sustainable, and economical binding system. The results promote the use of waste-based binders as an alternative to traditional cement-based systems and provide significant scientific contributions to the ongoing efforts in developing sustainable building materials.

Funding: This research was funded by the Scientific Research Projects Coordination Unit of Kahramanmaraş İstiklal University, grant number 2022/1-2.

References

Alonso, M. M., Palomo, A., & Fernandez-Jimenez, A. (2019). Alkali activation of biomass ash-based binders: A review. *Journal of Cleaner Production, 219,* 365-379.

Bakhoum, S. Loutfy E., Kamel Garas, G., Allam, E. M., & Ezz, H. (2017). The Role of Nanotechnology in Sustainable Construction: A Case Study of Using Nano Granite Waste Particles in Cement Mortar.

Baran, T., Yıldırım, H., & Ozkocak, A. (2020). The effects of hazelnut shell ash in cementitious systems. *Materials Today: Proceedings, 37,* 1123-1130.

Davidovits, J. (2015). Geopolymer Chemistry and Applications. Institut Géopolymère.

Duxson, P., Provis, J. L., Lukey, G. C., & Van Deventer, J. S. J. (2007). The role of inorganic polymer technology in the development of green concrete. *Cement and Concrete Research, 37(12),* 1590-1597.

Gunasekara, C., Law, D. W., & Setunge, S. (2020). Long-term performance of blended cement incorporating agricultural waste ashes. *Cement and Concrete Composites*, 114, 103738.

Islam, A., Alengaram, U. J., Jumaat, M. Z., & Bashar, I. I. (2021). The development of sustainable concrete incorporating agro-waste. *Resources, Conservation and Recycling*, 172, 105662.

Maddalena, R., Roberts, J. J., & Hamilton, A. (2018). Can Portland cement be replaced by low-carbon alternative materials? A study on the thermal properties and carbonation of mineral blends. *Journal of Cleaner Production*, 186, 933-942.

Mehta, P. K., & Monteiro, P. J. M. (2014). Concrete: Microstructure, Properties, and Materials. McGraw-Hill.

Omur, T., Kanat, D., & Kabay, N. (2024). Innovative use of hazelnut shell ash as an alkali activator: A comparative analysis with commercial activators. *Journal of Building Engineering, 90,* 109466.

Pacheco-Torgal, F., Labrincha, J. A., Leonelli, C., Palomo, A., & Chindaprasirt, P. (2018). Handbook of Alkali-Activated Cements, Mortars, and Concretes. Woodhead Publishing.

Pinheiro, M. D. M., et al. (2018). Olive stone biomass ash as an alkali activator for BFS-based AAMs. *Construction and Building Materials, 171,* 90-98.

Provis, J. L., & Bernal, S. A. (2014). Geopolymers and other alkali-activated materials: why, how, and what? *Materials and Structures, 47(1-2),* 11-25.

Sevinç, A. H. (2022). Investigating the properties of GGBFS hazelnut ash-based cement-free mortars. *Journal of Materials in Civil Engineering, 34(10),* 04022268.

Siddique, R., & Klaus, J. (2009). Influence of metakaolin on the properties of mortar and concrete: A review. *Applied Clay Science*, 43(3–4), 392–400.

Tashima, M. M., Soriano, L., Monzó, J., & Borrachero, M. V. (2019). Performance of alkali-activated binders containing agricultural residues. *Construction and Building Materials*, 206, 49-58.

Tufan, M., Akbaş, S., Güleç, T., Taşçıoğlu, C., & Hakkı Alma, M. (2015). Mechanical, thermal, and morphological properties and decay resistance of filled hazelnut husk polymer composites.

Van Deventer, J. S. J., Provis, J. L., & Duxson, P. (2012). Technical and commercial progress in the adoption of geopolymer cement. *Minerals Engineering, 29,* 89-104.

Chapter 3

Energy Yield Analysis of a Grid-Connected PV System and Feasibility Estimation for Green Hydrogen Production in Bandırma Region

Batın DEMİRCAN[1,2]

Abstract

In this study, the potential for green hydrogen production of a 10.8 kWp grid-connected photovoltaic (PV) system, designed for the Bandırma region of Turkey, was evaluated using PVsyst 7.2.16 software. The system comprises bifacial PV modules manufactured by Longi Solar and two inverters, each with dual-MPPT inputs and a nominal power rating of 7.5 kW. Simulation results indicate an annual total electricity yield of 15.32 MWh. Of this energy, 95.86 % is allocated to a proton exchange membrane (PEM) electrolyzer operating at a constant power of 1.5 kW for six hours per day, resulting in an annual green hydrogen production of 63.17 kg.

Economic analyses reveal that the system's total installation cost is approximately USD 12,300; when operating expenditures are included, the levelized cost of hydrogen production amounts to about USD 12.66 per kg. This figure lies within the expected range for small-scale installations, and it is projected that scale-up would reduce production costs to the vicinity of USD 5–7 per kg.

From an environmental standpoint, the system's hydrogen output alone avoids the emission of 631.7 kg of CO_2 per year; furthermore, the export of surplus PV electricity to the grid yields an additional reduction of 6.89 t of CO_2 annually. These findings demonstrate that such systems offer significant potential for integrating renewable energy sources and mitigating carbon emissions.

Keywrods: PVsyst, Electrolyzer, PV system, Green Hydrogen, Renewable Energy

[1] Balıkesir University, Balıkesir Vocational School, Department of Electronic and Automation, batindemircan@gmail.com ORCID No: 0000-0002-0765-458X

[2] Balıkesir University, Renewable Energy Research, Application and Development Center

1 Introduction

In recent years, green hydrogen, produced through the electrolysis of water using electricity generated from renewable energy sources, has emerged as a priority among carbon neutral energy solutions worldwide [1]. Green hydrogen is based on the principle of separating water into hydrogen and oxygen without reliance on fossil fuels and contributes to grid flexibility by storing surplus electricity generated from wind and solar power [2]. According to the report of the International Renewable Energy Agency, green hydrogen will become cost competitive after 2030 through photovoltaic and wind based production [3].

Among electrolysis technologies, alkaline water electrolyzers, which are the most widely used in industrial applications, and polymer electrolyte membrane electrolyzers, which allow high current densities and rapid dynamic response, are prominent. However, in recent years significant progress has also been made in anion exchange membrane water electrolyzers that do not contain noble metal groups and can use low cost catalysts [4]. Electrolyzer units integrated with photovoltaic systems support grid stability by supplying water electrolysis during periods of surplus production and increase the economic benefits of photovoltaic plants through hydrogen production [2]. The IEA World Energy Investments 2025 report also emphasizes that photovoltaic electrolyzer integration has gained priority in investments in low emission fuels [5].

This technological diversity enables system designs suitable for different scales and application scenarios [6]. A systematic review of the potential of green hydrogen to reduce carbon emissions has evaluated not only its role as an energy storage medium produced through water electrolysis but also its direct use in hard to decarbonize sectors such as heating, transportation, and the chemical industry. In the review by Elshafei and Mansour, it is stated that green hydrogen projects are currently costly, but costs are expected to decrease rapidly due to the decline in renewable energy costs, the achievement of economies of scale, and the maturation of technology [7]. The European Commission's EU Hydrogen Strategy report details the strategic importance of green hydrogen in transportation and heavy industry and the investment targets associated with it [8].

For the widespread adoption of green hydrogen, not only technological efficiency but also environmental and economic impact analyses covering the entire value chain are of critical importance. In the literature, systematic reviews have evaluated all stages from electrolysis to production, distribution, and the carbon free potential achieved at the end use [9]. In addition, the cost effectiveness of hydrogen integration into heavy industry is being discussed in the context of direct reduced iron technologies. Economy wide optimization

simulations conducted by Jordan et al. have shown that under the net zero carbon dioxide target by 2050, carbon capture and storage technologies provide both lower costs and higher cumulative emission reductions compared to hydrogen fed direct reduced iron [10]. The Turkey Hydrogen Technologies Strategy and Roadmap supports this transition by projecting that costs can be reduced below 2.4 USD per kilogram by 2035 and to 1.2 USD per kilogram by 2053 [11] . On the other hand, the Turkey National Energy Plan highlights the importance of such pilot scale photovoltaic electrolyzer projects by targeting an electrolyzer capacity of 5 gigawatts by 2035 [12].

In this study, a 10.8 kilowatt peak grid connected photovoltaic system specific to the Bandırma region of Turkey is analyzed. The annual distribution of solar energy and operating parameters in the relevant region are examined using PVsyst 7.2.16 software, and the potential for converting the obtained electricity generation data into green hydrogen in a polymer electrolyte membrane electrolyzer is investigated. Thus, a green hydrogen production system applicable specifically to Bandırma will be proposed in the light of both regional economic feasibility and annual greenhouse gas reduction figures.

2 Materials and Methods

In this study, the green hydrogen production potential based exclusively on solar energy was analyzed for a site located in the Bandırma district of Balıkesir province, Turkey. Using PVsyst 7.2.16 software [13], a grid-connected photovoltaic (PV) system was designed with the aim of operating a constant-power electrolyzer during daylight hours to produce hydrogen. Figure 1 shows the general schematic diagram of the PVsyst-based green hydrogen production system installed in the Bandırma region. The system directs a portion of the electrical output from the PV panels directly to the grid, while routing the remainder to an electrolyzer unit with a fixed load profile for green hydrogen generation. Within the simulation framework, PV generation, inverter configuration, load profile, and hydrogen production calculations were all modelled in PVsyst 7.2, and performance analyses were subsequently carried out.

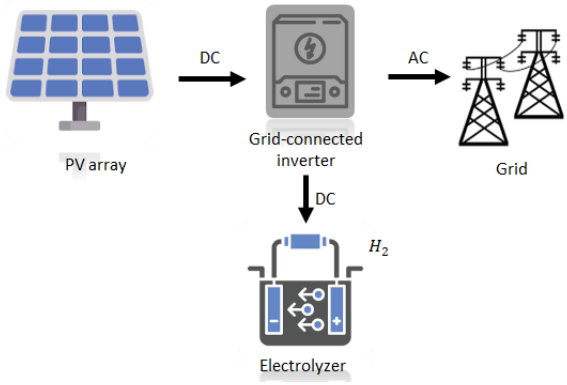

Figure 1. Green hydrogen production configuration integrated with a grid-connected photovoltaic system

2.1 Site Location, Meteorological Data and Photovoltaic Field Configuration

The simulation study was conducted using the Bandırma district, situated in the southern Marmara Region, as its basis. The location of the study area on the map is shown in Figure 2.

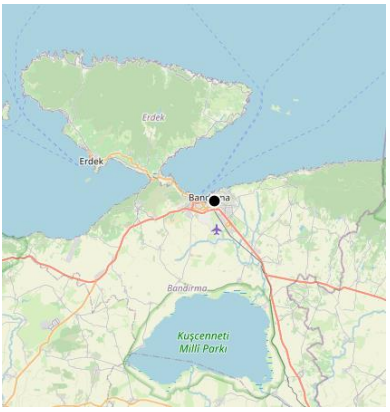

Figure 2. Geographical location of the Bandırma district where the study was conducted

The locational information for Bandırma is shown in Figure 3. This site was entered directly into the PVsyst software and served as the basis for the simulation.

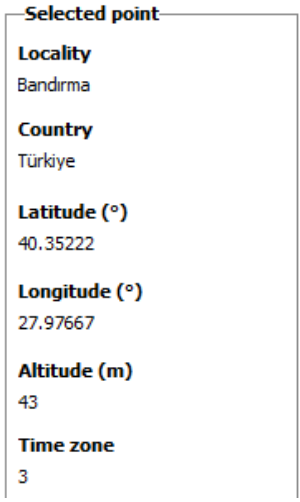

Figure 3. Coordinates and general parameters of the Bandırma location

Meteorological data were obtained from the Meteonorm 8.0 database integrated into PVsyst. This selection was performed manually, as illustrated in Figure 3.

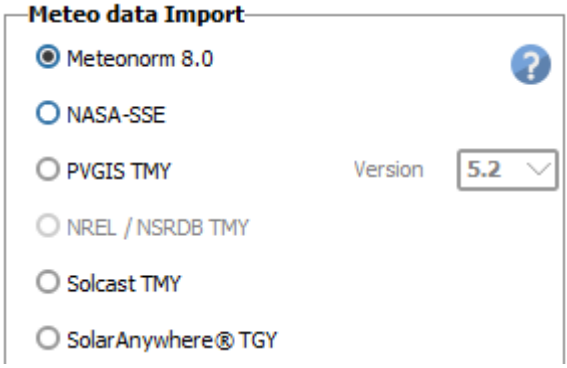

Figure 4. Selection of Meteorological Data Source (Meteonorm 8.0)

For the Bandırma site, the annual global horizontal irradiance (GHI) was determined to be 1563.5 kWh/m², and the mean ambient temperature was 14.72 °C. Throughout the simulation period, the albedo was held constant at 0.20, and shading effects were neglected. The PV system was mounted on a fixed-tilt plane, with a module tilt angle set to 30° and an azimuth orientation of 0° (due south). Figure 5 presents a graphical evaluation of the panel tilt and orientation in terms of annual irradiance optimization.

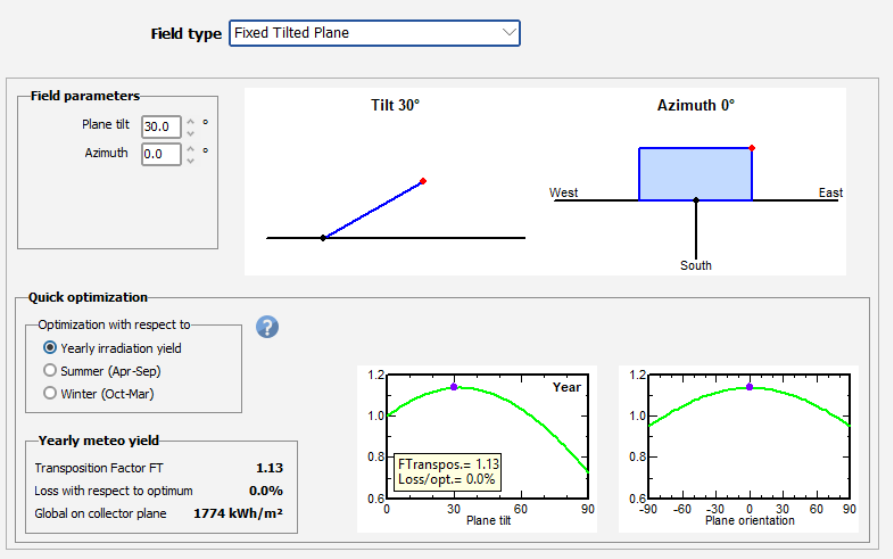

Figure 5. Annual Irradiance Optimization through PV Panel Tilt and Orientation

The system comprises 24 LONGi LR4-72HBD 450 M bifacial PV modules, yielding a total installed capacity of 10.8 kWp. Each 450 Wp module is arranged in three parallel strings of eight modules in series. Figure 6 details the PV module, string configuration, and inverter selection.

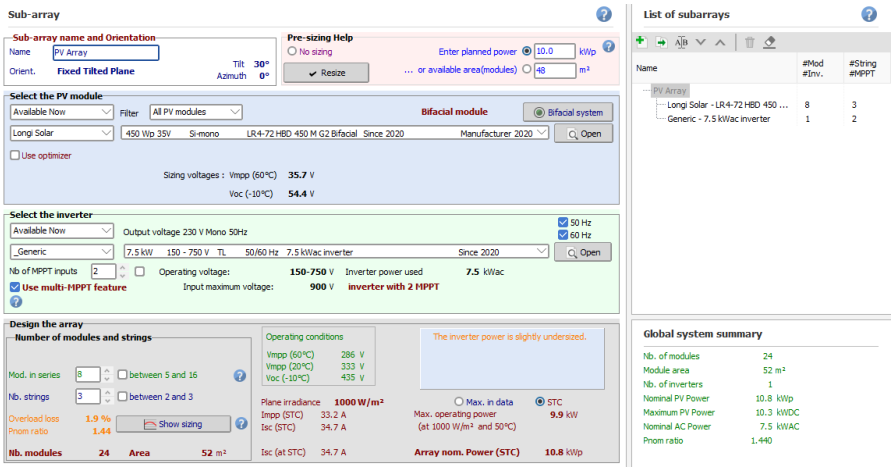

Figure 6. Presentation of PV module and inverter selection, including panel layout, connection configuration, and system overview

2.3 Inverter Description and Load Profile (Electrolyzer Load)

An inverter with a nominal power rating of 7.5 kW_a and two MPPT inputs was selected for the system. Its DC-input voltage window spans 150–750 V, and the DC/AC ratio (P_{nom} ratio) is 1.44 well within the acceptable range reported in the literature. The inverter model was generated using the "Generic" inverter database provided in PVsyst. A constant-power load was defined for hydrogen production. The specified 1.5 kW constant load was configured to operate only between 10:00 and 16:00, yielding a daily energy consumption of 9.0 kWh/day. This load profile ensures that energy is drawn for green hydrogen production solely during photovoltaic generation hours. Figure 7 presents the hourly load profile of the electrolyzer.

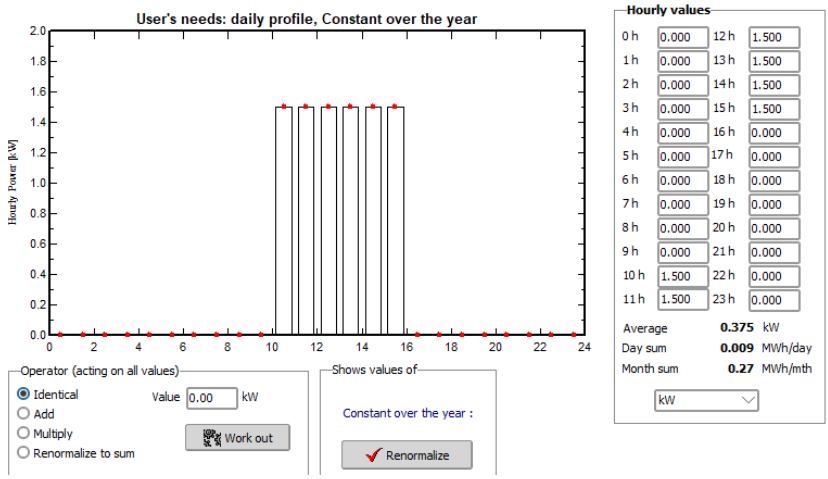

Figure 7. Daily hourly load profile of the constant-power (1.5 kW) electrolyzer defined in PVsyst

2.5 Simulation Settings and Reporting

The simulation year was defined using the Typical Meteorological Year (TMY) dataset provided by PVsyst. The key outputs obtained include total PV generation (MWh/year), energy delivered to the user load (kWh/year), energy exported to the grid, performance ratio (PR), specific yield (kWh/kWp/year), inverter losses, and overall system losses. All results are corroborated by PVsyst's PDF report and graphical outputs. The total energy supplied to the user load was calculated as 3,285 kWh/year, and this value was directly employed in the hydrogen production calculations.

3 Results

In this study, a grid-connected photovoltaic (PV) system for green hydrogen production was modeled for the Bandırma site using PVsyst 7.2.16, and its annual performance was evaluated. The simulation results were analysed from technical, economic, and environmental perspectives to elucidate the system's green hydrogen production potential.

3.1 PV System Performance and Energy Uncertainty, Reliability Assessment

The annual energy yield of the 10.8 kWp PV system planned for installation in the Bandırma region was calculated as 15,323 kWh/year. This corresponds to a specific yield of 1,419 kWh/kWp/year, indicating highly efficient operation relative to Turkey's solar-energy potential. The system's performance ratio (PR) was determined to be 81.1 %. Figure 8 summarizes the annual energy yield, nominal power, specific yield, and system losses.

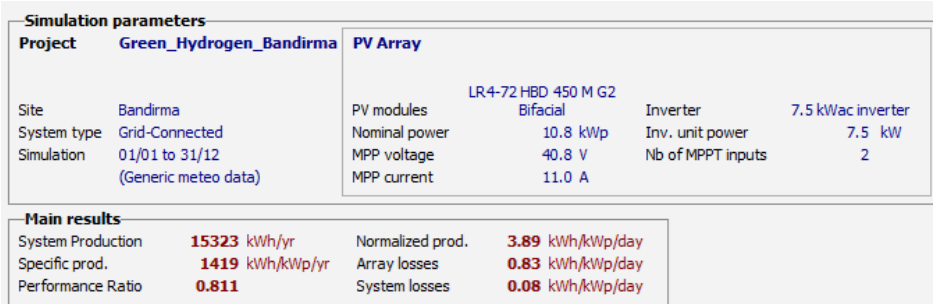

Figure 8. Key Simulation Parameters and Annual Performance Outputs of the PV System

Figure 9 presents the input–output relationship that characterizes the system's daily energy performance. On the horizontal axis, it shows the global irradiance incident on the horizontal plane (kWh/m²/day), and on the vertical axis, the corresponding electric energy output of the PV system (kWh/day).

The dataset covers the period from 1 January to 31 December, with each point representing one day's energy input–output performance. The observed trend indicates a directly proportional increase in electrical output with rising irradiance, confirming that the system operates smoothly and responsively to solar intensity. The high density of data points in the 2–8 kWh/m²/day range reflects that this irradiance interval is the most prevalent daily radiation level for the Bandırma region. Moreover, output values reaching up to 60 kWh/day

demonstrate that, under favorable conditions, the system can operate at near-maximum efficiency, approaching saturation at high irradiance levels.

The tight, narrowly dispersed linear cluster evidences the system's stable performance and its ability to convert energy with high precision, minimally affected by environmental factors such as temperature fluctuations, shading, or soiling. Such a strong linear relationship validates the adequacy of the system design and confirms that energy losses have been kept to a minimum. Figure 9 thus substantiates the PV system's high irradiance sensitivity, the robust correlation between input radiation and energy production, and the system's reliable operation under dynamic environmental conditions.

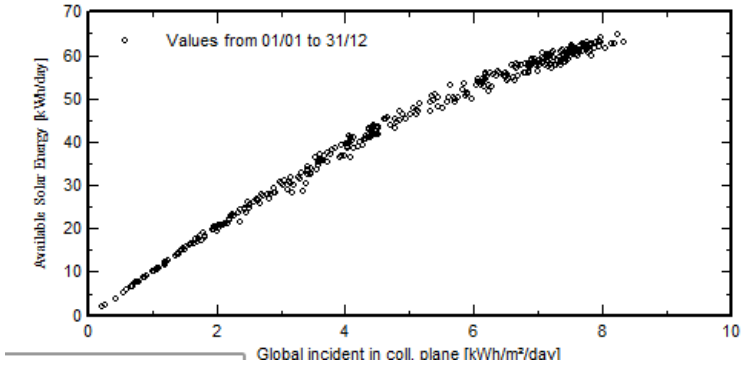

Figure 9. Relationship between Daily Global Irradiance and System Output

Figure 10 illustrates the performance ratio (PR) curve, defined as the ratio of the energy delivered to the grid over the year to the theoretical energy that could have been generated. The plot presents separate PR values for each month, thereby revealing how system efficiency responds to seasonal variations. Overall, the PR fluctuates between 0.75 and 0.85 throughout the year, with a mean value of 0.811, indicating excellent installation quality and overall system performance.

Notably, January, November, and December exhibit higher PR levels (approximately 0.85), despite shorter daylight hours; this suggests that colder ambient temperatures during these months positively influence module efficiency, thereby boosting performance. Cooler conditions reduce cell operating temperature, which is a primary factor contributing to the observed PR increase. During the transition periods of March–April and September–October, the PR values remained close to the annual average, indicating that the system delivers more balanced and stable performance during spring and autumn. Consequently, the analysis presented in Figure 9 demonstrates that the system operates at over 80 % efficiency for the majority of the year, experiencing only

minor efficiency losses during the summer months due to elevated temperatures and system limitations. This finding confirms that the system successfully maintains seasonal performance balance and provides reliable energy production.

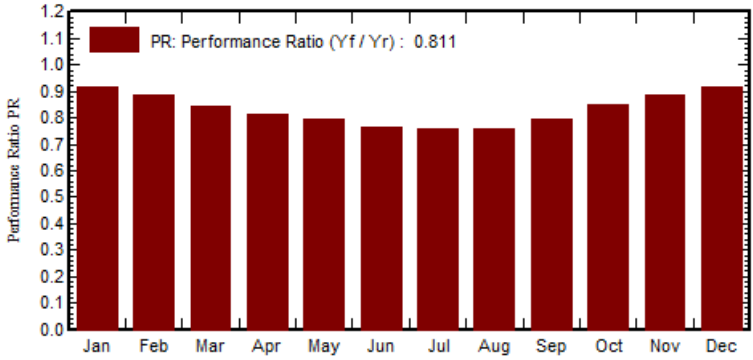

Figure 10. Monthly Variation of Performance Ratio (PR)

Figure 11 illustrates the probabilistic distribution of the PV system's annual energy yield under uncertainty. The P50 energy yield is calculated as 15,323 kWh, meaning there is a 50% probability that the system will produce this amount or more. Additionally, the P90 and P95 values 14,343 kWh and 14,068 kWh, respectively indicate that even under more conservative assumptions, the energy yield remains high. This demonstrates both the system's strong performance and its low investment risk profile.

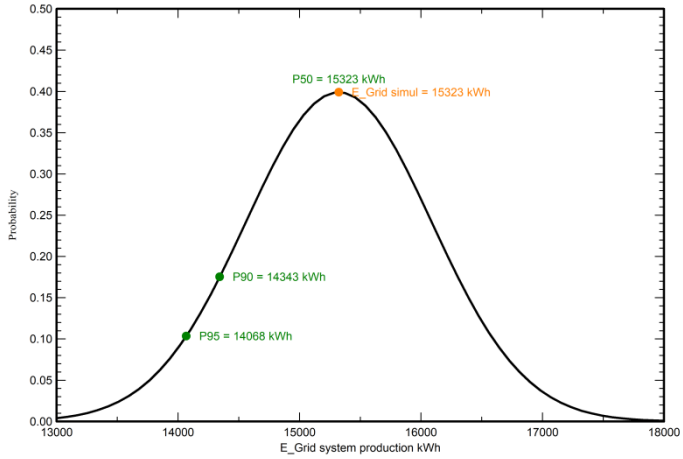

Figure 11. Probability Distribution of Annual Energy Yield Uncertainty for the PV System

3.3 Electrolyzer Load and Energy Consumption

A PEM (Proton Exchange Membrane) electrolyzer with a constant power demand was considered for green hydrogen production. The system was configured to operate only during the PV system's most efficient hours, specifically between 10:00 and 16:00. The electrolyzer's fixed daily consumption was defined as 1.5 kW, leading to a daily energy requirement of 9.0 kWh and an annual consumption of 3,285 kWh/year. Simulation results obtained via PVsyst software reveal that the PV system is capable of supplying the majority of the electrolyzer's energy demand. The solar fraction, defined as the ratio of energy consumption met directly by solar production without importing electricity from the grid, was calculated to be 95.86%. This high ratio clearly indicates substantial grid independence and a high level of system autonomy. The annual energy imported from the grid was only 0.14 MWh, representing a negligible portion of the total demand.

Figure 12 presents the monthly normalized energy production and associated losses of the PV system. The chart distinguishes between the useful inverter output (Yf), PV array losses (Lc), and system/inverter losses (Ls). The system exhibits peak performance during the summer months June, July, and August with normalized daily production ranging between 6–7 kWh/kWp/day. In contrast, production declines during the winter season due to reduced irradiance. This seasonal variation was considered in system design to ensure operational continuity. These findings confirm the PV system's high energy efficiency and its effective alignment with the defined load profile. Particularly for green hydrogen production, which requires consistent and time-specific energy delivery, the observed performance underscores the system's viability and sustainability.

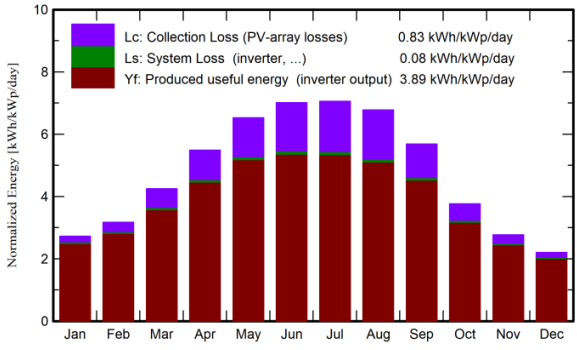

Figure 12. Monthly Normalized Energy Production and Losses (kWh/kWp/day)

3.4 Green Hydrogen Production Potential, Economic Evaluation and Carbon Emission Savings

Assuming an energy requirement of 52 kWh per kilogram of hydrogen for a PEM electrolyzer, the annual production capacity mH_2 can be calculated as follows [14], [15]:

$$H_2 production = \frac{3285\ kWh}{52\ kWh/kg} \approx 63.17 kg/yr$$

$$m_{H_2} = \frac{E_{annual}}{E_{per\ kg}} = \frac{3{,}285\ kWh/year}{52\ kWh/kg} \approx 63.17\ kg_{H_2}/yr$$

where

E_{annual} = 3,285 kWh/year is the total annual energy supplied to the electrolyzer, and

E_{annual} = 52 kWh/kg is the specific energy consumption per kilogram of hydrogen.

Production was seasonally uniform, with the average daily hydrogen yield ranging from 5.2 to 5.4 kg/day. Assuming a 20-year lifetime and an annual operation-and-maintenance rate of 1.5 %, the annualized costs can be derived as follows [16]:

Capital recovery factor (CRF):

$$CRF = \frac{1}{20} = 0.05$$

Annualized capital cost:

$$C_{cap,ann} = 12300\ \text{USD} \times 0.05 = 615\ \text{USD/yr}$$

Annual maintenance cost:

$$C_{om,ann} = 12300\ \text{USD} \times 0.015 = 184.5\ \text{USD/yr}$$

Total fixed annual cost:

$$C_{fixed,ann} = 615 + 184.5 \approx 800\ \text{USD/yr}$$

Given an annual hydrogen yield of 63.17 kg, the levelized cost of hydrogen (LCOH) is therefore [17], [18], [19]:

$$LCOH = \frac{C_{fixed,ann}}{m_{H_2} ann} = \frac{800\ USD/yr}{63.17\ kg/yr} \approx 12.66\ USD/kg$$

$$\frac{\$800}{63.17\ kg} \approx 12.66\$/\text{kg} - H_2$$

Although this value may appear high for a small-scale installation, it is anticipated that scaling up the system could reduce the cost to the USD 5–7 per kg-H_2 range reported in the literature. When hydrogen is produced by conventional methods (gray hydrogen), an average of 10 kg CO_2 is emitted per kilogram of H_2. Accordingly, for an annual production of 63.17 kg, approximately 631.7 kg of CO_2 would be emitted per year. Additionally, if the PV system's total electricity output of 15.32 MWh per year were used entirely to displace grid supplied power, assuming an emission factor of 0.45 kg CO_2 per kWh, a total annual CO_2 savings of 6,894 kg would be realized.

4 Conclusion

In this study, the potential application of a grid-connected 10.8 kWp photovoltaic system developed for the Bandırma site for green hydrogen production was examined in detail using PVsyst 7.2.16 software. The simulation outputs revealed significant findings in terms of the system's energy generation capacity, hydrogen production potential, economic efficiency, and environmental contributions.

The simulation indicated an annual photovoltaic generation of 15.32 MWh, of which 95.86% was allocated to a 1.5 kW constant-power electrolyzer configured specifically for green hydrogen production, demonstrating a high solar fraction. The electrolyzer's annual energy consumption was calculated as 3,285 kWh, and based on this value, the system's annual green hydrogen production was determined to be approximately 63.17 kg.

Economic analyses showed a capital cost of USD 12,300 and, including annual operation and maintenance expenditures, a levelized hydrogen production cost of approximately USD 12.66 per kilogram. Although this cost is expectedly higher for small-scale installations, it aligns with literature reports suggesting a reduction to USD 5 to 7 per kilogram for larger systems. From an environmental perspective, the green hydrogen output avoids around 631.7 kg of CO_2 emissions annually. Moreover, if all of the PV system's electricity is used to replace grid-supplied power, an additional reduction of approximately 6.89 tonnes of CO_2 per year can be achieved.

Thus, the system offers a sustainable and environmentally friendly solution not only for green hydrogen production but also for general energy supply. In conclusion, this work demonstrates the technical, economic, and environmental

feasibility of small-scale PV-based hydrogen production systems and provides a pioneering model for future higher-capacity installations.

It is important to note that PVsyst does not directly model electrolyzer dynamics or hydrogen production processes. Instead, the hydrogen yield in this study was estimated based on the PV system's energy output and a standard specific energy consumption of 52 kWh/kg H_2 for a PEM electrolyzer. Therefore, the results should be interpreted as an energy-based feasibility assessment rather than a detailed hydrogen system simulation. Future work could integrate more advanced modeling tools to capture electrolyzer performance, partial load behavior, and hydrogen storage dynamics for a more comprehensive analysis.

5

REFERENCES

[1] W. Cheng and S. Lee, "How Green Are the National Hydrogen Strategies?," *Sustainability (Switzerland)*, vol. 14, no. 3, Feb. 2022, doi: 10.3390/su14031930.

[2] A. Mohamed Elshafei and R. Mansour, "Green Hydrogen as a Potential Solution for Reducing Carbon Emissions: A Review," *Journal of Energy Research and Reviews*, vol. 13, no. 2, pp. 1–10, Feb. 2023, doi: 10.9734/jenrr/2023/v13i2257.

[3] I. Renewable Energy Agency, *World Energy Transitions Outlook 2024: 1.5°C pathway - Executive summary*. 2024. [Online]. Available: www.irena.org

[4] A. Franco and C. Giovannini, "Recent and Future Advances in Water Electrolysis for Green Hydrogen Generation: Critical Analysis and Perspectives," *Sustainability (Switzerland)*, vol. 15, no. 24, Dec. 2023, doi: 10.3390/su152416917.

[5] W. Energy Investment and th Edition, "World Energy Investment 2025 - 10th Edition," 2025. [Online]. Available: www.iea.org

[6] M. Klingenhof *et al.*, "All Platinum-Group-Metal-Free Alkaline Exchange Membrane Water Electrolyzers Using Direct Hydrothermal Catalyst Deposition on Raney Ni Substrate," *ACS Appl Energy Mater*, vol. 7, no. 16, pp. 6856–6861, Aug. 2024, doi: 10.1021/acsaem.4c01647.

[7] A. Mohamed Elshafei and R. Mansour, "Green Hydrogen as a Potential Solution for Reducing Carbon Emissions: A Review," *Journal of Energy Research and Reviews*, vol. 13, no. 2, pp. 1–10, Feb. 2023, doi: 10.9734/jenrr/2023/v13i2257.

[8] European Commission, "A Hydrogen Strategy for a climate neutral Europe," 2020.

[9] L. Du, Y. Yang, L. Zhou, and M. Liu, "Greenhouse Gas Reduction Potential and Economics of Green Hydrogen via Water Electrolysis: A Systematic Review of Value-Chain-Wide Decarbonization," Jun. 01, 2024, *Multidisciplinary Digital Publishing Institute (MDPI)*. doi: 10.3390/su16114602.

[10] K. H. Jordan, P. Jaramillo, V. J. Karplus, P. J. Adams, and N. Z. Muller, "The Role of Hydrogen in Decarbonizing U.S. Iron and Steel Production," *Environ Sci Technol*, vol. 59, no. 10, pp. 4915–4925, Mar. 2025, doi: 10.1021/acs.est.4c05756.

[11] T.C. Enerji ve Tabi Kaynaklar Bakanlığı, “Türkiye Hidrojen Teknolojileri Stratejisi ve Yol Haritası,” 2024.

[12] T.C. Enerji ve Tabi Kaynaklar Bakanlığı, “TÜRKİYE ULUSAL ENERJİ PLANI 2022,” 2022.

[13] PVsyst, “PVsyst.” Accessed: Jul. 27, 2025. [Online]. Available: https://www.pvsyst.com/

[14] D. Gielen, E. Taibi, and R. Miranda, “HYDROGEN: A RENEWABLE ENERGY PERSPECTIVE,” 2019, Accessed: Jul. 28, 2025. [Online]. Available: www.irena.org

[15] IEA, “Global Hydrogen .” Accessed: Jul. 28, 2025. [Online]. Available: https://www.iea.org/reports/global-hydrogen-review-2022

[16] A. Liponi, A. Baccioli, L. Ferrari, and U. Desideri, “Techno-economic analysis of hydrogen production from PV plants”, doi: 10.1051/e3sconf/202233401001.

[17] A. Liponi, A. Baccioli, L. Ferrari, and U. Desideri, “Techno-economic analysis of hydrogen production from PV plants,” 2022, doi: 10.1051/e3sconf/202233401001.

[18] Lazard, “Lazard’s Levelized Cost of Hydrogen Analysis-Executive Summary Overview of Analysis,” 2021.

[19] European Hydrogen Partnership, “Levelised Cost of Hydrogen Calculator | European Hydrogen Observatory.” Accessed: Jul. 29, 2025. [Online]. Available: https://observatory.clean-hydrogen.europa.eu/tools-reports/levelised-cost-hydrogen-calculator

Chapter 4

Controlling Entry/Exit Delamination in GFRP Composites: Taguchi Optimization of Drilling Parameters

Durmuş Ali BİRCAN[1],Bekir YILDIRIMCI[2], Yılmaz ERBİL[3]

Introduction

Composite materials have revolutionized modern engineering by offering unparalleled advantages, including high strength-to-weight ratios, corrosion resistance, and customizable mechanical properties. These characteristics have rendered them essential in aerospace, automotive, renewable energy, and defense industries, where performance under extreme conditions is critical [1, 2]. Among composites, Glass Fiber-Reinforced Plastics (GFRP) have garnered significant attention in defense applications, particularly for manufacturing protective components such as spall liners. These liners mitigate the hazardous effects of spallation, fragmentation caused by high-impact forces, enhancing the survivability of armored systems [3, 4]. The efficacy of GFRP in such roles stems from its exceptional impact absorption, flexibility, and lightweight nature, making it a material of strategic importance [5].

Despite these advantages, the machining of GFRP composites presents tough challenges. Drilling, a ubiquitous process for assembling structural components, often induces defects such as fiber pull-out, matrix cracking, and delamination, the separation of composite layers [6, 7]. Delamination, in particular, compromises structural integrity by reducing load-bearing capacity and fatigue resistance, thereby jeopardizing the safety and longevity of critical systems [8]. This defect arises primarily from excessive thrust forces during drilling, which exceed the interlaminar bond strength, especially at hole entry and exit regions [9, 10]. Consequently, mitigating delamination is paramount to ensuring the reliability of GFRP components in demanding applications.

[1] Çukurova University, Department of Mechanical Engineering, Adana, Türkiye
ORCID:0000-0002-9430-4587
[2] Çukurova University, Department of Mechanical Engineering, Adana, Türkiye
ORCID:0009-0006-1852-8366
[3]SECANT Savunma ve Havacılık A.Ş., Eskişehir, Türkiye
ORCID:0000-0003-2890-8961

Traditional approaches to optimizing drilling parameters, such as spindle speed, feed rate, and tool geometry, rely on iterative experimentation, which is both time-intensive and costly [11]. While advanced techniques like cryogenic cooling and diamond-coated tools have shown promise in reducing thermal and mechanical damage, their implementation often entails prohibitive expenses or technical complexities [12, 13]. Recent studies emphasize the critical influence of cutting parameters on delamination severity, with higher feed rates and lower speeds worsening defect formation [14, 15]. However, a systematic methodology to identify optimal parameter combinations remains indefinable, particularly for GFRP composites.

To address these limitations, this study employs the Taguchi optimization method, a robust statistical Design of Experiments (DoE), to systematically evaluate the effects of drilling parameters on delamination. The Taguchi approach minimizes experimental iterations while maximizing data reliability, enabling the identification of optimal conditions through Signal-To-Noise (S/N) ratio analysis [16]. By focusing on three critical factors (drill diameter, spindle speed, and feed rate) at multiple levels, this research aims to establish a parameter hierarchy and determine configurations that minimize peel-up and push-down delamination.

Literature Review

The machining of GFRP composites has attracted considerable research attention given their widespread adoption in high-performance industries such as aerospace, automotive, and defence. Among machining processes, drilling is critical for assembling composite structures but frequently introduces defects like delamination, which compromises mechanical integrity and long-term performance. Delamination, characterized by the separation of composite layers at hole entry (peel-up) and exit (push-down) zones, arises predominantly from excessive thrust forces [8, 10].

Important work by Hocheng and Dharan [11] established a mechanistic relationship between thrust forces and delamination, attributing defect formation to the critical interaction between uncut material thickness and interlaminar bond strength. Building on this foundation, Lin and Chen [13] demonstrated in Carbon Fiber-Reinforced Polymer (CFRP) drilling that optimizing speeds reduces thrust forces, thereby suppressing delamination. Although their study focused on CFRP, the insights remain applicable to GFRP composites due to analogous structural characteristics, including anisotropic behavior and layered reinforcement.

The influence of drilling parameters on delamination severity has been a central point of research. Khashaba et al. [14, 15] demonstrated that feed rate

significantly impacts thrust forces, with higher feed rates worsening peel-up delamination due to increased tool-workpiece interaction. Conversely, El-Sonbaty et al. [16] observed that cutting speed exerts minimal influence on thrust forces in GFR/epoxy composites, emphasizing instead the role of drill diameter and fiber volume fraction. Kilickap [17] further corroborated these findings, identifying feed rate and speed as dominant factors affecting delamination in GFRP, with lower feed rates reducing defect formation. Such discrepancies underscore the complexity of parameter interactions and the need for material-specific optimization strategies.

Advanced machining techniques, including cryogenic cooling [12] and diamond-coated tools [7], have been proposed to address thermal and mechanical damage during drilling. However, their practical implementation is often limited by cost and technical constraints, particularly in defense applications where cost-effectiveness and scalability are critical. In response, statistical optimization methods, such as the Taguchi DoE, have gained prominence for their ability to minimize experimental iterations while maximizing process efficiency. Mohan Kumar et al. [19, 20] successfully applied Taguchi S/N ratio analysis to optimize drilling parameters for Kevlar composites, achieving reduced delamination at higher speeds and lower feed rates. Their work highlights versatility of the method in composite machining, though its application to GFRP composites tailored for defense systems.

Figure 1. GFRP Defense Components: Ballistic Plates and Bulletproof Jacket

A critical gap in existing research lies in the systematic evaluation of parameter hierarchies for minimizing both peel-up and push-down delamination. While studies such as those by Vinayagamoorthy et al. [18] emphasize thrust force as the primary delamination driver, others, including Davim et al. [21], advocate for digital image analysis to quantify delamination factors.

The Taguchi orthogonal array approach offers a structured framework to address these challenges. By evaluating multiple parameters simultaneously, this methodology enables the identification of optimal drilling conditions while minimizing resource expenditure. Previous applications in composite machining, such as those by Aamir et al. [5], demonstrate its efficacy in balancing competing factors like production rate and defect minimization. Nevertheless, stringent requirements of the defense sector for GFRP components, demanding both high precision and durability under extreme conditions, necessitate further refinement of these techniques.

This study builds upon prior work by integrating Taguchi optimization with a comprehensive analysis of peel-up and push-down delamination mechanisms in GFRP composites. By examining the effects of spindle speed, feed rate, and drill diameter through a structured L9 orthogonal array, the research aims to establish a parameter hierarchy and deliver actionable insights for enhancing drilling quality in defense applications.

Material and Method

The development and experimental evaluation of GFRP composites demand careful selection of constituent materials and precise control of machining parameters. This section outlines the materials, fabrication methodology, and experimental framework employed to investigate drilling-induced delamination. The GFRP composites were fabricated using E-glass fibers (Metyx GW300) and a vinylester resin matrix (Crystic VE 679-03PA). The glass fibers were selected for their high tensile strength and cost-effectiveness, while the vinylester resin was chosen for its superior chemical resistance and mechanical durability compared to polyester, ensuring performance in aggressive environments, as presented in Tables 1 and 2.

Table 3.1. Mechanical and Physical Properties of Glass Fiber Reinforcement

Properties	Glass
	Metyx GW300
Areal Density (g/m^2)	306
Density (g/cm^3)	2.55
Tensile Strength (MPa)	3450
Young's Modulus (GPa)	72
Elongation at Break (%)	4.8
Fiber Diameter (Microns)	9 – 13

Table 3.2. Thermomechanical Properties of Vinylester Resin Matrix

Properties	Vinylester
	Crystic VE 679-03PA
Density (g/cm³)	1.06
Viscosity [mPa·s (at 25°C)]	250 – 450
Gel Time (minutes)	20 – 30
Tensile Strength (MPa)	90
Flexural Strength (MPa)	150
Elongation at Break (%)	4 – 6

The composite laminates, with a nominal thickness of 10 mm, consisted of 23 unidirectional plies arranged in a [0°/90°] alternating sequence. These laminates were designed with an areal density of 600 g/m² and a fiber-to-matrix weight ratio of 81:19, optimized to achieve high strength-to-weight properties critical for defense and aerospace applications. Fabrication was carried out via the Vacuum-Assisted Resin Infusion Method (VARIM) using a custom-designed aluminum mold with integrated flow channels to enhance resin distribution. This process minimized void content and ensured uniform consolidation. After curing at 80°C for 8 hours, the laminates were trimmed to 200×100×10 mm dimensions using an abrasive water jet cutter, a non-contact method selected to prevent mechanical stress and preserve edge integrity, as shown in Figure 2.

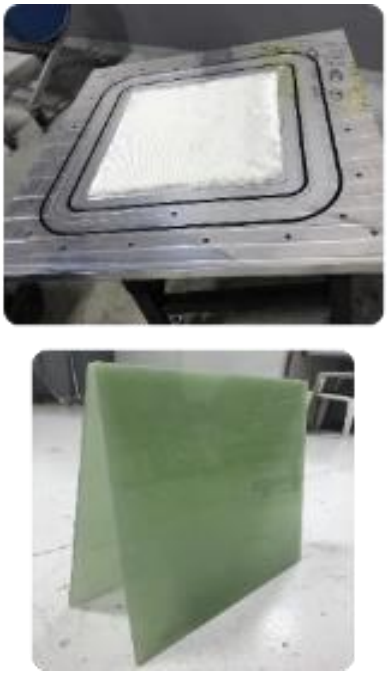

Figure 2. VARIM Process for GFRP Laminate Fabrication

High-Speed Steel (HSS) drill bits with diameters of 6 mm, 8 mm, and 10 mm were employed, each equipped with a 30° helix angle and 118° point angle to optimize chip evacuation and cutting performance. Experiments were conducted on a CNC milling machine (Figure 3), with spindle speed, feed rate, and drill diameter designated as key controlled variables (Table 3). Three levels were selected for each parameter: spindle speeds of 62, 422, and 945 Rpm; feed rates of 0.10, 0.18, and 0.24 mm/rev; and drill diameters of 6, 8, and 10 mm. These parameters were selected to reflect both industrial standards and extreme operational scenarios encountered in defense applications.

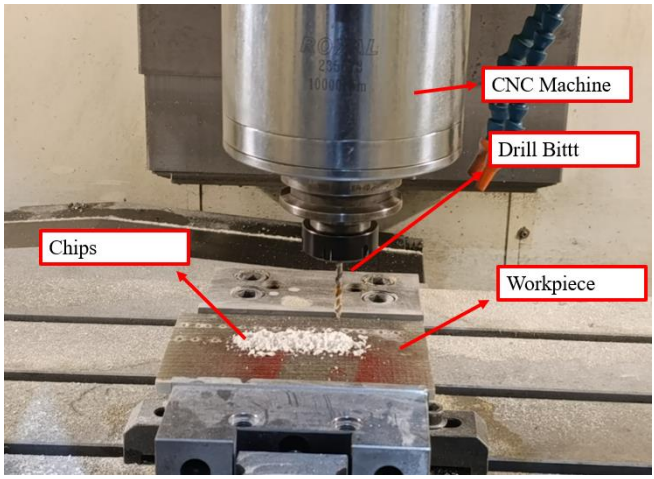

Figure 3. CNC Drilling Experimental Setup for GFRP Composites

Table 3. Drilling Parameters and Taguchi Levels for GFRP Experiment

Spindle Speed (Rpm)	Feed Rate (mm/rev)	Drill Diameter (mm)
62	0.10	6
422	0.18	8
945	0.24	10

Drilling-induced damage was assessed by quantifying entry (peel-up) and exit (push-down) delamination using a digital optical microscope at 200× magnification, integrated with image analysis software. The delamination factor (F_d), calculated as the ratio of the maximum damaged diameter (D_{max}) to the nominal hole diameter (D_{drill}) (Equation 1, Figure 4b), was adopted as the primary evaluation metric for hole quality. Each experimental condition was replicated three times to ensure statistical reliability, and the average F_d values were recorded.

$$F_d = \frac{D_{max}}{D_{drill}} \qquad \text{(Eq.1)}$$

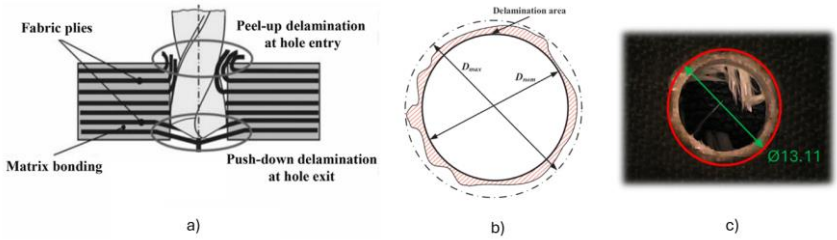

Figure 4. Optical Microscopy Analysis of Peel-Up and Push-Down Delamination

A Taguchi L9 orthogonal array (Table 4) was employed to systematically evaluate the effects of drilling parameters on delamination. This design reduced the number of experiments from 27 (full factorial) to 9 while maintaining analytical robustness. The S/N ratio, calculated using Equation 2, was applied under the "smaller is better" criterion to identify optimal parameter combinations for minimizing F_d. Minitab software facilitated data analysis, including main effects plots and response tables.

$$\eta = -10 \log_{10}\left(\frac{1}{n}\sum_{i=1}^{n} y_i^2\right) \qquad \text{(Eq.2)}$$

Table 4. L9 Orthogonal Array with Delamination Factors and S/N Ratios

Drilling Diameter (mm)	Spindle Speed(Rpm)	Feed Rate(mm/rev)	F_d Peel-up	F_d Push-down	S/N F_d Peel-up	S/N F_d Push-down
6	62	0.10	1.2183	1.217	-1.715	-1.7059
6	422	0.18	1.2513	1.2811	-1.9473	-2.1516
6	945	0.24	1.1879	1.2101	-1.4959	-1.6561
8	62	0.18	1.2247	1.2058	-1.7608	-1.6257
8	422	0.24	1.2253	1.2633	-1.765	-2.0304
8	945	0.10	1.1329	1.2014	-1.0841	-1.5939
10	62	0.24	1.2679	1.2962	-2.0615	-2.2534
10	422	0.10	1.1183	1.1725	-0.9711	-1.382
10	945	0.18	1.1458	1.2889	-1.182	-2.2047

A polynomial regression model was developed to correlate drilling parameters with delamination factors. Predictive accuracy of the model was validated through R-squared values and alignment between experimental and predicted

results. Surface plots further visualized interactions between spindle speed, feed rate, and drill diameter across different tool sizes.

Results & Discussion

The experimental investigation using the Taguchi L9 orthogonal array (Table 4) explained critical relationships between drilling parameters and delamination in GFRP composites. The analysis of S/N ratios for peel-up and push-down delamination demonstrated different optimal parameter configurations for minimizing each defect type. For peel-up delamination, the optimal parameters comprised a drill diameter of 10 mm, speed of 945 Rpm, and feed rate of 0.10 mm/rev, yielding the highest S/N ratio (Table 5). Spindle speed emerged as the most influential factor, followed by feed rate and drill diameter. Conversely, for push-down delamination, the optimal parameters shifted to an 8 mm drill diameter, speed of 945 Rpm, and feed rate of 0.10 mm/rev, with feed rate dominating as the primary factor, followed by drill diameter and speed as shown in Table 6.

Table 5. S/N Ratio Response for Peel-Up Delamination

Level	Drilling Diameter (mm)	Spindle Speed (Rpm)	Feed Rate (mm/rev)
1	-1.719	-1.846	-1.257
2	-1.537	-1.561	-1.63
3	-1.405	-1.254	-1.774
Delta	0.315	0.592	0.517
Rank	3	1	2

Table 6. S/N Ratio Response for Push-down Delamination

Level	Drilling Diameter (mm)	Spindle Speed (Rpm)	Feed Rate (mm/rev)
1	-1.838	-1.862	-1.561
2	-1.75	-1.855	-1.994
3	-1.947	-1.818	-1.98
Delta	0.197	0.043	0.433
Rank	2	3	1

The advantage of high speeds in reducing peel-up delamination aligns with the mechanistic understanding of reduced thrust forces at elevated speeds, as suggested by Lin and Chen [13]. Lower feed rates further reduce tool-workpiece interaction forces, thereby limiting interlaminar shear stresses that initiate layer separation [14]. This parameter synergy, high speeds paired with low feed rates, is visually corroborated in Figures 5 and 6, where main effects plots exhibit

significant delamination factor reduction under these conditions. Divergent optimal drill diameters for the two delamination modes likely stem from mechanical trade-offs. Larger diameters enhance torsional rigidity, minimizing vibration-induced peel-up defects, whereas smaller diameters reduce exit-layer bending stresses, thereby lessening push-down delamination [10, 21]. This contrast underscores the role of tool geometry in balancing chip evacuation efficiency and structural resistance during composite machining.

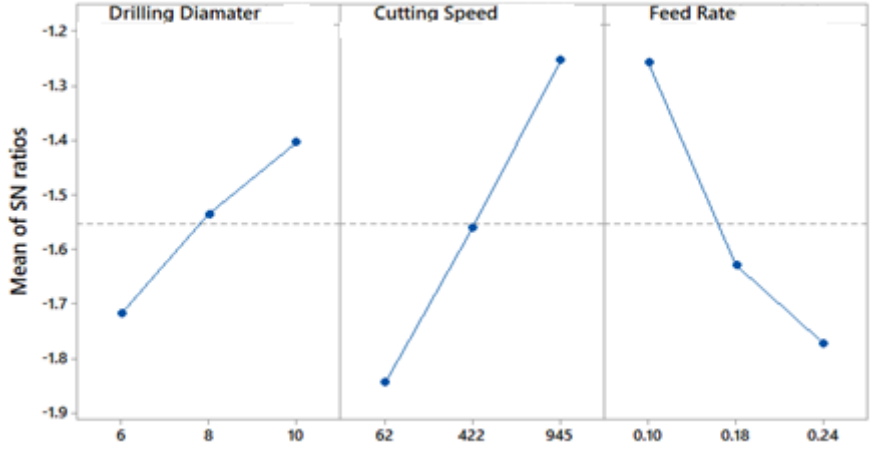

Figure 5. Taguchi S/N Ratio Main Effects for Peel-Up Delamination

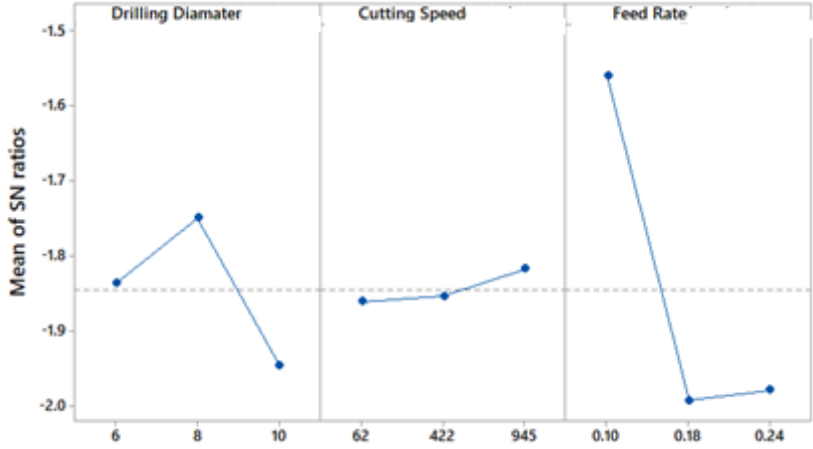

Figure 6. Taguchi S/N Ratio Main Effects for Push-Down Delamination

Figures 7 and 8 provide a compelling visual contrast of the results obtained using the optimum and sub-optimum drilling parameters. Figure 7, illustrating the optimized configuration, 10 mm drill diameter, 945 Rpm spindle speed, 0.10 mm/rev feed rate, displays negligible burr formation and minimal delamination at both entry and exit zones. This contrasts sharply with Figure 8, where a high

feed rate and low speed result in significant fiber pull-out, matrix cracking, and extensive delamination. These morphological anomalies correlate with elevated F_d values, directly corroborating the quantitative trends identified through S/N ratio analysis. The distinct divergence in defect severity underscores the necessity of precise parameter selection to minimize material damage and ensure structural integrity in drilling operations.

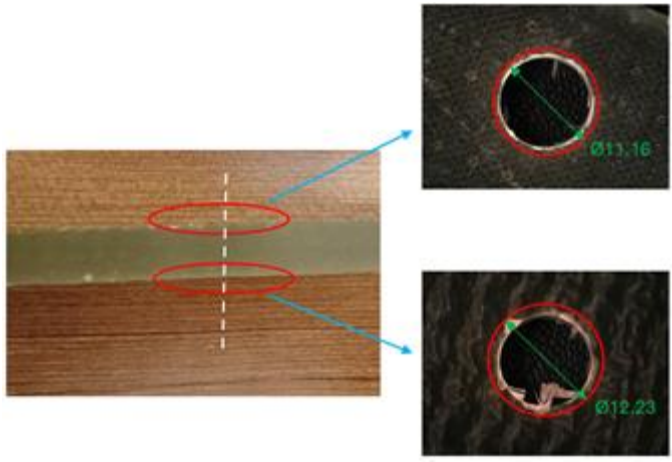

Figure 7. Optimized Drilling Result: Minimal Delamination at High Speed (945 Rpm) and Low Feed Rate (0.10 mm/rev), 10 mm Drill

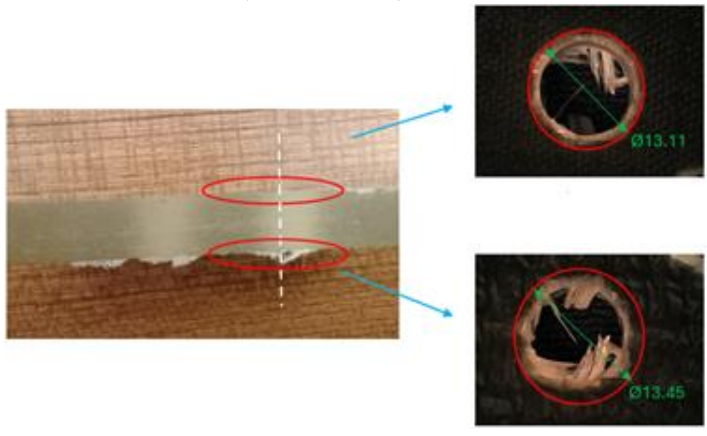

Figure 8. Suboptimal Drilling Outcome: Severe Delamination and Fiber Damage at Low Speed (62 Rpm) and High Feed Rate (0.24 mm/rev), 10 mm Drill

The regression analysis revealed strong predictive performance, with adjusted R^2 values of 81.20% and 88.10% for peel-up and push-down delamination, respectively, as illustrated in Figure 9. Surface plots (see Figures 10–12) explained the relationship between machining parameters and delamination behavior. For the 6 mm drill bit (Figure 10), minimal entry-zone delamination

occurred at low feed rates and high spindle speeds, whereas excessive feed rates exacerbated defects due to elevated thrust forces. A parallel trend emerged for the 8 mm drill bit (Figure 11), though push-down delamination demonstrated non-linearity, showing a slight increase at moderate feed rates. This deviation may stem from localized heat accumulation or progressive tool wear, factors potentially attributable to prolonged machining cycles, as noted in prior studies [7, 12]. In contrast, the 10 mm drill bit (see Figure 12) demonstrated consistent delamination suppression across both entry and exit zones when used with low feed rates and high speeds, thereby emphasising its suitability for precision-critical industrial operations.

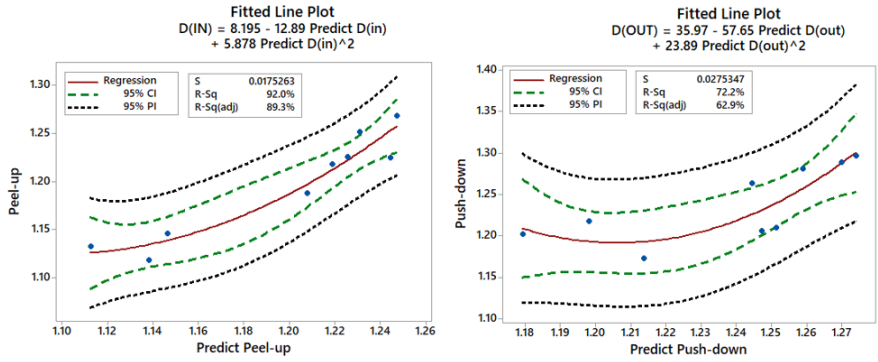

Figure 9. Regression Model Validation for Delamination Factor Predictions

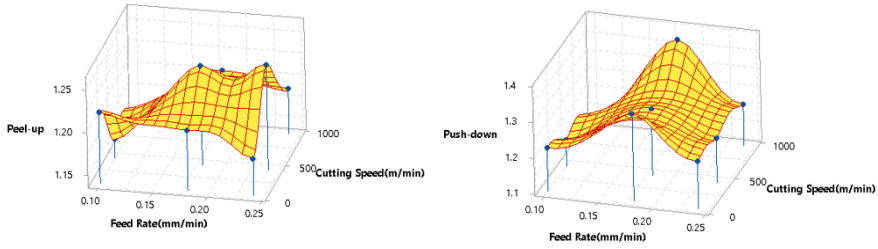

Figure 10. Parametric Interaction Surface Plot: Delamination vs. Speed/Feed (6 mm Drill)

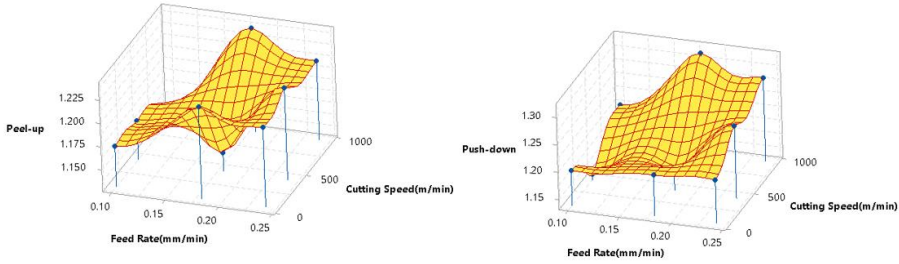

Figure 11. Parametric Interaction Surface Plot: Delamination vs. Speed/Feed (8 mm Drill)

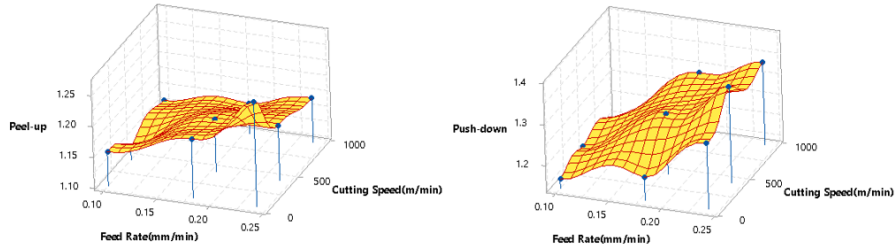

Figure 12. Parametric Interaction Surface Plot: Delamination vs. Speed/Feed (10 mm Drill)

The findings are consistent with previous studies that have supported the use of Taguchi optimization for composite machining [5, 19], yet extend its applicability to defence-grade GFRP. The established parameter hierarchy, prioritizing spindle speed to mitigate peel-up delamination and feed rate to suppress push-down delamination, offers practical guidelines for industrial applications. When drilling critical defense components such as spall liners or armored structures, employing a 10 mm diameter drill at a speed of 945 Rpm and a feed rate of 0.10 mm/rev may significantly improve hole integrity while complying with rigorous military standards [3, 4]. However, the inverse relationship between drill diameter and delamination mechanisms underscores the need for application-specific parameter calibration, particularly in multidirectional load-bearing systems where balanced mechanical performance is paramount.

Conclusions

The present study investigated the minimization of delamination defects in drilling GFRP composites, a material of strategic importance in defense applications such as spall liners and armored systems. By employing the Taguchi optimization method, this research identified critical parameter configurations to mitigate both peel-up and push-down delamination, thereby enhancing the structural integrity and operational reliability of machined components.

Significant results revealed distinct optimal parameter sets for each delamination mode. Peel-up delamination was minimized using a 10 mm drill diameter, a spindle speed of 945 Rpm, and a feed rate of 0.10 mm/rev, with speed emerging as the most influential factor. Conversely, push-down delamination was optimally suppressed with an 8 mm drill diameter, the same high speed, and low feed rate, where feed rate dominated as the primary contributing factor. The

divergent influence of drill diameter underscores the necessity of balancing torsional rigidity and exit-layer bending stresses, depending on specific defect mechanisms.

The Taguchi L9 orthogonal array demonstrated exceptional efficacy in reducing experimental iterations while maintaining analytical robustness, enabling the identification of parameter hierarchies through S/N ratio analysis.

From an industrial perspective, these findings provide actionable guidelines for machining defense-grade GFRP components. Adopting high speeds paired with low feed rates, alongside diameter-specific tool selection, can significantly enhance hole quality, reduce post-machining defects, and align with stringent military standards. However, the trade-offs between drill diameter and delamination mechanisms necessitate application-specific calibration, particularly in multidirectional load-bearing systems.

References

[1] Xu, J.; Geier, N.; Shen, J.; Krishnaraj, V.; & Samsudeensadham, S. A review on CFRP drilling: fundamental mechanisms, damage issues, and approaches toward high-quality drilling. Journal of Materials Research and Technology. 2023, *Volume 24*, Pages 9677-9707.

[2] Rampal, G.; Kumar, S.; Mavinkere Rangappa, S.; Siengchin, S.; & Zafar, S. A review of recent advancements in drilling of fiber-reinforced polymer composites. Composites Part C: Open Access. 2022, *Volume 9*,100312.

[3] Bircan, D. A.; Çetinkaya, İ.; & Erbil, Y. Delamination Investigation and Optimization in Drilling Operations of Glass Fiber Reinforced Plastics (GFRP) Composites. 7th International Antalya Scientific Research and Innovative Studies Congress. Antalya, May 11-13, 2024,

[4] Bircan, D. A.; Yildirimci, B.; & Erbil, Y. Minimizing delamination factor in glass fiber reinforced plastic composite drilling through Taguchi optimization. In Proceedings of the International Conference on Global Practice of Multidisciplinary Scientific Studies-VI. Lisbon, 2024; p 2111-2122.

[5] Aamir, M.; Tu, S.; Tolouei-Rad, M.; Giasin, K.; & Vafadar, A. Optimization and modeling of process parameters in multi-hole simultaneous drilling using Taguchi method and fuzzy logic approach. Materials 2020, *13*(3), 680.

[6] Voss, R.; Henerichs, M.; & Kuster, F. Comparison of conventional drilling and orbital drilling in machining carbon fiber reinforced plastics (CFRP). CIRP Annals 2016, *65*(1), 137-140.

[7] Fernández-Pérez, J.; Díaz-Álvarez, J.; Miguélez, M. H.; & Cantero, J. L. Combined analysis of wear mechanisms and delamination in CFRP drilling. Composite Structures 2021, *255*, 112774.

[8] Iqbal, A.; Zhao, G.; Zaini, J.; Jamil, M.; Nauman, M. M.; Khan, A. M.; Zhao, W.; He, N.; & Suhaimi, H. CFRP drilling under throttle and evaporative cryogenic cooling and micro-lubrication. Composite Structures 2021, *267*, 113916.

[9] Kannan, S.; & Pervaiz, S. Surface morphology of inclined CFRP holes when machined under cryogenic environment. Materials and Manufacturing Processes 2020, *35*(11), 1228–1239.

[10] Dharan, C. K. H.; & Won, M. S. Machining parameters for an intelligent machining system for composite laminates. International Journal of Machine Tools and Manufacture 2000, *40*(3), 415-426.

[11] Hocheng, H. & Dharan, C. K. H. Delamination during drilling in composite laminates. ASME Journal of Engineering for Industry 1990, *112*, 236-239.

[12] Gaitonde, V. N.; Karnik, S. R.; Rubio, J. C.; Correia, A. E.; Abrao, A. M.; & Davim, J. P. A study aimed at minimizing delamination during drilling of CFRP composites. Journal of Composite Materials 2011, *45*(22), 2359-2368.

[13] Lin, S. C.; & Chen, I. K. Drilling of carbon fiber-reinforced composite material at high speed. Wear 1996, *194*, 156–162.

[14] Khashaba, U. A.; El-Sonbaty, I. A.; Selmy, A. I.; & Megahed, A. Machinability analysis in drilling woven GFR/epoxy composites: Part I Effect of machining parameters. Composites Part A: Applied Science and Manufacturing 2010, *41*, 391-400.

[15] Khashaba, U. A. Drilling of polymer matrix composites: a review. Journal of Composite Materials 2013, *47*, 1817–1832.

[16] El-Sonbaty, I.; Khashaba, U. A.; & Machaly, T. Factors affecting the machinability of GFR/epoxy composites. Composite Structures 2004, *63*, 329–338.

[17] Kilickap, E. Optimization of cutting parameters on delamination based on Taguchi method during drilling of GFRP composite. Expert Systems with Applications 2010, *37*, 6116-6122.

[18] Vinayagamoorthy, R.; Manoj, I. V.; Narendra Kumar, G.; & others. A central composite design based fuzzy logic for optimization of drilling parameters on natural fiber reinforced composite. Journal of Mechanical Science and Technology 2018, *32*, 2011–2020.

[19] Mohan Kumar, A.; Parameshwaran, R.; Rajasekar, R.; Harissh Ragavendra, V. C.; & Praveenraj, N. Effect of thrust force, torque, and induced temperature on Kevlar reinforced composites during drilling process. Materials Today: Proceedings 2021, *45*(2), 522-528.

[20] Mohan Kumar, A.; Rajasekar, R.; Manoj Kumar, P.; Parameshwaran, R.; Karthick Alagar.; & Muhibbullah, M. Comparative analysis of drilling behaviour of synthetic and natural fiber-based composites. Advances in Materials Science and Engineering 2021, 9019334.

[21] Davim, J. P.; Rubio, J. C.; & Abrao, A. M. A novel approach based on digital image analysis to evaluate the delamination factor after drilling composite laminates. Composites Science and Technology 2007, *67*(9), 1939-1945.

[22] Davim, J. P.; Reis, P.; & Antonio, C. C. Experimental study of drilling glass fiber reinforced plastics (GFRP) manufactured by hand lay-up. Composites Science and Technology 2004, *64* (2), 289-297.

[23] Geng, D.; Liu, Y.; Shao, Z.; Lu, Z.; Cai, J.; Li, X.; Jiang, X.; & Zhang, D. Delamination formation, evaluation and suppression during drilling of composite laminates: A review. Composite Structures 2019, *216*, 168-186.

[24] Mohan, N. S.; Kulkarni, S. M.; & Ramachandra, A. Delamination analysis in drilling process of glass fiber reinforced plastic (GFRP) composite materials. Journal of Materials Processing Technology 2007, *186*, 265-271.

[25] Karataş, M. A.; & Gökkaya, H. A review on machinability of carbon fiber reinforced polymer (CFRP) and glass fiber reinforced polymer (GFRP) composite materials. Defence Technology 2018, *14*, 318-326.

Chapter 5

An Overview Of The Electropolishing Method

Furkan CENGİZ[1]

Abstract

This paper reviews the fundamental aspects and recent advances in the electropolishing process. Theoretical approaches to the material removal mechanisms are introduced, highlighting the complex interplay of electrical and chemical reactions. Electropolishing is influenced by multiple factors, including current density, temperature, electrolyte composition, and workpiece motion. However, no single theory fully explains the process, particularly in light of recent developments that have further complicated the understanding of material removal. With the growing application of laser machining, additive manufacturing, and biomedical device fabrication, electropolishing has become increasingly important as a post-processing technique to meet industrial surface quality requirements. The process relies on electrochemical reactions between anodic and cathodic electrodes under DC/AC power supply, and its effectiveness varies depending on material type, electrolyte, and operating conditions. Beyond surface finishing, electropolishing is also employed for passivation, deburring, and micro-pattern formation. Finally, this review outlines future perspectives in electropolishing research to support further technological development.

Keywords: Electropolishing, Finishing, Post-process, Roughness

[1] Kilis 7 Aralık Üniversitesi Sağlık Hizmetleri Meslek Yüksekokulu Optisyenlik Programı, furkan.cengiz@kilis.edu.tr, ORCID: 0000-0003-0011-5476

1. Introduction

Electropolishing (EP), sometimes referred to as electrochemical polishing, anodic polishing, or electrolytic polishing, is a finishing technique that uses an anodic dissolving process to remove material from a metal or alloy by removing it off the workpiece surface ion by ion. Faraday made the initial discovery of the electrochemical process principle in the nineteenth century (McGeough, 1974). The well-known electrodeposition and dissolving techniques were both built on the principles of electrolysis, which were introduced in 1833. Because EP is a non-contact, damage-free process, it differs significantly from conventional mechanical finishing methods including cutting, grinding, milling, and buffing as the ultimate finish, according to the principles of electrolysis (Faraday's Law). The removal of roughness, the lack of grain-boundary and crystallographic harm, and the formation of smooth, brilliant surfaces are the hallmarks of the polishing phenomena. Usually, the workpiece acts as the anode and is submerged in a temperature-controlled electrolyte solution. It is connected to the DC/AC power supply's positive polarity, while the cathode is connected to its negative polarity. From the anode, where surface metal dissolves in the electrolyte, current flows to the cathode. A reduction reaction takes place at the cathode surface, typically producing hydrogen. The essential electrolyte is typically a highly viscous concentrated acid medium, like sulfuric acid, phosphoric acid, and their mixes, or in solutions of acetic acid and perchloric acid (Landolt, 1987). The metal finishing industry has made extensive use of EP thanks to its ease of use and capacity to polish intricate structures. Polishing stainless steel cutlery and preparing samples for transmission electron microscopy are just two of the many uses for the EP process. This technique is also helpful for biomedical and semiconductor applications, including superconductive niobium cavities, pharmaceutical, and coronary stents semiconductor installations, and implants for the cardiovascular and orthopaedic systems (Rokicki and Hryniewicz, 2012).

Additionally, the medicinal, aerospace, and defense industries have benefited greatly from additive manufacturing in recent years but its broad range of applications is severely constrained by the poor surface quality of metals produced using this process (Z. Chaghazardi and R. Wüthrich, 2022). In order to satisfy surface quality standards, post polishing techniques like sandblasting, electropolishing, plasma spraying, etching, and laser polishing are frequently used for additive manufacturing components (Bhaduri et al., 2017). Due to its artlesness and capacity to polish complex structures, EP is a potential method for polishing additive manufacturing components when compared to other polishing methods. The rapid advancement of laser machining

necessitates the employment of a post-treatment approach to improve the resulting poor surface smoothness, and EP is a potential method to apply in this process, particularly when polishing complicated structures. As a result, conducting an evaluation of the literature in EP is urgently required.

2.EP Process

The most principle EP system is a conventional electrochemical cell with an anode and a cathode in an electrolyte solution, as displayed in Fig. 1. The cathode electrode of a power supply is the tool electrode, and the anode electrode is the workpiece to be polished, which is connected to the positive terminal. The electrolyte experiences an electrolytical current when the power supply provides a voltage between the electrodes. An electrolysis technique is used to transfer electrons from the anode's surface to the cathode's surface. It oxidizes and loses electrons for the anode. The process of material removal is brought about by the metal atoms on the workpiece surface transferring to metal ions and then dissolving in the electrolyte solution. In terms of the cathode, it is decreased and gains electrons. The reduction reaction causes hydrogen to be produced from the cathodic surface in a typical EP process.

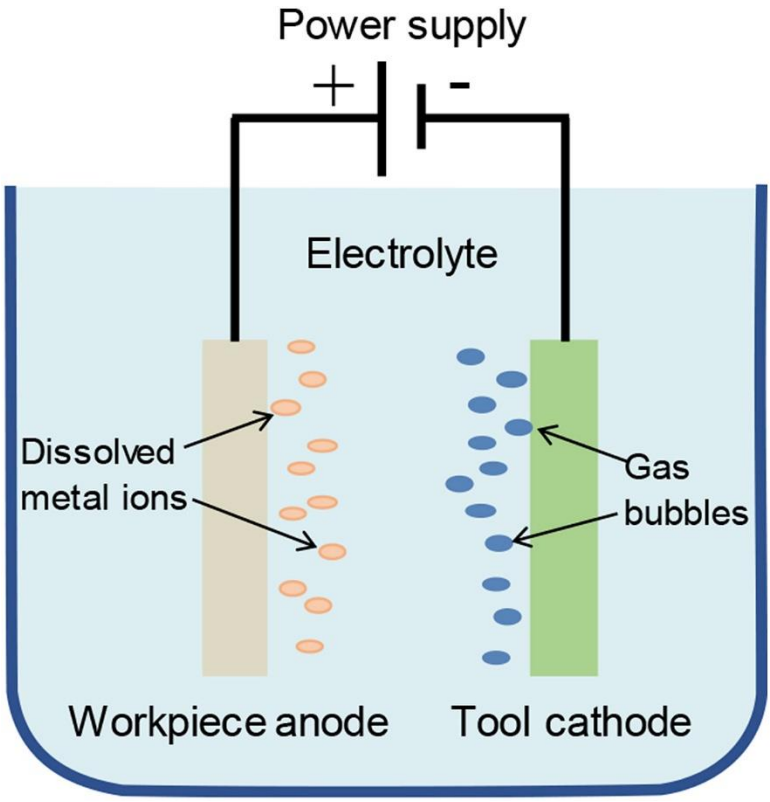

Fig 1. EP Method

The workpiece material, electrolyte composition, EP duration, temperature, and other process variables all affect the material removal volume; some of these will be covered in Section 3. The two process factors that are most commonly considered to attain surface roughness control are the current density and EP time. (Hahn & Marder, 1988). Faraday's two laws of electrolysis are followed in the material dissolving process in the EP process:

1. The electricity is proportional to the volume of material deposited or dissolved.

$$m \propto Q$$

Q is the amount of charge transferred, and m is the amount of material dissolved or deposited.

2. Equal amounts of energy dissolve or deposit material in proportion to its ch emical equivalent weight.

Faraday's law states that 1 g of workpiece material requires nF/M coulombs of electricity. n is the atomic valency, F is the Faraday constant, and M is the atomic weight. The dissolved workpiece part m [g] reasoned by current I [A] throughout EP time t [s] can then be expressed using Eq. (1) (Lee & Shin, 2011a)

$$m = \frac{MIt}{nF}[\mathrm{g}] \quad (1)$$

As a result, the current I and EP time t can be tuned to achieve the desired material removal mass. When the density of the workpiece part is ρ, Eq. (2) can be used to compute the theoretical material removal volume.

$$V = \frac{MIt}{nF\rho}[\mathrm{mm}^3] \quad (2)$$

3. Primary Process Factors

Surface smoothening in the EP process is typically divided into two steps: anodic leveling (macro-smoothening) and brightness (micro-smoothening) (Jacquet, 1956). The anodic levelling method eliminates surface roughness heights above 1 μm caused by potential distribution differences between protrusion and valley positions. A locally increased rate of material disintegration results from the over current density at the prominent site. Surface roughness heights below 1 μm are eliminated in the anodic brightening process, which is the outcome of suppressing the impact of surface defects and crystallographic orientation on the electrochemical dissolving process. By adjusting the process variables, the anodic leveling effect can be achieved without the brightness effect, and vice versa (Sautebin et al., 1980). There is no standard parameter set for different workpiece materials because EP is a complicated process with many influencing factors. Electrolyte temperature and composition, polishing time, beginning surface roughness, and other variables all affect the EP process.

3.1.Temperature

The electrolyte temperature in an EP process is typically directly related to the process's mass transport because a lower temperature slows the migration of soluble metal ions out of the electrode surface and donor ions into the surfa ce. Additionally, the low temperature decreases the solubility of metal ions in solution, which has the effect of lowering the current density (Zhao et al., 2011). Because of the low viscosity and constant availability of fresh electrolyte, the EP effect intensifies as the electrolyte temperature rises. Selective dissolution

between the protrusion and valley positions is encouraged by this mechanism. It is believed that as the electrolyte temperature rises, the viscous layer on a workpiece surface thins because of the increased diffusion rate and decreased viscosity of the electrolyte. Fig. 2 displays the current density-voltage curve in the EP of porous austenitic stainless steel (PASS) in phosphoric-sulfuric mixed acid at 80, 70, and 60°C (Chen et al., 2005). As the temperature rose, the current density also rose, and because of the improved surface roughness, the greater current density contributes to a better EP effect. Eliaz and Nissan (Eliaz and Nissan, 2007) obtained comparable outcomes in the EP method of 316LVM stainless steel. Ma et al. discovered that electropolishing aluminum samples with a volume ratio of 1:8 perchloric acid to ethanol at a high temperature of 40 °C had a detrimental impact on the EP process. The study found that as temperature rises from 10°C to 30°C, the limiting current plateau zone expands. At 40°C, there is no limiting plateau zone, resulting in a continuous increment in current density. They concluded that high temperatures should be avoided because they cause etching pits on the aluminium gap (Ma et al., 2009).

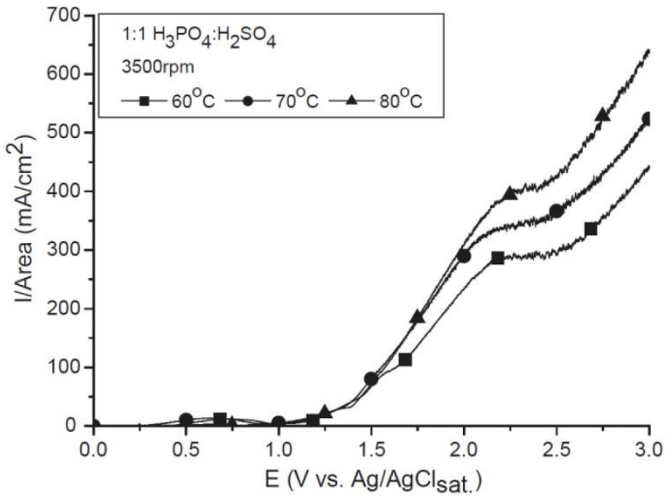

Fig 2. At temperatures of 60, 70, and 80°, the PASS current density-voltage curve

3.2.Electrolyte composition

Carrying current, heat, and reaction products is an electrolyte's primary role. Organic, inorganic, or organic/inorganic combinations can be employed as electrolytes in an EP process. The most well-known electrolytes are used to polish stainless steel (Han and Fang, 2019). They typically contain 50% to 75% by weight acids, 5% to 15% by weight deionized water, and one or more

inhibitors. A 1:1 or 2:1 mixture of sulfuric and phosphoric acids typically makes up the electrolyte's acid component. Nevertheless, different metals could require different kinds of electrolyte, and the eventual EP effect is directly influenced by the electrolyte's characteristics (Landolt, 1987). The volume ratio of acid is crucial in the EP process of different materials. In copper EP, the average surface roughness (Ra) decreased with increasing acid concentration, and a higher acid concentration resulted in a greater polishing effect (Chang and Wang, 2004). Fig. 3 depicts the anodic polarization behavior of 30Nb-Ti alloys electropolished using methanolic sulfuric acid as the electrolyte at temperatures of 253 K for 1 M, 3 M, and 5 M sulfuric acid solutions (Neelakantan et al., 2011). It turned out that when the concentration of sulfuric acid increased, the limiting current density's amplitude reduced. Furthermore, Chen et al. (Chen et al., 2005) and Fushimi et al. (Fushimi, Stratmann, & Hassel, 2006) reported that growing the volume rate of sulfuric acid in the mixed acid including phosphoric-sulfuric mixed acid reduced the current density. The decrease in current density as sulfuric acid increases indicates that the SO_4^{2-} ion is not essential for mass transport in the limiting current plateau zone. It is plausible that the movement of metal ions, as opposed to acceptor ions, which adhere to the salt film mechanism, limits the EP in these systems. Declining metal ion solubility in the electrolyte is another reason for the widened plateau zone and decreased current density brought on by an increase in acid content (Acquesta and Monetta, 2021).

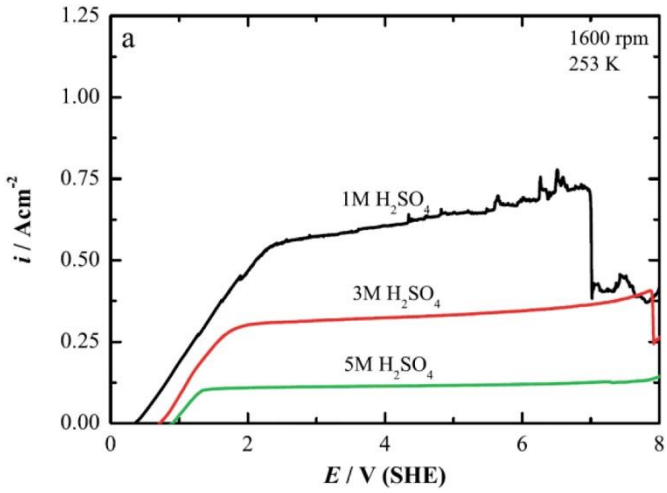

Fig 3. NbTi anodic polarization curves at 253 K with different methanolic sulfuric acid concentrations. The voltage was swept down from 8.207 V to 0.207 V at a scan rate of 10 mV/s. (Neelakantan et al., 2011)

3.3. Electropolish time

Faraday's equation shows that EP time is directly correlated with the amount of material eliminated. More time will guarantee greater metallic disintegration and a higher polishing rate when ideal electrical conductivity and voltage range are present. Fig. 4a illustrates that, under favorable conditions, the material removal rate increases up to a certain point. In general, it follows a sigmoidal relationship (Miao, 2006). The impact of temperature and duration on the electropolishing of Co-Cr alloys for surface characterisation and biocompatibility was examined by Aihara (Aihara, 2009). The bath temperature was raised from 3 to 60 minutes and lowered from 35 to 0 °C (Fig. 4b). Increasing time produced surfaces that were hydrophilic and smooth. According to controlled EP effects, Cr-Co samples that were biocompatible and non-toxic were produced by lowering the temperature and lengthening the duration.

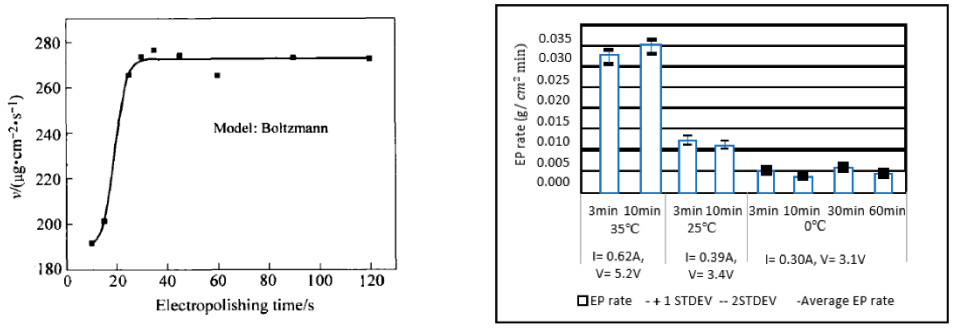

(a) (b)

Fig 4. (a) The sigmoidal law governs the electropolishing time effect. (Sun et al., 2021) (b) EP rate of Co-Cr samples in phosphoric acid at temperatures of 35 °C, 25 °C, and 0 °C

Núñez electropolished stainless steel in different ratios of phosphoric, sulfuric, and chromic acids to examine the importance of current density and time. By increasing the treatment period to 25 minutes and the current density to 48 A/dm2, surface finish (Ra) was significantly improved, reaching maximum polishing ranges of 80–90%, as shown in Fig. 4 (Núñez, García-Plaza, Hernando, & Trujillo, 2013).

3.4. Roughness of the initial surface

It is crucial to note that the final electropolished surface quality is influenced by the workpiece's initial surface roughness, and that the EP process has a

limited capacity to ameliorate surface roughness. When employing an acid electrolyte, the electropolished nitinol surfaces in Ra with varying initial surface roughness of 1 μm and 2 μm are displayed in Fig. 4 (Lee & Shin, 2011b). The workpiece surface roughness improved quickly up to 50 s from its starting roughness of Ra = 1 μm to less than Ra = 0.5 μm, but after that time, there was no discernible improvement. After 300 seconds, the surface roughness increased significantly to Ra = 0.98 μm from its original roughness of Ra = 2. Additionally, there was no discernible change in surface roughness after 300 seconds. Because EP has a restriction on polishing quality, the workpiece's beginning surface should be carefully evaluated for a quick and efficient EP operation.

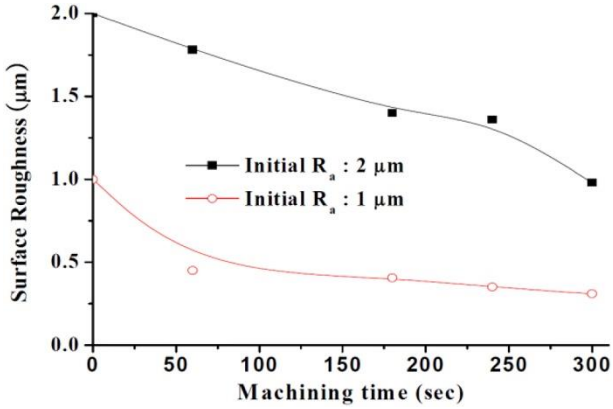

Fig 5. *The initial anode surface roughness features as a function of machining time (Lee & Shin, 2011b)*

4. Conclusion

When it comes to applications that demand a high degree of precision, cleanliness, and corrosion resistance, electropolishing (EP) has shown to be a very successful surface finishing technology for enhancing the surface quality of metallic components. As demonstrated throughout this chapter, the EP process relies on a complex interplay of electrochemical principles, including current density, temperature, electrolyte composition, treatment time, and initial surface conditions. These parameters collectively govern the efficiency of material removal, surface leveling, and micro-brightening effects.

Recent advances in additive manufacturing and laser-based fabrication techniques have increased the demand for post-processing solutions that can address the inherent surface roughness of as-built components. In this regard, EP stands out as a particularly promising technique due to its non-mechanical nature, ability to polish complex geometries, and compatibility with a wide

range of metals and alloys. Moreover, the continued exploration of electrolyte formulations and process optimizations holds great potential for further expanding the industrial applicability of EP, particularly in biomedical, aerospace, and microelectronics sectors.

Despite its advantages, challenges remain in standardizing EP parameters for diverse material systems and geometries. Therefore, future research should focus on developing predictive models for surface evolution during EP, integrating real-time process monitoring, and tailoring electrolyte chemistries to specific manufacturing methods. Overall, EP remains a vital and evolving surface engineering process with substantial significance for next-generation manufacturing technologies.

REFERENCES

Acquesta, A., & Monetta, T. (2021, December 1). The Electropolishing of Additively Manufactured Parts in Titanium: State of the Art. *Advanced Engineering Materials*, Vol. 23. John Wiley and Sons Inc. https://doi.org/10.1002/adem.202100545

Aihara, H. (2009). *SURFACE AND BIOCOMPATIBILITY STUDY OF ELECTROPOLISHED Co-Cr Alloy L605*.

Bhaduri, D., Penchev, P., Batal, A., Dimov, S., Soo, S. L., Sten, S., … Dong, H. (2017). Laser polishing of 3D printed mesoscale components. *Applied Surface Science*, *405*, 29–46. https://doi.org/https://doi.org/10.1016/j.apsusc.2017.01.211

Chang, S.-C., & Wang, Y.-L. (2004). Effects of applied voltages on planarization efficiency of Cu electropolishing. *Journal of Vacuum Science & Technology B: Microelectronics and Nanometer Structures Processing, Measurement, and Phenomena*, *22*(6), 2754–2757. https://doi.org/10.1116/1.1819898

Chen, S. C., Tu, G. C., & Huang, C. A. (2005). The electrochemical polishing behavior of porous austenitic stainless steel (AISI 316L) in phosphoric-sulfuric mixed acids. *Surface and Coatings Technology*, *200*(7), 2065–2071. https://doi.org/10.1016/j.surfcoat.2005.06.008

Eliaz, N., & Nissan, O. (2007). Innovative processes for electropolishing of medical devices made of stainless steels. *Journal of Biomedical Materials Research - Part A*, *83*(2), 546–557. https://doi.org/10.1002/jbm.a.31429

Fushimi, K., Stratmann, M., & Hassel, A. W. (2006). Electropolishing of NiTi shape memory alloys in methanolic H2SO4. *Electrochimica Acta*, *52*(3), 1290–1295. https://doi.org/10.1016/j.electacta.2006.07.030

Hahn, T. S., & Marder, A. R. (1988). Effect of electropolishing variables on the current density-voltage relationship. *Metallography*, *21*(4), 365–375. https://doi.org/https://doi.org/10.1016/0026-0800(88)90001-8

Han, W., & Fang, F. (2019). Electropolishing of 316L Stainless Steel Using Sulfuric Acid-Free Electrolyte. *Journal of Manufacturing Science and Engineering*, *141*(10). https://doi.org/10.1115/1.4044518

Jacquet, Pierre A. (1956). ELECTROLYTIC AND CHEMICAL POLISHING. *Metallurgical Reviews*, *1*(1), 157–238. https://doi.org/10.1179/mtlr.1956.1.1.157

Landolt, D. (1987). Fundamental aspects of electropolishing. *Electrochimica Acta*, *32*(1), 1–11. https://doi.org/https://doi.org/10.1016/0013-4686(87)87001-9

Lee, E. S., & Shin, T. H. (2011a). An evaluation of the machinability of nitinol shape memory alloy by electrochemical polishing. *Journal of Mechanical Science and Technology*, *25*(4), 963–969. https://doi.org/10.1007/s12206-011-0209-2

Lee, E. S., & Shin, T. H. (2011b). An evaluation of the machinability of nitinol shape memory alloy by electrochemical polishing. *Journal of Mechanical Science and Technology*, *25*(4), 963–969. https://doi.org/10.1007/s12206-011-0209-2

Ma, D., Li, S., & Liang, C. (2009). Electropolishing of high-purity aluminium in perchloric acid and ethanol solutions. *Corrosion Science*, *51*(4), 713–718. https://doi.org/10.1016/j.corsci.2009.01.030

McGeough, J. A. (1974). *Principles of electrochemical machining*. Chapman and Hall and Halsted Press Division, Wiley. Retrieved from https://cir.nii.ac.jp/crid/1130000797072855040.bib?lang=ja

Miao, W. (2006). Electropolishing parameters of NiTi alloy. *Transactions of Nonferrous Metals Society of China* , *16*, 130–132. Retrieved from http://www.nitinol.de/processes/electropolishing.htm.

Neelakantan, L., Pareek, A., & Hassel, A. W. (2011). Electro-dissolution of 30Nb-Ti alloys in methanolic sulfuric acid - Optimal conditions for electropolishing. *Electrochimica Acta*, *56*(19), 6678–6682. https://doi.org/10.1016/j.electacta.2011.05.049

Núñez, P. J., García-Plaza, E., Hernando, M., & Trujillo, R. (2013). Characterization of Surface Finish of Electropolished Stainless Steel AISI 316L with Varying Electrolyte Concentrations. *Procedia Engineering*, *63*, 771–778. https://doi.org/https://doi.org/10.1016/j.proeng.2013.08.255

Rokicki, R., & and Hryniewicz, T. (2012). Enhanced oxidation–dissolution theory of electropolishing. *Transactions of the IMF*, *90*(4), 188–196. https://doi.org/10.1179/0020296712Z.00000000031

Sautebin, R., Froidevaux, H., & Landolt, D. (1980). Theoretical and Experimental Modeling of Surface Leveling in ECM under Primary Current Distribution Conditions. *Journal of The Electrochemical Society*, *127*(5), 1096. https://doi.org/10.1149/1.2129823

Sun, X., Wei, X., Li, Z., Lou, D., Wang, Y., & Liu, H. (2021). Study on Improving the Performance of Nitinol Cardiovascular Stent by "Fiber Laser—Electropolishing." In J. Xu & K. M. Pandey (Eds.), *Mechanical Engineering and Materials* (pp. 31–40). Cham: Springer International Publishing.

Z. Chaghazardi, & R. Wüthrich. (2022). Review—Electropolishing of Additive Manufactured Metal Parts. *Journal of Electrochemical Society*, *169*(4).

Zhao, X., Corcoran, S. G., & Kelley, M. J. (2011). Sulfuric acid-methanol electrolytes as an alternative to sulfuric-hydrofluoric acid mixtures for electropolishing of niobium. *Journal of Applied Electrochemistry*, *41*(6), 633–643. https://doi.org/10.1007/s10800-011-0276-1

Chapter 6

Biomedical Applications of Electromagnetic Waves

Taha Fatih ATEŞ[1], Ali Osman ÖZKAN[2]

ABSTRACT

Electromagnetic waves are playing an increasingly vital role in biomedical engineering, particularly in diagnostic and therapeutic applications. Generated by the oscillatory motion of electrically charged particles, these waves enable non-invasive, rapid, and reliable analyses through their capacity to directly measure the dielectric properties of biological tissues. This distinctive capability has rendered electromagnetic waves indispensable in critical domains such as cancer diagnosis, tissue monitoring, and biosensor applications. The distribution of electromagnetic fields in biological media, as described by Maxwell's equations and influenced by the frequency-dependent dielectric properties of tissues, facilitates highly accurate modeling and measurement.

Microwave imaging offers a non-ionizing and cost-effective alternative for tumor detection, while microwave biosensors provide highly sensitive measurements with minimal sample volumes, making them valuable for both laboratory research and clinical practice. The integration of metamaterial-based sensors and microfluidic systems further enhances their sensitivity, supporting successful applications in biomarker analysis, glucose monitoring, and cancer cell detection. Similarly, microwave ablation and electromagnetic hyperthermia target specific tissue regions, providing minimally invasive and safe therapeutic options that stand as strong alternatives to conventional surgical approaches.

Looking forward, the incorporation of artificial intelligence and machine learning algorithms enables the automated processing of biosensor data and highly accurate classification of biological conditions. Deep learning models, by extracting meaningful insights from complex electromagnetic data, lay the foundation for advanced clinical decision support systems. Furthermore, the development of IoT-enabled portable and wearable sensors opens new possibilities for remote patient monitoring and personalized healthcare management.

[1]Lecturer; KTO Karatay University Department of Electronics and Automation, Vocational School of Trade and Industry, taha.fatih.ates@karatay.edu.tr, ORCID: 0000-0003-2163-681X

[2]Asst. Prof. Dr; Necmettin Erbakan University Electrical and Electronics Engineering, alozkan@erbakan.edu.tr, ORCID: 0000-0002-2226-9786

Electromagnetic wave–based biomedical technologies are advancing rapidly through interdisciplinary collaboration, paving the way for transformative developments in healthcare. Systems that combine metamaterial-assisted sensors, AI-driven algorithms, and IoT integration are expected to deliver smarter, faster, and more patient-centered solutions in both diagnostics and therapeutics, marking the dawn of a new era in modern medicine.

Keywords: Electromagnetic, Biomedical, Sensor, Microwave

1. Introduction

1.1. Electromagnetic Waves

Electromagnetic waves are generated by the oscillatory motion of electrically charged particles. A vibrating charge produces a time-varying electric field, which, according to Maxwell's equations, induces a perpendicular magnetic field. Conversely, a time-varying magnetic field produces an electric field. Together, these oscillating electric and magnetic field components, oriented orthogonally, propagate in a direction perpendicular to both, forming an electromagnetic wave. Accordingly, electromagnetic waves are classified as transverse waves, with the electric field, magnetic field, and propagation direction mutually orthogonal. Electromagnetic waves are employed across a wide range of applications, including radios, microwave ovens, mobile phones, radar systems, and biomedical technologies (Čáp et al., 2021; Dash & Khuntia, 2011; Someda, 2017).

1.2. Biosensors

A biosensor is a device that detects a biological response and converts it into a measurable electrical signal. Advances in biosensor technologies have significantly contributed to the field of medicine. These devices are widely used in applications such as the early detection of various cancers, monitoring vital parameters like heart rate, analyzing biomolecules such as proteins, and measuring blood glucose levels. Biological materials are regarded as dielectric substances that exhibit specific conductivities when exposed to an electric field, with their dielectric properties playing a fundamental role in the sensing process (Johnson & Guy, 1972; Mehrotra et al., 2019; Turner et al., 1987; Yang, 2011).

1.3. The Role of Electromagnetic Waves in the Biomedical Field

Electromagnetic waves have become powerful tools in biomedical engineering for both diagnostic and therapeutic purposes. While conventional biomedical methods are often invasive or time-consuming, electromagnetic waves allow for direct measurement of tissue and cellular dielectric properties, enabling rapid and non-invasive diagnostics. Technologies operating in the microwave, radio frequency (RF), and terahertz ranges have become particularly prominent, especially in cancer detection, tissue monitoring, and biosensor applications. These techniques analyze the frequency-dependent electromagnetic responses and S-parameters of biological tissues to provide valuable diagnostic information (Farmer et al., 2012; Harsanyi, 2000).

Compared to other biological detection methods, electromagnetic-based technologies offer distinct advantages, including high sensitivity, rapid response

time, and contactless measurement capabilities. Their operation is based on the interaction of electromagnetic fields with biological structures. When living organisms are exposed to external electromagnetic fields, observable changes occur in the dielectric properties of tissues. Measuring these variations enables the extraction of meaningful biological data, further strengthening the potential of electromagnetic-based sensing. In recent years, the use of electromagnetic waves has expanded beyond diagnostics, becoming increasingly common in therapeutic applications as well (Chen et al., 2020; Clements & Comeau, 2019; Huang et al., 2021; Hwang et al., 2020).

2. Theoretical Foundations

2.1. Maxwell's Equations in Biomedical Media

The behavior of electromagnetic waves is governed by Maxwell's equations, which describe the propagation of electric and magnetic fields in both space and time. In biological media, these waves exhibit similar behavior; however, due to the lossy nature of tissues, they undergo both reflection and attenuation. In such cases, the wave equations are expressed through a complex dielectric constant, where energy losses are associated with the electrical conductivity and dielectric losses of the tissues (Frankel, 1974; Huray, 2010; Sandeep et al., 2024).

In biomedical applications, the distribution of electromagnetic fields within tissues depends on boundary conditions and the intrinsic properties of the tissues. Soft tissues typically exhibit high dielectric constants, whereas bone tissues display lower dielectric values (Gabriel & Peyman, 2018). Early research on the dielectric properties of human tissues at microwave frequencies primarily focused on the therapeutic potential of microwaves (O'Loughlin et al., 2018). The variations among different tissue types result in electromagnetic waves being absorbed to different depths. Consequently, accurate modeling of electromagnetic wave propagation in biological media is essential for the design of reliable diagnostic and therapeutic systems.

2.2. Dielectric Properties of Biological Tissues

The dielectric properties of biological tissues are among the most critical parameters governing their interaction with electromagnetic waves. Both the dielectric constant and the loss tangent vary with frequency, meaning that a tissue exhibits distinct dielectric behaviors across different frequencies. Moreover, tissues of different types can demonstrate markedly different dielectric properties even at the same frequency.

Identifying the optimal frequency for the tissue of interest is therefore crucial to achieving effective detection. Dielectric properties also play a key role in

clinical diagnostics. For instance, cells with higher water content generally exhibit higher dielectric constants. Such distinctions form the basis for microwave-based imaging and biosensor technologies. Because biosensors rely on dielectric properties for detection, precise characterization of these properties is vital to ensure high measurement accuracy. Thus, biosensor designs must prioritize sensitivity, which depends heavily on the accurate determination of dielectric parameters.

When designing these systems, it is essential to account for factors that influence changes in dielectric properties, including water content, temperature variations, and pathological conditions.

3. Diagnostic Applications

Electromagnetic waves are widely employed in biomedical science for non-invasive imaging. Diagnostic research has demonstrated the use of microwave imaging, terahertz spectroscopy, nuclear magnetic resonance (NMR), ultra-wideband (UWB) radar, and biosensor technologies for detecting tumors, characterizing tissues, and monitoring cardiac and respiratory functions. The operational frequencies extend from radio and microwave bands to very low frequencies and even the terahertz range.

The primary advantages reported in the literature include non-ionizing radiation, enhanced image contrast, portability, and high sensitivity, whereas limitations involve restricted tissue penetration, resolution constraints, and technical complexity (Nikolova, 2014). Documented diagnostic imaging techniques include electromagnetic imaging ("Handbook of Biological Effects of Electromagnetic Fields," 1996; Rozzell & Lin, 1987a), radiometry (Nikolova, 2014), nuclear magnetic resonance (Rozzell & Lin, 1987b), infrared spectral imaging (Staderini, 2002), terahertz imaging (Amini et al., 2021), microwave biosensors (Choudhury & El-Nasr, 2015) and active microwave imaging (Chandra et al., 2015).

3.1. Microwave Imaging

Microwave imaging detects dielectric contrasts within biological tissues by transmitting electromagnetic waves through them. This technique has gained particular significance in breast cancer diagnostics due to its non-ionizing nature and relatively low cost. Studies report that microwave imaging systems can successfully distinguish malignant from benign tumors with high accuracy (Cheng & Fu, 2018; Mirbeik-Sabzevari & Tavassolian, 2019). Nevertheless, the field of microwave tissue imaging continues to offer many unexplored opportunities (O'Loughlin et al., 2018).

As microwave signals penetrate tissue, they undergo scattering processes, altering their velocity, propagation path, amplitude, phase, and polarization. These scattering effects form the basis of active imaging. In contrast, passive imaging systems rely on radiometry principles. Radiometers, typically narrowband receivers, generate images based on the natural microwave radiation emitted from tissues a few centimeters beneath the skin.

At a given temperature, thermal noise peaks in the infrared spectrum, whereas radiation intensity in the microwave range is comparatively weaker. Consequently, microwave radiometry has emerged as a low-cost, portable, and non-invasive diagnostic method, particularly for temperature monitoring, functional imaging, and inflammation detection in clinical settings (Groumpas et al., 2022).

Microwave radiometric cancer detection relies on the principle that malignant tumors and surrounding normal tissues exhibit measurable temperature contrasts (Nikolova, 2014). Aggressive tumors, which typically have higher growth rates, produce more metabolic heat and thus display elevated temperatures. In patients, the natural temperature difference between malignant and normal tissues generally ranges from 1°C to 3°C (Carr, 1989). Malignant lesions, which tend to exhibit higher conductivity than normal tissues, are more prone to heating (Carr et al., 1981; Nikolova, 2014).

Radar-based microwave imaging represents another diagnostic approach. Such systems benefit from the increased conductivity of tissue at higher frequencies, ensuring sufficient signal penetration, but require UWB signals to achieve the necessary resolution (AlSawaftah et al., 2022; Fear, 2005).

Ongoing advancements in microwave imaging aim to determine optimal frequency ranges and achieve clinically acceptable resolutions for various tissues (AlSawaftah et al., 2022; Chandra et al., 2015). Emerging methods, including novel algorithms and metamaterial-based focusing techniques, have the potential to enhance imaging sensitivity. Additionally, machine learning–driven data analysis has become a promising avenue for improving diagnostic accuracy from measured data.

3.2. Biosensors

Biosensors are devices designed to directly detect the electromagnetic properties of biological samples—including cell cultures, protein solutions, DNA samples, and biological fluids—using high-frequency measurement technologies. These sensors allow precise determination of frequency-dependent parameters such as dielectric constant, loss tangent, and conductivity.

Microwave frequencies are particularly well-suited for such applications due to their sensitivity to water content, as water exhibits a high dielectric constant. This property makes microwave biosensors especially effective for distinguishing between healthy and cancerous cells, identifying protein structural changes, monitoring drug responses, and measuring blood glucose levels (Kim et al., 2022; Patel et al., 2024; Shamim et al., 2024).

Most microwave biosensor designs employ structures such as microstrip lines, ring resonators, or cavity resonators. Biological samples are placed in regions where the electromagnetic field is most concentrated, maximizing sensitivity while minimizing sample volume. Sensor outputs are generally obtained via S-parameters, with changes in dielectric properties leading to resonance frequency shifts and amplitude attenuations. These variations are analyzed to derive insights about the biological medium. Unlike optical sensors, microwave sensors do not require transparency, making them suitable for measurements even in turbid biological fluids (Kumar Sharma et al., 2023; Tlili et al., 2024).

Metamaterial-based biosensors further enhance sensitivity. Structures such as Split Ring Resonators (SRRs) and Complementary Split Ring Resonators (CSRRs) provide fine control over resonance characteristics, enabling the detection of subtle biological variations (Khodaie & Heidarzadeh, 2024). Research demonstrates that CSRR-based sensors can effectively monitor parameters such as glucose concentrations, cancer cell densities, and protein conformational changes at very low levels.

A high quality factor (Q-factor) is another essential parameter that improves sensitivity. Resonators with high Q-factors respond more precisely to minor frequency changes, which is particularly critical in low-concentration biological analyses. Additionally, integrating microfluidic systems into modern sensor designs reduces sample volumes to microliter scales while improving measurement repeatability (Kulkarni et al., 2022; Xie et al., 2023).

For example, CSRR-based sensors have successfully differentiated the dielectric spectra of samples with varying glucose levels. Likewise, studies on human breast cancer cell lines have reported resonance frequency shifts linked to cell proliferation. These findings highlight the potential for microwave biosensors to extend beyond laboratory research into clinical applications. Furthermore, their portability and integration with embedded systems pave the way for future development of wearable biosensor platforms (Geetharamani & Aathmanesan, 2020; Reimer & Pistorius, 2023; W. Wu et al., 2024).

4. Therapeutic Applications

4.1. Microwave Ablation

Microwave ablation involves delivering high-frequency electromagnetic energy to tissues, producing localized heating that destroys targeted pathological tissue. This technique is particularly employed in the treatment of liver, lung, and kidney tumors. Its ability to penetrate tissues deeply, create extensive ablation zones, and shorten procedure times offers significant clinical advantages.

Recent clinical studies have shown that the minimally invasive nature of microwave ablation shortens patient recovery times and reduces the risk of complications. Furthermore, the development of metamaterial-based antennas has improved energy focusing capabilities, thereby minimizing collateral damage to surrounding healthy tissues. These advancements position microwave ablation as a powerful alternative to traditional surgical methods (Selmi et al., 2019; Spiliotis et al., 2021; X. Wu et al., 2016; Yu et al., 2025).

4.2. Electromagnetic Hyperthermia

Electromagnetic hyperthermia is a therapeutic technique that raises the temperature of tumor tissues in a controlled manner to thermally weaken cancer cells. When combined with radiotherapy or chemotherapy, hyperthermia often exhibits synergistic effects, improving overall treatment outcomes. Microwave- and RF-based hyperthermia systems deliver focused energy to the targeted region, minimizing damage to adjacent healthy tissues.

Metamaterial-based focusing structures allow for more precise targeting of electromagnetic energy to the tumor site. This strategy reduces energy loss in non-targeted areas and enhances therapeutic efficacy. Recent literature emphasizes promising results from advanced antenna arrays and control algorithms in hyperthermia therapy (Gel'vich & Mazokhin, 2001; Mahmoud & Montaser, 2022; Majchrzak & Paruch, 2011; Obrador et al., 2023).

5. Future Trends

5.1. Integration of Artificial Intelligence and Machine Learning

In recent years, the application of artificial intelligence (AI) and machine learning (ML) techniques in electromagnetic wave–based diagnostic and therapeutic systems has expanded significantly. These approaches have demonstrated high accuracy in areas such as microwave imaging, dielectric property analysis, and classification of measurement data obtained from microwave biosensors.

Machine learning algorithms are particularly effective in extracting complex features from biological data. Recent advances, including deep learning and

convolutional neural networks (CNNs), enable direct feature extraction from microwave biosensor data, achieving high-precision classifications without human intervention.

The integration of ML into the processing of microwave biosensor data facilitates noise reduction, precise classification of biological states, and clinically valuable outcomes. Additionally, AI-driven optimization algorithms play a critical role in treatment planning. In microwave ablation and hyperthermia therapies, for example, the distribution of electromagnetic energy can be personalized to patient-specific tissue properties, thereby improving therapeutic efficacy while minimizing collateral damage to healthy tissues. Techniques such as particle swarm optimization, genetic algorithms, and reinforcement learning are increasingly employed to adaptively fine-tune treatment parameters.

Looking ahead, the integration of AI with electromagnetic biosensors is expected to drive the development of advanced clinical decision support systems, real-time patient monitoring, automated diagnostics, personalized treatment planning, and portable or wearable microwave sensor platforms. These innovations will render electromagnetic wave–based biomedical technologies more intelligent, efficient, and patient-centered, contributing to transformative advances in healthcare.

5.2. IoT and Portable Systems

The Internet of Things (IoT) is enabling electromagnetic-based biomedical devices to become portable and remotely monitored. Integrating microwave biosensors with cost-effective embedded systems allows real-time patient data collection, streamlining clinical follow-up and disease management. Such systems are particularly promising for home healthcare services and the management of chronic conditions.

Furthermore, the development of wearable electromagnetic sensors facilitates continuous patient monitoring. Studies have reported successful outcomes using radio frequency–based subcutaneous sensors for applications such as glucose tracking and cellular activity monitoring. This trend indicates that, in the near future, electromagnetic waves will not only transform diagnostics and therapeutics but also revolutionize personalized healthcare management.

6. Conclusion

The biomedical applications of electromagnetic waves have emerged in recent years as a rapidly advancing interdisciplinary field. Techniques such as microwave imaging, biosensor technologies, ablation, and hyperthermia provide non-invasive, rapid, and highly sensitive alternatives for both diagnostic and

therapeutic procedures. The accurate modeling and measurement of the dielectric properties of biological tissues directly influence the performance of electromagnetic-based systems. In this context, integrating fundamental electromagnetic principles—such as Maxwell's equations and the frequency dependence of tissue dielectric properties—into clinical applications has been instrumental in the development of reliable and effective solutions.

Microwave biosensors, capable of delivering highly sensitive measurements with minimal sample volumes, have become a particularly promising technology, especially when combined with metamaterial-based structures to enhance performance. Designs incorporating Complementary Split Ring Resonators (CSRRs), Split Ring Resonators (SRRs), and microfluidic systems demonstrate great potential in accelerating the translation of laboratory innovations into clinical practice. Similarly, microwave ablation and electromagnetic hyperthermia have established themselves as important minimally invasive techniques, offering targeted and safer approaches for cancer treatment.

Looking forward, AI- and ML-assisted data analysis will further enhance the accuracy and reliability of microwave-based diagnostic and therapeutic systems. Deep learning–driven automated data processing will play a pivotal role in tissue classification and the creation of personalized treatment plans. Meanwhile, IoT-enabled portable sensor systems will facilitate real-time patient monitoring, driving transformative innovations in remote healthcare services and personalized health management.

In conclusion, the potential of electromagnetic waves in biomedical applications continues to expand, with interdisciplinary research expected to yield direct contributions to clinical practice. In the coming years, the integration of electromagnetic wave–based systems with artificial intelligence, metamaterial designs, and IoT technologies is poised to establish them as standard tools in both diagnostics and therapeutics.

7. References

AlSawaftah, N., El-Abed, S., Dhou, S., & Zakaria, A. (2022). Microwave Imaging for Early Breast Cancer Detection: Current State, Challenges, and Future Directions. *Journal of Imaging*, *8*(5), 123. https://doi.org/10.3390/jimaging8050123

Amini, T., Jahangiri, F., Ameri, Z., & Hemmatian, M. A. (2021). A Review of Feasible Applications of THz Waves in Medical Diagnostics and Treatments. *Journal of Lasers in Medical Sciences*, *12*(1), e92–e92. https://doi.org/10.34172/jlms.2021.92

Čáp, I., Čápová, K., Smetana, M., & Borik, Š. (2021). Electromagnetic and Acoustic Waves in Bioengineering Applications. In I. Čáp, K. Čápová, M. Smetana, & Š. Borik, *Electromagnetic and Acoustic Waves in Bioengineering Applications*. IntechOpen. https://doi.org/10.5772/intechopen.101655

Carr, K. L. (1989). Microwave radiometry: Its importance to the detection of cancer. *IEEE Transactions on Microwave Theory and Techniques*, *37*(12), 1862–1869. https://doi.org/10.1109/22.44095

Carr, K. L., El-Mahdi, A. M., & Shaeffer, J. (1981). Dual-Mode Microwave System to Enhance Early Detection of Cancer. *IEEE Transactions on Microwave Theory and Techniques*, *29*(3), 256–260. https://doi.org/10.1109/TMTT.1981.1130337

Chandra, R., Zhou, H., Balasingham, I., & Narayanan, R. M. (2015). On the Opportunities and Challenges in Microwave Medical Sensing and Imaging. *IEEE Transactions on Biomedical Engineering*, *62*(7), 1667–1682. https://doi.org/10.1109/TBME.2015.2432137

Chen, Y.-T., Lee, Y.-C., Lai, Y.-H., Lim, J.-C., Huang, N.-T., Lin, C.-T., & Huang, J.-J. (2020). Review of Integrated Optical Biosensors for Point-of-Care Applications. *Biosensors*, *10*(12), 209. https://doi.org/10.3390/bios10120209

Cheng, Y., & Fu, M. (2018). Dielectric properties for non-invasive detection of normal, benign, and malignant breast tissues using microwave theories. *Thoracic Cancer*, *9*(4), 459–465. https://doi.org/10.1111/1759-7714.12605

Choudhury, P. K., & El-Nasr, M. A. (2015). Electromagnetics for biomedical and medicinal applications. *Journal of Electromagnetic Waves and Applications*, *29*(17), 2275–2277. https://doi.org/10.1080/09205071.2015.1103984

Clements, J. C., & Comeau, L. A. (2019). Use of High-Frequency Noninvasive Electromagnetic Biosensors to Detect Ocean Acidification Effects on

Shellfish Behavior. *Journal of Shellfish Research*, *38*(3), 811. https://doi.org/10.2983/035.038.0330

Dash, S. K., & Khuntia, S. R. (2011). *Fundamentals of electromagnetic theory* (2nd ed). PHI Learning.

Farmer, A., Friedli, A. C., Wright, S. M., & Robertson, W. M. (2012). Biosensing using surface electromagnetic waves in photonic band gap multilayers. *Sensors and Actuators B: Chemical*, *173*, 79–84. https://doi.org/10.1016/j.snb.2012.06.015

Fear, E. C. (2005). Microwave Imaging of the Breast. *Technology in Cancer Research & Treatment*, *4*(1), 69–82. https://doi.org/10.1177/153303460500400110

Frankel, T. (1974). Maxwell's Equations. *The American Mathematical Monthly*, *81*(4), 343–349. https://doi.org/10.1080/00029890.1974.11993557

Gabriel, C., & Peyman, A. (2018). Dielectric Properties of Biological Tissues; Variation With Age. In *Conn's Handbook of Models for Human Aging* (pp. 939–952). Elsevier. https://doi.org/10.1016/B978-0-12-811353-0.00069-5

Geetharamani, G., & Aathmanesan, T. (2020). Split ring resonator inspired THz antenna for breast cancer detection. *Optics & Laser Technology*, *126*, 106111. https://doi.org/10.1016/j.optlastec.2020.106111

Gel'vich, E. A., & Mazokhin, V. N. (2001). Technical Aspects of Electromagnetic Hyperthermia in Medicine. *Critical Reviews in Biomedical Engineering*, *29*(1), 77–97. https://doi.org/10.1615/CritRevBiomedEng.v29.i1.30

Groumpas, E. I., Koutsoupidou, M., & Karanasiou, I. S. (2022). Biomedical Passive Microwave Imaging and Sensing: Current and future trends [Bioelectromagnetics]. *IEEE Antennas and Propagation Magazine*, *64*(6), 84–111. https://doi.org/10.1109/MAP.2022.3210860

Handbook of biological effects of electromagnetic fields. (1996). *Choice Reviews Online*, *33*(11), 33-6361-33–6361. https://doi.org/10.5860/CHOICE.33-6361

Harsanyi, G. (2000). *Sensors in Biomedical Applications: Fundamentals, Technology and Applications* (0 ed.). CRC Press. https://doi.org/10.1201/9781420012910

Huang, P., Xu, L., & Xie, Y. (2021). Biomedical Applications of Electromagnetic Detection: A Brief Review. *Biosensors*, *11*(7), 225. https://doi.org/10.3390/bios11070225

Huray, P. G. (2010). *Maxwell's equations* (Online-Ausg). Wiley.

Hwang, J., Choi, Y., Lee, K., Krishnan, V., Pelled, G., Gilad, A. A., & Choi, J. (2020). Regulation of Electromagnetic Perceptive Gene Using

Ferromagnetic Particles for the External Control of Calcium Ion Transport. *Biomolecules*, *10*(2), 308. https://doi.org/10.3390/biom10020308

Johnson, C. C., & Guy, A. W. (1972). Nonionizing electromagnetic wave effects in biological materials and systems. *Proceedings of the IEEE*, *60*(6), 692–718. https://doi.org/10.1109/PROC.1972.8728

Khodaie, A., & Heidarzadeh, H. (2024). Design and analysis of a multi-modal refractive index plasmonic biosensor based on split ring resonator for detection of the various cancer cells. *Optical and Quantum Electronics*, *56*(9), 1439. https://doi.org/10.1007/s11082-024-07381-9

Kim, S., Malik, J., Seo, J. M., Cho, Y. M., & Bien, F. (2022). Subcutaneously implantable electromagnetic biosensor system for continuous glucose monitoring. *Scientific Reports*, *12*(1), 17395. https://doi.org/10.1038/s41598-022-22128-w

Kulkarni, M. B., Ayachit, N. H., & Aminabhavi, T. M. (2022). Biosensors and Microfluidic Biosensors: From Fabrication to Application. *Biosensors*, *12*(7), 543. https://doi.org/10.3390/bios12070543

Kumar Sharma, M., Singh, S. P., Badola, P., Kumar, M., Saini, J. P., & Lay Ekuakille, A. (2023). Noninvasive Microwave-Multielement Sensor for Breast Phantoms Analysis and Tumor Detection. *IEEE Sensors Journal*, *23*(17), 20207–20214. https://doi.org/10.1109/JSEN.2023.3296740

Mahmoud, K. R., & Montaser, A. M. (2022). Design of Multiresonance Flexible Antenna Array Applicator for Breast Cancer Hyperthermia Treatment. *IEEE Access*, *10*, 93338–93352. https://doi.org/10.1109/ACCESS.2022.3203431

Majchrzak, E., & Paruch, M. (2011). Identification of electromagnetic field parameters assuring the cancer destruction during hyperthermia treatment. *Inverse Problems in Science and Engineering*, *19*(1), 45–58. https://doi.org/10.1080/17415977.2010.531473

Mehrotra, P., Chatterjee, B., & Sen, S. (2019). EM-Wave Biosensors: A Review of RF, Microwave, mm-Wave and Optical Sensing. *Sensors*, *19*(5), 1013. https://doi.org/10.3390/s19051013

Mirbeik-Sabzevari, A., & Tavassolian, N. (2019). Tumor Detection Using Millimeter-Wave Technology: Differentiating Between Benign Lesions and Cancer Tissues. *IEEE Microwave Magazine*, *20*(8), 30–43. https://doi.org/10.1109/MMM.2019.2915472

Nikolova, N. K. (2014). Microwave Biomedical Imaging. In J. G. Webster (Ed.), *Wiley Encyclopedia of Electrical and Electronics Engineering* (1st ed., pp. 1–22). Wiley. https://doi.org/10.1002/047134608X.W8214

Obrador, E., Jihad-Jebbar, A., Salvador-Palmer, R., López-Blanch, R., Oriol-Caballo, M., Moreno-Murciano, M. P., Navarro, E. A., Cibrian, R., & Estrela, J. M. (2023). Externally Applied Electromagnetic Fields and Hyperthermia Irreversibly Damage Cancer Cells. *Cancers*, *15*(13), 3413. https://doi.org/10.3390/cancers15133413

O'Loughlin, D., O'Halloran, M., Moloney, B. M., Glavin, M., Jones, E., & Elahi, M. A. (2018). Microwave Breast Imaging: Clinical Advances and Remaining Challenges. *IEEE Transactions on Biomedical Engineering*, *65*(11), 2580–2590. https://doi.org/10.1109/TBME.2018.2809541

Patel, S. K., Wekalao, J., Albargi, H. B., Jalalah, M., Almawgani, A. H. M., & Armghan, A. (2024). Design and Simulation of Metasurface-Enhanced Graphene Biosensors for Cancer Biomarker Detection. *Plasmonics*, *19*(6), 3119–3130. https://doi.org/10.1007/s11468-024-02224-5

Reimer, T., & Pistorius, S. (2023). Review and Analysis of Tumour Detection and Image Quality Analysis in Experimental Breast Microwave Sensing. *Sensors*, *23*(11), 5123. https://doi.org/10.3390/s23115123

Rozzell, T. C., & Lin, J. C. (1987a). Biomedical Applications of Electromagnetic Energy. *IEEE Engineering in Medicine and Biology Magazine*, *6*(1), 52–57. https://doi.org/10.1109/MEMB.1987.5006376

Rozzell, T. C., & Lin, J. C. (1987b). Biomedical Applications of Electromagnetic Energy. *IEEE Engineering in Medicine and Biology Magazine*, *6*(1), 52–57. https://doi.org/10.1109/MEMB.1987.5006376

Sandeep, S., Vard, A., Guxens, M., Bloch, I., & Wiart, J. (2024). RF-EMF Exposure Assessment of Fetus During the First Trimester of Pregnancy. *IEEE Access*, *12*, 75311–75322. https://doi.org/10.1109/ACCESS.2024.3404369

Selmi, M., Bin Dukhyil, A. A., & Belmabrouk, H. (2019). Numerical Analysis of Human Cancer Therapy Using Microwave Ablation. *Applied Sciences*, *10*(1), 211. https://doi.org/10.3390/app10010211

Shamim, S., Mohsin, A. S. M., Rahman, Md. M., & Hossain Bhuian, M. B. (2024). Recent advances in the metamaterial and metasurface-based biosensor in the gigahertz, terahertz, and optical frequency domains. *Heliyon*, *10*(13), e33272. https://doi.org/10.1016/j.heliyon.2024.e33272

Someda, C. G. (2017). *Electromagnetic Waves* (2nd ed.). CRC Press. https://doi.org/10.4324/9781420009545

Spiliotis, A. E., Gäbelein, G., Holländer, S., Scherber, P.-R., Glanemann, M., & Patel, B. (2021). Microwave ablation compared with radiofrequency ablation for the treatment of liver cancer: A systematic review and meta-

analysis. *Radiology and Oncology*, *55*(3), 247–258. https://doi.org/10.2478/raon-2021-0030

Staderini, E. M. (2002). UWB radars in medicine. *IEEE Aerospace and Electronic Systems Magazine*, *17*(1), 13–18. https://doi.org/10.1109/62.978359

Tlili, B., Chibuike, O., & Keshkar, M. (2024). Non-Invasive Glucose Detection Using a Triple Cell Square CSRR Sensor: Experimental Validation. *2024 IEEE International Symposium on Antennas and Propagation and INC/USNC-URSI Radio Science Meeting (AP-S/INC-USNC-URSI)*, 2555–2556. https://doi.org/10.1109/AP-S/INC-USNC-URSI52054.2024.10685880

Turner, A. P. F., Karube, I., & Wilson, G. S. (Eds.). (1987). *Biosensors: Fundamentals and applications*. Oxford University Press.

Wu, W., Xiao, X., Wang, Z., Sun, J., & Zhang, X. (2024). Highly sensitive blood glucose monitoring sensor with adjustable resonant frequency based on MP-CSRR. *Sensors and Actuators A: Physical*, *366*, 115004. https://doi.org/10.1016/j.sna.2023.115004

Wu, X., Liu, B., & Xu, B. (2016). Theoretical evaluation of high frequency microwave ablation applied in cancer therapy. *Applied Thermal Engineering*, *107*, 501–507. https://doi.org/10.1016/j.applthermaleng.2016.07.010

Xie, B., Wang, C., Meng, F., Li, X., & Wu, Q. (2023). Q-factor enhanced resonator biosensor optimized by adaptive genetic algorithm for glucose detection. *Microwave and Optical Technology Letters*, *65*(3), 746–752. https://doi.org/10.1002/mop.33560

Yang, J. (Ed.). (2011). *Recent Application in Biometrics*. InTech. https://doi.org/10.5772/970

Yu, M., Wang, B., Qu, Y., Sun, W., Liang, M., Mao, X., Jiang, Y., Wang, J., Tang, X., Pan, H., Zhao, Y., Xie, H., Ding, Q., Wang, S., & Zhou, W. (2025). Comparison of local effects and systemic T-cell responses in patients with breast cancer treated by radiofrequency ablation versus microwave ablation. *Cancer Cell International*, *25*(1), 261. https://doi.org/10.1186/s12935-025-03896-7

Chapter 7

Climate Change Effects on Water Resources (A Bibliometric Analysis)

Zeyneb KILIÇ [1]

1. INTRODUCTION

Global warming inevitably affects ecosystem and processes of hydrological cycle. Water is indispensable for health, food production, industry, sustainable ecosystems and other sectors. The decrease of water, increases desertification and prevents sustainable life. Forecasting the future influence of climate change and taking precautions against the negativities caused by climate change is one of the most important issues of today's humanity. Global warming caused by climate change and other reasons; this leads to decrease in water resources, change in precipitation regimes, energy shortage, decrease in quality of life, extreme weather events, floods and droughts [1]. Nowadays, climate change stands out as one of the most important and complex challenges. The negative impacts of climate change are seen not only on the environment, but also in the economic, social and political spheres. If these negative impacts are not controlled, they will continue to harm the entire environment and society [2]. Climate change can also change the natural cycle of water and river flow regimes. The natural cycle of water has invaluable ecological and economic benefits for life on earth. Water is vital for the survival of humanity, and access to unpolluted fresh water is vital for protecting human well-being [3]. Therefore, rational and sustainable use of water, protection of existing water resources, water education and water management issues are important [4]. The rapid increase in the number of studies in the literature makes it difficult to compile and follow them. Bibliometric analysis methods are very valuable in terms of systematically evaluating current publication trends and providing a strategic direction to the research process. With these analyses; the general status of academic activities in a field, key themes and trends can, the most influential authors, institutions, countries and collaboration networks between researchers and organizations can be determined [5]. Bibliometric analyses contribute to the identification of potential collaboration opportunities and the identification of knowledge gaps in the

[1]Assist. Prof. Dr., Adıyaman University, Engineering Faculty, Department of Civil Engineering-Hydraulic, Adıyaman, Türkiye.
* Corresponding author e-mail: zkilic@adiyaman.edu.tr
ORCID: 0000-0003-4954-6955

relevant literature. In this context, bibliometric analyses not only map past literature, but also help make strategic decisions that will guide future research.

In this study, "climate change" and "water resources" papers were used to evaluate with bibliometric analysis. 1982-2023 data were obtained from Web of Science; which is the most widely and largest database of bibliometric analysis. Only the Science Citation Index Expanded civil engineering database and article document type was used. As a result; 13.417 documents were found on water resources. Information on co-authorship, previous studies, related keywords and authors was obtained. The article examined research articles published on water resources, climate change, drought and water resources management. The aim of this research is to analyze the current status of the concepts of climate change and water resources and to provide a holistic perspective to researchers and literature. It is hoped that this study will support studies on the subject.

2. MATERIAL AND METHOD

2.1. Data Collection

Bibliometric analysis methods are used functionally in examining water concerns related to climate change and determining water management systems. Bibliometric analysis provides information based on numerical data about authors, countries, publication performance of journals, collaboration networks, strengths and weaknesses about research field. It also provides important contributions in terms of identifying gaps in the literature, revealing potential research opportunities, and evaluating the impact of scientific outputs [6]. There are many databases that can be used in bibliometric research. Scopus, Web of Science (WoS), Google Scholar are the most important of these databases. The majority of high impact factor journals are scanned in WoS [7]. In this research, Science Citation Index (SCI), which includes the WoS civil engineering document type, was used. Articles published on water resources, climate change, drought, and water resources management (1982-2023) were evaluated. Evaluations were made by determining the distribution of published articles on the subject by year and country, the distribution of keywords, the authors with the most publications and citations and the most productive journals.

3. RESULT AND DISCUSSION

3.1. Distribution of Published Articles by Year

Table 1 shows the number of publications by year; so this table shows how scientific interest in climate change and water resources has evolved over time. The number of publications was quite low from the 1982s to 1999, which can be interpreted as the subject not yet being widely included in the academic area. While less than 20 articles were produced per year until the 1982s and 1990s,

studies continued to increase with 34 works in 1991. A significant increase in the number of paperss has been observed since the 2000s. It is seen that studies on the subject continued with an accelerated increase especially after 2005. The number of studies increased even more after 2015. The years 2021-2022-2023 are the period with the most articles. This situation shows that academic interest and awareness about research topic has increased over time. Table 1 show that the subject has entered the global research area seriously in the last 10 years. Publications on the subject can contribute to decision-making processes, similar studies, researchers, politicians and practitioners. In 2000-2010 years, there is a gradual, slow but steady increase in the number of papers since the beginning of the 2000s. It started with 64 publications in 2001 and became 313 in 2010.

Table 1. Number of Papers by Year

2023 : 1358	**2016 :** 607	**2009 :** 251	**2002 :** 69	**1995:** 60	**1988 :** 12
2022 : 1257	**2015 :** 655	**2008 :** 168	**2001 :** 64	**1994 :** 35	**1987 :** 5
2021 : 1237	**2014 :** 617	**2007 :** 174	**2000 :** 62	**1993 :** 36	**1986 :** 13
2020 : 1016	**2013 :** 531	**2006 :** 126	**1999 :** 52	**1992 :** 45	**1985 :** 8
2019 : 738	**2012 :** 443	**2005 :** 93	**1998 :** 45	**1991 :** 36	**1984 :** 6
2018 : 778	**2011 :** 344	**2004 :** 78	**1997 :** 41	**1990 :** 23	**1983 :** 3
2017 : 703	**2010 :** 313	**2003 :** 74	**1996:** 65	**1989 :** 19	**1982 :** 5

This period coincided with the period when global policies such as the United Nations Sustainable Development Agenda began to be addressed; which may have led to an increase in studies on the subject. While the number of studies on the subject was 344 in 2011, this number increased and reached 1358 in 2023. The rising publication trend may also mean that; stronger collaborations are being established between researchers.

3.2. Distribution of Works and Citations by Country

USA is the most productive country with 260 documents and 42,521 citations. The second and third countries, China and the UK, have 237 and 109 documents, respectively. The distribution of papers by other countries is as follows: Australia (92), Canada (78), Iran (50); Netherlands (43), Spain (41), France (40), Germany (39), Norway (35), India (35), Italy (33), Sweden (30), Türkiye (21). The highest number of citations was observed in USA publications (42.521), followed by China and the UK.

Table 2. Number of Publications and Citations by Country

Country-Paper-Citation	Country-Paper-Citation	Country-Paper-Citation
USA - 260 - 42521	Iran – 50 - 6987	Norway – 35 - 6408
China - 237 - 34670	Netherlands – 43 - 8315	India – 35 - 4472
England - 109 -20684	Spain – 41 - 10314	Italy – 33 - 4906
Australia - 92 - 13074	France – 40 - 5869	Sweden – 30 - 5948
Canada - 78 - 13582	Germany – 39 - 5753	Türkiye – 21 - 3414

The relevant work collaborations among the top 15 countries are shown in Figure 1, which shows the scientific production and joint publication network between countries. Thicker lines represent more intensive collaboration, and larger nodes represent more joint publications and a central role. The United States and China stand out as the two most active countries in international collaboration. The thick lines indicate strong collaboration between these two countries. Canada, Australia, United Kingdom are other countries with extensive collaboration. England, Germany, France, Italy, Netherlands, and Spain are generally closely associated with each other and shown in green in Figure 1, represent European-based research networks. Sweden and Norway showed with blue; these countries are linked to other countries through lesser but more significant collaborations. Türkiye, Iran, India particularly linked to the United States and China, play a more limited but strategic role in producing publications.

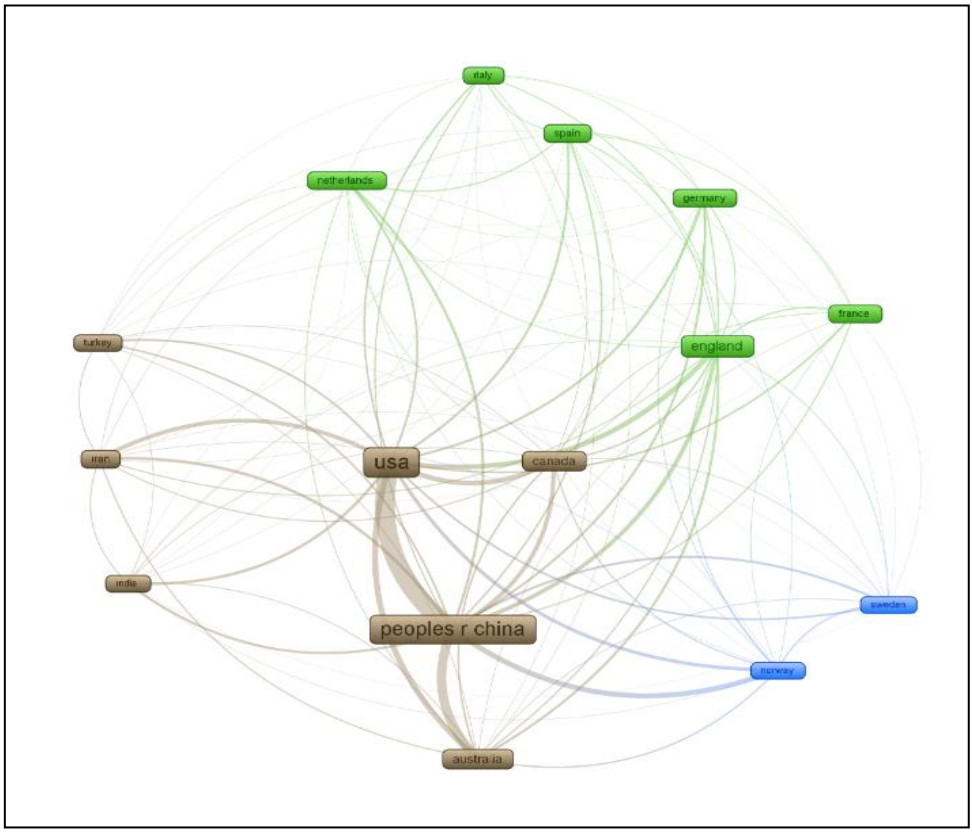

Figure 1. International Cooperation Network Between Countries

3.3. Distribution Numbers of Keywords Related to the Topic

Climate change is significantly higher ratio than other keywords. Other three topics (drought, precipitation, water resources) play an important role in the continuous expansion of the research (Table 3).

Table 3. Distribution of Keywords Related to the Topic in Literature

Keywords	Number	Keywords	Number
Climate change	246	Evapotranspiration	26
Drought	57	Trend analysis	20
Precipitation	36	Hydrology	18
Water resources	34	Groundwater	17
Streamflow	31	Hydrological modelling	15

Figure 2 is a bibliometric co-occurrence network showing the key concepts and their interconnections in the scientific literature on climate change and water resources. Figure 2 shows the distribution of keywords used by year. As the frequency of keywords increases, their labels also increase. The size of the nodes

indicates the years, and the color transitions indicate the frequency of keyword use. Words that appear clearly and large are the keywords preferred in the studies. The purple colored parts indicate the places where the studies on the subject are less intense; the yellow colored parts indicate the places where the studies on the subject are more quantitative.

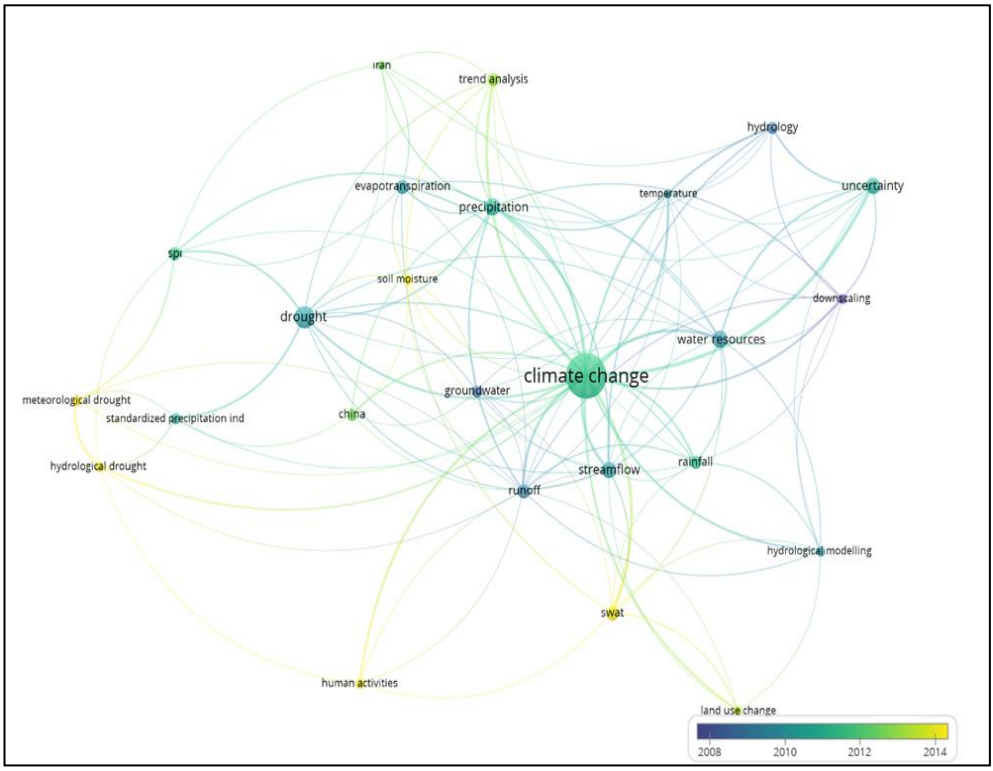

Figure 2. Keyword Map

Climate change is the node with the largest and most dense connections, which indicates that this topic is the most cited, most associated and analyzed keyword in the literature. Others are concepts frequently used in studies analyzing the physical effects of climate change and are directly or indirectly connected to the main theme of climate change. The keywords groundwater and water resources are prominent in studies in the context of water management and water security. Countries such as China and Iran in particular have been prominent in studies on drought.

3.4. Author and Citation Analysis

Xu, chog-yu (China) is the author with the most works and the most citations in the field, followed by Singh vijay (2292) and Guo shenglian (1619). This

shows the significant contributions and influence of the first three authors in the field. Although authors such as Yang Dawen and Chen Xi have published relatively fewer articles, their citation counts are high. This shows that their publications are followed with interest by the academic community and have high impact. The authors on the list are mostly researchers of Asian origin, which indicates the increasing influence of countries, especially China, in research in this field (Table 4).

Table 4. Authors Articles and Citations

Co-Author	Documents	Citations
Xu, chong-yu	18	3554
Singh, vijay	15	2292
Guo, shenglian	11	1619
Zhang, zengxin	10	1301
Huang, qiang	10	1375
Yang, dawen	9	1595
Chen, xi	7	1478

Figure 3 is a bibliometric co-authorship network, showing academic collaborations between authors. The red areas where the density associated with the author is high. Each node (dot) represents an author, while the lines between the nodes represent the academic studies published jointly. The colors indicate the clusters to which the authors belong. The citation network of the most cited authors studying the relationship between water resources and nearby regions shows three clusters of authors with different characteristics (Figure 3). In this analysis, authors who published at least three articles in the selected regions were included. Figure 3 shows the number of times two independent authors were cited simultaneously in different studies.

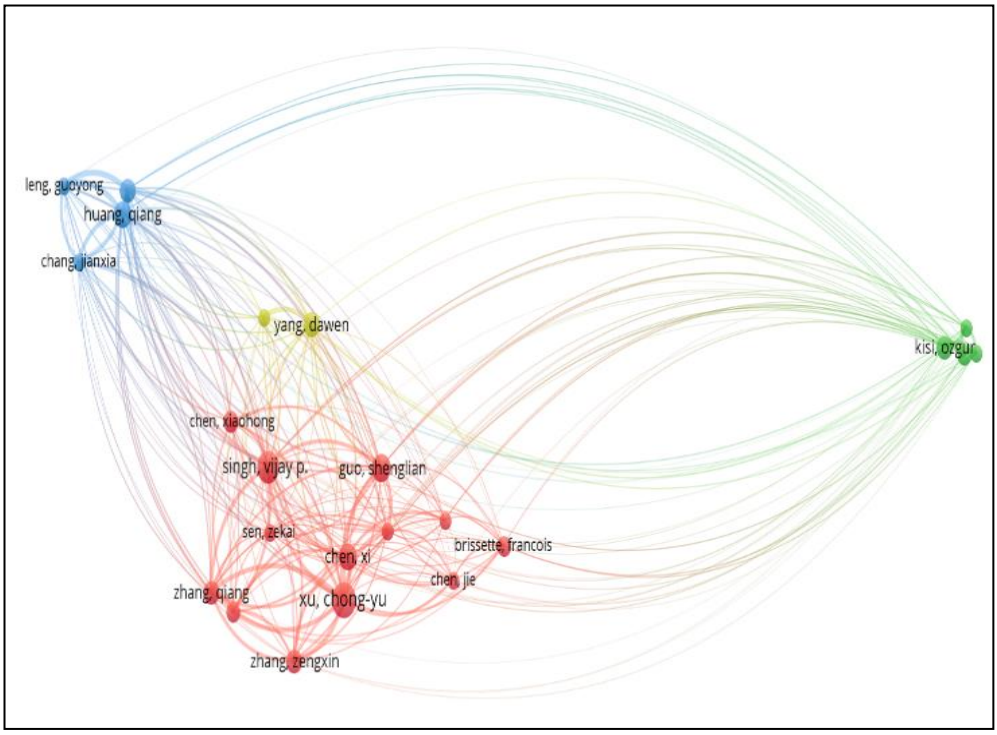

Figure 3. Bibliometric Collaboration Network on the Subject

Almost all of the authors in the red cluster are Chinese; Xu Chong-Yu, Singh Vijay P., Guo Shenglian, Chen Xi and Zhang Qiang have very intense collaborations and are closely connected. The red cluster may represent many universities and research institutions based in China, and international collaborations are also noteworthy. The blue cluster consists of names such as Leng Guoyong, Huang Qiang, Chang Jianxia. The blue cluster is less connected than the others and is a group that collaborates intensively within itself. The green cluster is an independent cluster consisting of authors from Turkey, primarily Özgür Kişi. The researchers in the green cluster have not established extensive partnerships, but have indirect connections with authors in other clusters. Yang Dawen plays a bridging role by establishing weak connections to both red and blue clusters, and may be an important author who provides interdisciplinary or multinational transition in the literature. There are collaborations at various levels between Chinese, Turkish and international researchers (especially those based in the US and Canada). In particular, the red cluster is the most active group in terms of both the number of publications and the density of collaboration. This collaboration network analysis shows that scientific productivity is directly related not only to the number of publications but also to the density of collaboration and global interaction (Figure 3).

3.5. The Most Productive Journals

The 12 most productive journals are shown in Figure 4. The "Journal of Hydrology" journal, shown with the large red circle in the center, is one of the most important journals in the field of research, the most cited publication source in the field and the one that cites other journals the most. This shows how central the "Journal of Hydrology" journal is in fields such as hydrology, climate change, water management.

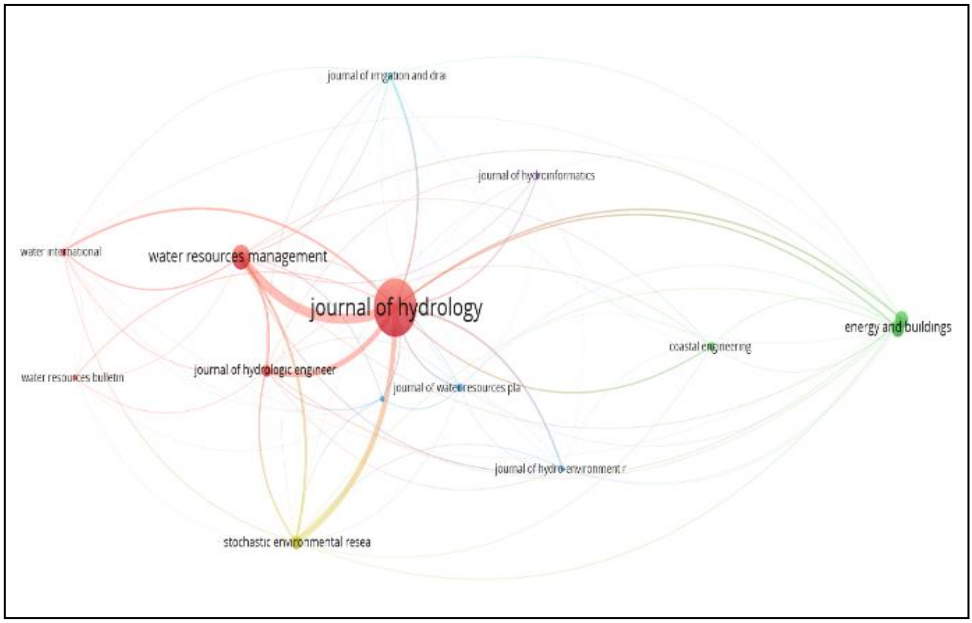

Figure 4. The 12 Most Productive Journals

Strong connections are shown with thick arcs. The presence of connections with Water Resources Management, Journal of Hydrologic Engineering, Water International and Stochastic Environmental Research journals with very thick arcs indicates that there are intense citation relationships between these journals, that research topics overlap and that mutual information exchange on the subject is strong. Topics such as global climate change, water resources, water health and water security have encouraged the rapid development of water-related research in recent years. Many countries have conducted successful research in this field and continue to do so. With the development of technological tools on the subject, research has spread to all water resources, both groundwater and surface water. Modeling to assess the effects of climate change yields successful results. According to the results obtained from this study; studies on the subject have intensified after 2019. The first two countries with the most publications are the USA and China, while the index with the most publications is determined as SCI Expanded. The USA and China are

generally places with high co-author connections. Accordingly, it can be said that there are not enough academic studies on the subject in the national literature. It is recommended that future studies conduct research and studies in this direction and address the issue with different analyses. In order to eliminate confusion on the subject and to reveal the connections more clearly, it is necessary to thoroughly examine the facts and problems. In order to increase the sensitivity and scientific rigor of scenario simulations for future climate change, mechanistic and applied studies should be included in the subject. In addition, it is important to determine the various factors that negatively affect water in various environments and to examine the interaction of these factors. Moving from theoretical analysis of mechanistic research to practical applications for strategy formulation is an important research direction to better understand the relationship between future climate change and water and water management [8]. Nowadays, with the development of machine learning and artificial intelligence, research methods and technologies between climate change and water and water resources are continuously improved [9]. Bibliometric analysis provides comprehensive information about publications and new directions on floods, water problems, sustainable use of water, and climate change, and provides data that will form the basis for and shed light on future studies on the subject. Such studies help to better understand the current state of knowledge, identify additional research areas, increase collaboration, and promote knowledge sharing.

4. CONCLUSION

In this study, it was determined how research on the subject changed worldwide, how much was done, and how different countries focused on different research areas on the subject. Articles containing bibliometric analysis may have some methodological limitations and potential restrictions. Therefore, different databases and technological methods can be used for more comprehensive scans. Better understanding the connection between climate change and water resources and finding solutions to related problems requires the integration of disciplines such as ecology, climatology, hydrology, technology, analytical science, and social sciences. A better understanding of the strategies used by countries and sectors to adapt to the effects of climate change on water resources can be facilitated by interdisciplinary collaborations. Scientists working on the subject can better understand the complex interactions between natural systems, water status, human activities, and climate change by combining different perspectives, interpretations, experiences, knowledge, and approaches. In this way, more comprehensive and successful results can be obtained. In addition, within the scope of water resources and climate change adaptation, joint strategies and efforts can be developed to reduce disaster risk and reduce economic losses

REFERENCES

[1] Van der Pol, T.D., Van Ierland, E.C., Gabbert, S., Weikard, H.P., and Hendrix, E.M.T. (2015). Impacts of Rainfall Variability and Expected Rainfall Changes on Cost-Effective Adaptation of Water Systems to Climate Change. *Journal Environment Management,* 154, 40–47.

[2] Zhuang, Y., and Zhang, J. (2020). Diurnal Asymmetry in Future Temperature Changes Over The Main Belt and Road Regions. *Ecosystem Health Sustainability,* 61, 1-10.

[3] Kılıç, Z. (2020). The İmportance of Water and Conscious Use Of Water. *International Journal of Hydrology,* 4(5), 239–241.

[4] Kılıç, Z. (2021). Water Pollution Causes, Negative Effects and Prevent Methods. *İstanbul Sabahattin Zaim Ünv Fen Bilimleri Dergisi,* 3, 2, 32-35.

[5] Kılıç, Z. (2025). Bibliometric Analysis of Computational Fluid Dynamics (Cfd) On Hydraulic Energy. *Black Sea Journal of Engineering and Science,* 8(3), 598-604.

[6] McBurney, M.K., and Novak, P.L. (2002). What Is Bibliometrics And Why Should You Care? Paper Presented At The Proceedings. *IEEE International professional communication conference.*

[7] Demir, H., & Erigüç, G. (2018). Bibliyometrik Bir Analiz Ile Yönetim Düşünce Sisteminin Incelenmesi. *İş ve İnsan Dergisi,* 5(2), 91-114.

[8] Ding, M., and Zeng, H. (2022). A Bibliometric Analysis of Research Progress İn Sulfate-Rich Wastewater Pollution Control Technology. *Ecotoxicology and Environmental Safety,* 238, 113626.

[9] Longyang, Q. (2019). Assessing the Effects of Climate Change On Water Quality of Plateau Deep-Water Lake-A Study Case of Hongfeng Lake. *Science of the Total Environment,* 647, 1518-1530.

Chapter 8

Problematic Soils and Proven Solutions: A Practical Guide to Geotechnical Ground Improvement

Abiola Ayopo Abiodun [1]

Abstract

This handbook provides a practical roadmap for identifying problematic soils and for selecting, designing, and applying effective ground improvement techniques to meet clearly defined performance goals. It distils both research and field experience into field-ready guidance for managing soils such as collapsible loess, contaminated fills, expansive clays, frost-susceptible silts, liquefiable sands, peat and organic deposits, soft compressible soils, sulphate-bearing soils, sensitive and quick clays. Each soil class is described with diagnostic indicators, primary risks, recommended treatments, design precautions, and acceptance benchmarks. The guide covers improvement methods including chemical stabilisation, mechanical densification, drainage and consolidation, grouting, lightweight replacement, thermal methods, reinforcement and inclusions, and barriers or containment systems. Selection is supported by clear criteria, constructability insights, quality assurance (QA) and quality control (QC) procedures, and durability considerations. Emphasis is placed on quantifiable performance in terms of bearing capacity, deformation control, stiffness, hydraulic behaviour, and long-term resilience, supported by both laboratory and in situ testing. Sustainability principles are embedded throughout, highlighting low-carbon binders, recycled materials, leachate assessments, and whole-life cost-risk evaluation. Case snapshots illustrate common pitfalls and successful implementations, while decision matrices and performance criteria enable transparent validation with clients and regulators. The result is a comprehensive, evidence-based guide to transforming difficult ground into reliable foundations and durable platforms.

Keywords: soil stabilization, ground improvement, problematic soils, geotechnical testing, performance-based design, field trials, sustainable civil engineering, soil classification, quality assurance and control in geotechnics.

[1] PhD, MSc, BSc (Hons) Faculty of Engineering and Architecture, Cyprus West University, Famagusta 99450, North Cyprus via Mersin 10 Turkey
Email: a.abiodun@cwu.edu.tr | ORCID: 0000-0003-1655-2312

Table of Contents

1 Introduction and How to Use This Guide

Problematic soils such as expansive clays, collapsible loess, peat or organic deposits, frost-susceptible silts, liquefied sands, soft compressible clays or silts, sulphate-bearing strata, and contaminated fills pose major risks to civil structures [1-2]. Repeated failure patterns such as cracking, heave, and lateral expansion can often be traced back to three causes:

(1) incorrect soil diagnosis;

(2) inadequate quality assurance and control;

(3) suboptimal application of stabilisation methods.

This guide provides step-by-step methods for soil diagnosis, treatment selection, design control and project quality oversight to transform difficult ground into reliable foundations. It supports efficient reference use in lab testing, fieldwork, and technical reporting. Selected acronyms, notations, and abbreviations used throughout this book are clearly defined in the glossary.

1.1 Who should read it?

This book is for civil geotechnical engineers, construction site engineers, government regulators, real estate developers and postgraduates seeking to:

- stabilise problematic soils for safe and durable engineering structures;
- apply structured diagnostic tools for site assessment and technical reporting;
- match soil classifications with effective ground improvement solutions;
- select appropriate stabilisers and binders to meet performance criteria;
- implement rigorous QA/QC protocols to verify treatment success.
-

1.2 What does success look like?

Ground improvements are successful if performance targets are met over the design life. Typical metrics include strength and stiffness (degree of improvement (D) $\geq$ 70%, undrained shear strength (Su) $\geq$ 25–50 kPa), deformation (total S and differential Δ) within limits, hydraulic improvement (k or drainage), stability, volume control (plasticity index (PI), swell potential, swell pressure); constructability and durability [3]. Accepted field tests include cone penetration test (CPT), standard penetration test (SPT), plate load, vane shear, and bearing checks.

1.3 Categories of ground improvement

The categories of ground improvement provided in this book are as:

1. Mechanical densification and replacement techniques [4].
2. Drainage-based consolidation methods [5].

3. Chemical or cementitious stabilisation method [6].
4. Grouting and columnar inclusions techniques [7].
5. Bio-electrochemical and thermal methods [8].

1.4 How to navigate the book

- Section 2 presents the problem soils, diagnostics, risks, go-to remedies.
- Sections 3–9 analyze the guide's objectives, constraints, and implementation strategies.
- Section 10 provides a decision matrix chart.
- Section 11 offers checklists and field forms.
- Section 12 presents the final conclusions and practical takeaways.
- Finally, the book closes with a detailed glossary, list of abbreviations, and complete references.

1.5 Limits and ethics

This manual is not a substitute for standards, project specifications, or professional judgement. Readers should always verify their use by site visits, rigorous field tests, and appropriate approvals. Red flags such as sulphate soils, quick clays, or gas-producing soils require precautionary measures. Where appropriate, low-carbon and low-risk options are highlighted in details.

2 Problematic Soils: Classification and Diagnostic Indicators

This section outlines each soil class profile, with diagnostics, risks, treatment, quality assurance and control, and implementation cautions.

2.1 Expansive (shrink and swell) soils

Clay soils with a plasticity index (PI) > 25–35%; free swell (FS) > 50%; swelling potential (Sp) > 5%; swell pressure > 100 kPa; heave after wetting; and cracks after drying. Such soils pose risks of heaving beneath structures, pipeline distortion, wall and slab cracks, and highway deformation [9-10].

To reduce PI and increase strength, use lime, lime-cement mixtures, silica fume, fly ash, GGBS and agro-industry ash to stabilise these soils [11]. Geocomposites, groundwater barriers, geogrid substructures and capillary breaks are often used to control the moisture fluctuation. Deep piers or solid inclusions are used to circumvent the active zone of these soils [12].

It is important to avoid the use of lime or cement during stabilisation if the sulphate content of the soil is > 1% to avoid the formation of ettringites. To avoid the risk of ettringite, sulphate-resistant (SR) binders or mechanical

solutions should be used. After stabilisation, it is crucial to confirm that a 50% drop in pressure and unconfined compressive strength (UCS) > 1 MPa is achieved. In these clays, the retention of uniform moisture during compaction and construction is important [13].

2.2 Soft, highly compressible clays or silts

These clay or silt soils have low strength (Su < 25 kPa), high moisture content, high slip evident, high compression and rebound index: (Cc and Cr), high coefficient of compressibility a_v and high preconsolidation pressure $\sigma'p$.

These soils often lead to bearing failures, extensive consolidation, settling, tilting and instability, and long periods of consolidation [14].

The appropriate treatment is consolidation, surcharging or vacuum preloading for settling; stone columns, and granular piles for loading; reinforcement for drainage and stability and light filling to reduce voids [15].

It is essential to monitor settlement plates and piezometers: target > 90% consolidation; check the degree of consolidation and settling time, pore pressure dissipation and the stability factors for each soil stabilisation phase.

2.3 Organic and peat soils

Associated with water content > 200%; loss on ignition (LOI) ≥ 20%; very low Su; high compressibility; and gas pockets. They pose risks of overloading, embankment instability, buoyancy, long-term slippage, and gas hazards [16]. Difficulties can be overcome by shallow excavation or by replacement at the surface deeper deposits require deep mixing with cement and ash columns in a stable layer together with various load bearing grids. Electro-osmotic drainage and electrokinetic offer localised stiffening around the piles [17]. A vital step is to install gas-venting pipes to prevent CH_4-induced uplift of foundations. It is crucial to verify that UCS ≥ 0.5 MPa, ensure that creep is < 1% per log cycle; and that long-term settlement monitoring is mandatory [18].

2.4 Collapsible loess and metastable silts

Loess silts have an open, metastable structure which is slightly cemented with clay or carbonate. Their dry densities of 1100 to 1400 $kg.m^{-3}$ appear deceptively stable, but increasing humidity causes sudden rearrangements and settlements of 5 to 15%. The risk is confirmed by double oedometer tests showing a collapse strains exceeding 3% under a pressure of $\sigma' = 200$ kPa. Pre-wetting followed by a strong compaction ≥ 95 % maximum dry density (MDD) stabilises the unstable soils, thereby reducing the instability. However, where access is limited, permeable grouting with low-viscosity cement or

silicate will stabilise the soil. The use of lime-cement restricts the edge wetting in these soils and ground-granulated blast-furnace slag (GGBS) blends can reduce carbon content by 60%. Also, the use of raft or mat foundations offers improvement in collapsible loess and metastable silts [19].

The most vital quality assurance (QA) and precautions are to control site drainage; to plan for unexpected precipitation which may cause breakdown prior to soil treatment. Verify that there is a residual collapse of < 1% residual in double-oedometer post treatment, retaining a ± 2% optimum moisture content (OMC) and an energy of ≥ 2.5 MJ. m^{-3} [20–21].

2.5 Liquefied or loose sands and silty sands

These soils are characterised by Dr < 60%; (N1)60 < 15; Vs < 180 m. s^{-3}; susceptible to fines; high cyclic resistance ratio; groundwater liquefaction, lateral spreading, settling, loss of soil mass, and floatation of structures. The appropriate soil stabilisation is vibrocompaction for granular fill, dynamic compaction for rapid compaction at the site of construction [22]. Also, the use of stone columns can both densify and provide drainage and compaction grouting in confined spaces in these soils. Where densification is not feasible, concreted columns designed for kinematic loads offer stability in loose sands.

Monitoring of pre and post CPT and Vs profiles for Dr ≥ 70%, Qc > 5 MPa and ensuring excess pore pressure, Δu < 20 kPa after 10 cycles [23].

2.6 Sulphate-bearing clays including pyritic shales

These are clays containing gypsum or pyrite producing sulphate content that exceeds 1% water-soluble sulphate, total potential sulphate, with the presence of acidic pore water. The use of lime or cement to stabilise such soils is at high risk of triggering ettringite-induced heave exceeding 50 mm [24]. But, if stabilisation is mandatory, it is ideal to specify sulphate-resisting cement and calcium-aluminate pozzolan-rich binders with fly-ash > 25% [25].

It is vital to use non-carbonate binders or kinetic solutions, and to monitor pH, moisture, barrier layers, and drainage during and after soil stabilisation.

Other important measures include pH and sulphate tests, binder tests, long-term swell tests, and protection of concrete according to standard guidelines.

2.7 Frost-susceptible silts

These soils are identified by fine silt fractions, capillary rise and exposure to cold weather. They cause frost heaving, loss of support and weakening during the spring thaw. The soil mitigation methods are non-frost-sensitive

sealing, insulation layers, and drainage control to reduce the activity of fines. Monitoring thermal modelling and seasonal moisture control is vital [26].

2.8 Sensitive and quick clays

They are known for their marine and metastable structure, high sensitivity (St > 30), and very low remolded strength. The soil poses risks of landslides, severe spreading failures and extreme stress loosening [27]. They are stabilised using load-bearing platforms, vibration control, soil mixing or columns, piles, and drainage methods. Pre- and post-risk monitoring may be performed by conservative stability analysis, emergency response planning, and instrument slopes. Using an in-situ vane, CRS tests guide remoulded Su targets with a vibration limit of $< 3\ \mathrm{mm.s^{-1}}$ during adjacent works. Install real-time slope inclinometers and piezometers to maintain $\Delta u > 5$ kPa [28-29].

2.9 Contaminated fills and industrial by-products

They contain the heavy metals, organic or toxic materials, variable gas composition (CH_4 or CO_2), hydrocarbons, asbestos and high salinity. The soil poses serious health hazards, gas migration, and chemical attack on binders.

The soil stabilisation with cement, GGBS, or MgO binds the contaminants and improves low-permeability sealing walls to restrict leaching. Selective excavation allows the membranes to trap gas and venting to allow escape, which is an efficient and alternative engineered solution and substitution. Regulatory approval and long-term monitoring are required to confirm UCS ≥ 0.5 MPa, show $\geq 90\%$ reduced leachate toxicity, continuous gas monitoring, prevent methane from exceeding 1% v/v and maintain apt oversight [30-31].

2.10 Lateritic and residual soils

Tropical residual soils are rich in Fe and Al oxides, which seem stable in situ, but degrade when saturated and collapse the soil, causing settlement. Cement or lime and microcolumns or rafts can strengthen the different soil profiles; pre-wetting and soil compaction can stabilise the soil. Stabilisation is effective by using lime, cement or on-site coal dust as a substitute for 30% cement in the mixing of the lateritic and residual soils [32].

During stabilisation, monitor and regulate slake-durability performance and control moisture during construction. Target a durability index of > 80% retained UCS after 12 wet–dry cycles. Maintain tight moisture control during compaction, as strength is highly sensitive to ±1% variation in water content. Use SCPTu profiling on a 30 m grid to map subsurface variability [33].

2.11 Frozen and permafrost soils

Ice-rich permafrost with > 50% ice content can lose strength rapidly upon thawing, causing 30–50% ground settlement. To preserve frozen ground, use thermosyphons or passive cooling embankments. Install elevated piles with ventilated voids to minimise heat transfer. For temporary ground support, apply artificial ground freezing (brine or LN_2), which creates 1–2 MPa frozen barriers around shafts. Install thermistor strings with alarms at temperature (T) > –1 °C, verify UCS of ≥ 1 MPa at design temperatures, and monitor cyclic heave or settlement using D-GPS within ±5 mm tolerance [34].

2.11 Dispersive soils

These soils are characterised with high sodium adsorption ratio (SAR) > 10 which causes aggressive slope erosion in slopes and embankments. These soils can be treated with gypsum or lime to flocculate clay by replacing Na^+, confirm improvement using the Pinhole test > 1 min per 50 mL and crumb tests; use of reinforce slopes with armoring, salt-tolerant vegetation, and protect reservoir linings through early isolation. After stabilisation, it is important to monitor SAR to remain < 6 for 5 years, and seal borrow pits to prevent dispersive fines from clogging culverts [35].

3 Selecting an Improvement Strategy

3.1 Start with clear, testable performance objectives

Successful improvements start with explicit, quantifiable goals traceable through design, construction, and delivery. For strength and stiffness, the typical goals are Su ≥ 25–75 kPa, Dr ≥ 70–80%, CBR ≥ 8–15%, and an increase of E_{50}. For permeability and drainage, aim for k reduction or U ≥ 90–95% often achieved by PVD, surcharge or vacuum. Manage volume change by limiting total or differential settlement and swell strain below < 1–2%. PI ≤ 12–20% to ensure moisture tolerance. Finally, link each target to reliable acceptance tests such as CPT, SPT, and plate load test [36].

3.2 A five-step decision pathway

(1) Determine soil conditions and properties; (2) define improvement targets and constraints; (3) screen viable soil improvement methods; (4) shortlist using risk-screening; (5) validate through testing, inspection, and adherence to the ITP (Inspection and Test Plan) [37].

3.3 Balancing stabilisation goals with real-world constraints

Different kinds of stabilisation performance schedules vary. Fast methods include vibro-compaction, dynamic deep compaction, permeation grouting,

jet grouting, rapid impact compaction, rigid inclusions, micropiles and temporary freezing. Moderate method options include rock columns, deep soil mixing, lime and cement stabilisation and geogrid-reinforced platforms. Slow by design include prefabricated vertical drainage systems (PVD) with a surcharge or vacuum. As a rule of thumb, combine columns and DSM for immediate loading, PVD and preload for creep management are hybrid solutions, especially in densifying soft deposits in tight programmes [38].

For sustainability, it is ideal to use mechanical solution where feasible. For chemical alternatives, using pozzolanic admixtures are preferable, and using design of experiments (DoE) helps avoid binder waste. When possible, reuse local materials to evaluate life-cycle such as durability and leaching [39].

For the soil chemistry, high sulphates and pyrite, standard lime or cement without testing should not be used; instead, use sulphate-resistant binders or mechanical options. For organic soils or peat, anticipate higher binder demand and delayed strength development; use DSM and rigid inclusions. For saline and dispersive clays, use gypsum or lime to reduce dispersion [40].

For design or logistics constraints, noise or vibration limits may rule out DDC or vibro-methods, therefore, use compaction grouting, DSM, or rigid inclusions. If space or access is limited, use grouting, micropiles, or electro-kinetic methods. For deep soft soils, use DSM and PVD; for shallow weak soils use binders or replacement and compaction for deep loose sands [41].

3.3 Method selection by primary objectives

To increase strength and stiffness: Lime or cement is suitable for expansive soils, DSM or rigid inclusions for soft and organic clays, vibro-compaction or grouting for sands, and geogrid-reinforced method suitable for landfills [42].

To control settlement: PVD with surcharge or vacuum for soft clays; stone columns for drainage and stiffness; lightweight fills to reduce $\sigma'v$ [43].

To mitigate liquefaction: Densification of loose saturated sand using vibro-compaction, dynamic deep compaction (DDC), use stone columns or piles for drainage and stiffness; if unsuitable, consider deep foundations instead [44].

To reduce permeability or isolate contaminants: Apply stabilisers, binders, slurry walls, geomembranes, or jet-grout cut-offs in contaminant soils [45].

To reduce plasticity and volume change properties in compressible and expansive soils, use lime to lower the PI, apply moisture barriers or capillary brakes and deep foundations to transfer loads beyond the active zones [46].

3.3 Proving the option: treatability and trials

Verification of performance must adhere to established standards that are commonly used in ground improvement practices. For binder-treated soils, parameters such as unconfined compressive strength (UCS) at 7, 28, and 90 days, reductions in plasticity index (PI), swell pressure, hydraulic conductivity (k), and durability under cyclic wet–dry or freeze–thaw conditions, including sulphate-induced swelling, should be assessed. For mechanical densification, the density and stiffness increases are confirmed by test plates, CPT grids, light weight deflectometers (LWD), plate-load tests, and shear wave velocity (Vs) profiling. Thresholds for acceptance examples are Qc ≥ 10 MPa, U ≥ 90% in 120 days, UCS ≥ 1.5 MPa, swell ≤ 1% should be predefined and incorporated in the inspection and test plan (ITPs) [47-48].

3.4 Hybridizing for robustness

In previous studies, the integration of several stabilisation methods was used to stabilise challenging ground conditions. For instance, columns and DSM with a basal geogrid and a staged preload to stabilise very soft soils; vibro- compaction with stone columns to improve density and drainage of loose sand; lime-treatment with a PVD preload for ground reinforcement; chemical treatment with geomembranes for brownfield sites. Thus, hybrid approaches mitigate risks and speed up construction timelines [49].

3.5 Design pitfalls to avoid

It is advisable to avoid over-cementing sands, which results in high stiffness but leads to brittle failure; optimise binder dosage and confirm post-peak response. Neglecting soil chemistry may result in sulphate attack or organic interference; test pore water and solids early. Under-instrumented preloads obscure U ≥ 90% progress. Unrepresentative testing leads to inaccurate acceptance decisions. Spatial variability requires dense CPT and SCPTu grids and responsive quality assurance and quality control [50].

4 Treated Soil Nomenclature and Properties

This guide adopts a uniform, hyphenated nomenclature to make the treatment method and the host material readily recognizable in the method statements and reports. Common formats used are lime-treated soil, cement-treated soil, fly ash-treated soil, GGBS-treated soil, laterite treated with silica fume, geopolymer-treated fill, bio-cemented sand, EK-treated soil, resin-treated sand, and jet-grouted concrete surface. Where relevant, curing duration (7, 14, 28, 90, or 120 days), design targets (UCS, CBR, or k), and validation

methods are specified to ensure success. The summaries below outline key mechanisms, property improvements, and primary cautions. However, field-specific treatability trials remain essential for validation [51].

4.1 Lime-treated soils

Problematic soils stabilised with lime undergo rapid flocculation and agglomeration improving workability and significantly reducing plasticity index (PI). Pozzolanic reactions over 7–120 days increase UCS to approximately 0.5–1.5 MPa and permeability and volumetric changes often decrease. Prior studies caution that soils containing sulphates or pyritic shales may produce ettringite or thaumasite. Therefore, sulphate profiling, swell testing, and durability checks under wet–dry cycles are essential [52].

4.2 Cement-treated soils

Calcium silicate hydrate (C-S-H) bonding promotes early strength gain in cement-treated silty sands and low-PI clays. Typical dosages of 3–8% by dry mass added for subgrades yield UCS of approximately 1–3 MPa at 28 days, CBR ≥ 8–15%, and stiffness 3–10 times the of natural soils. It is paramount to avoid over-cementation of treated soils, which may exhibit brittleness and shrinkage. Therefore, it is advisable to optimise dosage, or consider fiber reinforcement or granular confinement. In sulphate-bearing soils, use SR binders compliant with ASTM or BS concrete protection standards [53-54].

4.3 Fly-ash-treated soils

Class F and C fly ashes combine with lime or cement to reduce Portland cement use, improve long-term strength, and refine pore structure. UCS at 28–90 days is often comparable to cement-only mixes, with similar permeability reductions. Due to variability in ash content, conduct treatability and leachate tests when environmental receptors are present [55].

4.4 GGBS and silica fume (SF) treated soils

Replacing Portland cement with GGBS reduces the carbon footprint and improves sulphates and chloride resistance through microstructural densification. Initial strength gain may be delayed with high GGBS content. Silica fume (SF), being highly reactive, requires careful mixing to maintain uniform workability [56].

4.5 Geopolymer-stabilised soils

Also known as alkaline-activated aluminosilicates (low-calcium fly ash), these form durable gels delivering ≥ 1 MPa within 7 days and 1–3 MPa at 28 days for subgrade use, with low permeability and a reduced CO_2 footprint. Strength depends on the precursor chemistry, activator molarity, and curing. Always use DoE to optimise stabiliser-soil mix and curing conditions [57].

4.6 Bio-cemented sands

Using microbially induced calcite precipitation (MICP) and enzyme induced calcite precipitation (EICP) methods these treatments promote interparticle bonding, elasticity, and stiffness while maintaining ductility compared to cemented sands. UCS, permeability, and volumetric behavior improve, but treatment uniformity, temperature, ammonium by-product control, and CPT profiling are required [58].

4.7 Electrokinetically (EK) treated soils

These use low-voltage DC to induce electroosmotic ion transport, promoting in-situ drainage, strength gain, and volume change control. Strength improvements of 20–200% can occur within days to weeks. Effects include pH front propagation, electrode corrosion, energy consumption, and remediation needs. Calibration using pore pressure sensors, suction devices, and compliance with electrical safety protocols is critical [59].

4.8 Resin-grouted soils

Stabilised with low-viscosity polyurethane, epoxy, or acrylic polymers, which allow for rapid water sealing, void filling, and stiffness with minimal tools and rapid curing for leakage drops. Maintaining control over resin-soil interaction, temperature, cyclic durability, and concrete compatibility is necessary [60].

4.9 Jet-grouted soilcrete

High-energy fluid jets form soilcrete columns yield a UCS ≈ 1–10 MPa and permeability ≤ 10^{-8} ms^{-1} suitable for cut-offs, rafts, or underpinning. Performance depends on jet energy, lift and rotation rates, and erodibility. Monitoring coring and curing is essential [61].

4.10 Naming of treated soils is not performance

A treated soil must meet target threshold values by relevant laboratory experiments and field tests. For example, lime-treated soils with UCS ≥ 1.0

MPa at 28 days, PI ≤ 15 and swell ≤ 1%; jet-grouted soil with k ≤ 10^{-8} ms^{-1} and biocemented sand with a post-treatment Qc ≥ 10 MPa and Vs ≥ 150 ms^{-1} are acceptable threshold values [62].

5 Mechanical Densification and Replacement Techniques

Mechanical improvements improve particle distribution and interparticle stresses, increasing the stiffness, strength and stability of the soil without requiring significant binder additives. These methods are best used in granular soils located above or near the groundwater table and are often combined with preloading or vacuum-assisted consolidation. Soil replacement techniques involve partial or total excavation of unsuitable surface soils and substitution with more mechanically competent, soil-based materials. The method selection depends on layer thickness, particle gradation, fines content, groundwater conditions, site accessibility, vibration tolerance, and proximity to adjacent structures. Performance validation should rely on results-based field tests rather than device usage metrics [4; 35]. Typical examples are:

5.1 Dynamic compaction (DC)

Heavy weights (10-25 t) are dropped repeatedly from 10 to 30 m above the ground on very loose, dry ground, with improvement depths of depth of 6 to 12 m. drop energy, spacing, rest intervals, and hammer inclination. Ideal for heterogeneous fills where vibro-methods are unsuitable. Downsides include vibration, noise, offsite disruptions, and large exclusion zones. Precautions should address heave, settlement, pore pressure rise, and validation by Vs or LWD for Dr or E targets [22, 63].

5.2 Rapid impact compaction (RIC)

A 5-9 t hammer generates high frequency impacts, and efficiently stabilises dry loose soil to depths of 3-6 m, with a better damping effect and smaller safety zones. Suitable for embankments, roads and shallow foundations near sensitive structures. QA involves testing CPT validation, LWD and PLT checks based on Qc and E curves, and settlement in loose soils [38, 64].

5.3 Vibro-compaction

Depth vibrators compact loose silty sands (fines < 10-15%) under saturated conditions to aid particle rearrangement. Typical operating depth ranges from 10–20 m. Risks include poor fines control, excess pore pressure and vibration effects. Apply trial-optimized compaction sequences. Validation requires CPT, Vs, SPT (N), and pore pressure change (Δu) profiles [42, 65].

5.4 Excavation and replacement

Poor soils are removed and replaced with well-graded, moisture-conditioned, competent fills. Best suited where soil thickness is low and in-situ treatment is constrained by debris or contamination. Interface control is vital, using geotextile separation, proper selection of fill, and capillary breaks for frost or shrinkage risk mitigation. Validation includes density and moisture tests (nuclear or sand cone), LWD, PLT, and CPT along critical sections. QA criteria should define target density, layer thickness, deformation tolerance, stiffness, and moisture control [4].

6 Drainage-Based Consolidation Methods

The purpose of this method is to accelerate the pore pressure dissipation in soft, compressible soils, so that settlement occurs predictably under controlled and monitored conditions on the ground prior to loading. Its proper application improves settlement predictability and undrained shear strength via effective stress gain, and reduces long-term creep with minimal carbon impact [7, 66].

In principle and in application, the consolidation rate depends on the drainage path length and the soil's coefficient of consolidation (cv). Prefabricated vertical drainage channels (PVDs) reduce the drainage channels by converting radial flow into a drainage blanket, thereby reducing the time-to-value over a lifespan. Vacuum preloading supplies isotropic efficient stress where the surcharge is restricted. For very low permeable, compressible organic soils, electro-osmosis helps to drain the water [67].

6.1 Preloading and vacuum preloading

These are used to strengthen soft soils with high-water content, high compressibility, and low shear strength, through induced consolidation and creep. Vacuum methods apply 60–80 kPa suction, particularly where embankment height or stability limits filling. Success depends on correct drain spacing, continuous seal integrity, staged loading, and real-time instrumentation. Acceptance criteria include settlement–time curves and achieving $U \geq 90$–95%, supported by settlement data and coefficient of consolidation (C_p) back-analysis against design [15, 68-69].

6.2 P Prefabricated vertical drains (PVDs) and surcharge

PVD (prefabricated vertical drainage) and surcharge are mainly used to improve the properties of soft, compressible, and saturated soils, such as clays, silts, peats, and organic soils. These soils are characterised by low permeability and a tendency to harden slowly under stress, which leads to

problems of settlement. Optimal drain spacing depends on soil permeability, drain capacity, and the required consolidation degree. Supporting systems include drainage blankets, embankments with slope stability monitoring, and base reinforcements when needed. Quality protocols include checking verticality, spacing, anchorage and pre-drilling through the crust to ensure drainage efficiency and timely soil strengthening [38, 70].

6.3 Sand drains

Involve boring large-diameter holes filled with clean, well-graded sand to facilitate radial drainage in thick deposits. This method is well-suited for reclamation projects with locally available sand. Precautions include borehole cleanliness, sand grading, and continuous backfilling [71].

6.4 Electro-osmosis and electro-osmotic vertical drains

These are most effective in stabilizing and dewatering fine-grained soils. They improve stability and reduce settlement by decreasing water content and increasing shear strength. Theys significantly improve drainage, when combined with vertical drains. Design considerations include current density, spacing, durability, energy limits, and corrosion control. Persistent monitoring of pH changes, ion migration, and effluent quality is essential [67, 72].

7 Chemical and Cementitious Stabilisation Methods

These methods are most effective for improving the properties of granular (coarse-grained), silty, and certain cohesive soils. They are particularly valuable for soils with low bearing capacity or those vulnerable to erosion and deformation. The objective is to modify soil composition and pore-liquid interactions to improve strength, stiffness, durability, workability, and permeability, quantified using the properties of treated soil such as the PI, UCS, E, k, and pressure-permeability indices. Results depend on binder type and dosage, moisture content, curing conditions, and chemical compatibility.

7.1 Lime stabilisation

This is commonly applied to improve clay soils, especially those with high plasticity and clay content. Widely used in road construction, lime is added to subgrades and subbases to increase strength and durability. In fine plastic soils, cation exchange and elevated pH rapidly reduce PI and moisture sensitivity; pozzolanic reactions then improve UCS and stiffness while reducing permeability and swelling. Field dosage is typically 2–6% CaO, targeting PI $\leq$ 12–20% and UCS $\geq$ 1.0–1.5 MPa at 28 days. Essential controls

include lime quality, uniform mixing, OMC targeting, and appropriate compaction energy. Acceptance criteria include reductions in PI and swell, moisture control, and increases UCS and CBR at 7, 28, and 90 days [73-74].

7.2 Portland-cement stabilisation

Effective across granular soils, silts, and clays, this technique improves strength, durability, and resistance to erosion and mechanical deterioration, especially in pavement bases and sub-surface structures. While suitable for many soil types, granular and sandy soils respond best, while clays may require prior lime treatment. Cement rapidly improves durability and stiffness in granular or low-PI soils. Typical doses are 3–8% for subgrades, with higher contents required for solidification. Precautions must address brittle failure and shrinkage, using blends, fibers or moisture regulation. Validation includes testing for density, UCS, strength ratio, and durability under cycles [75-76].

7.3 Blended binders

These materials which include fly ash, GGBS, cement kiln dust (CKD), rice husk ash (RHA), silica fume, metakaolin are applied primarily in soft soil stabilisation. They offer a sustainable alternative to Portland cement and increase sulfate resistance and long-term durability. Lime–Fly Ash (LFA) or Lime–Cement–Fly Ash (LCF) blends suit expansive soils; lime–GGBS is ideal for sulfate-rich clays. Mix designs should follow DoE principles to meet PI, UCS, swell, and k targets [77].

7.4 Geopolymers

Suitable for soft soils, especially high-compressibility, low-shear strength clays, geopolymers provide early strength gain, lower permeability, and reduced CO_2 emissions. Key variables include precursor type, activator chemistry, and curing duration. Risks include reactivity variance, mixing uniformity, and setting time. Targets include UCS at 7, 28, and 90 days, microstructural integrity, and leachability control in contaminated soils [78].

7.5 Deep soil mixing (DSM)

Applied to soft, high-moisture soils (e.g., clays and peat), DSM involves mechanically mixing the soil with binders such as cement to improve strength and stiffness. Design should specify targets for UCS, modulus, column layout, and cyclic durability. Controls include binder dosage, mixing uniformity, and energy input. UCS validation is conducted using core samples aligned with

CPT and SCPTu data. Blended systems (lime–GGBS and cement–GGBS) improve chemical durability beyond that of pure Portland cement [79].

7.6 Electro-chemically improved stabilisation

Designed for fine-grained soils like clays and peats, this technique uses electrical current to mobilise ions and pore fluids, accelerating reactions with lime or cement. This improves strength and uniformity even in low-permeability materials. Critical controls include current density, electrode durability, power supply, suction regulation, pH management, and strength profiling [80].

8 Grouting and columnar inclusions techniques

These are soil improvement techniques primarily used for the stabilisation of soft, weak, or loose soils. They are particularly effective in problematic soils such as peat, organic silts, and very fine clays, which lack adequate shear strength to support structures. The aim is to create a composite ground system with appropriate strength, stiffness, and hydraulic performance for deformation control. Target objectives include improving bearing capacity, controlling settlement, and increasing resistance to liquefaction. Design must integrate the inclusion–matrix interaction and be validated through rigorous field tests, quality assurance (QA) and quality control (QC) measures [81].

8.1 Permeation grouting

This method uses low-viscosity grouts (e.g., microfine cement, ultrafine slag, silica sol, and silicate–organic blends) to infiltrate connected pores below the fracture pressure, making it ideal for clean sands and gravels. Key variables include viscosity, gel time, pressure, stage length, and take volume. Grout refusal ensures no fracturing. Outcomes include increased stiffness, reduced permeability, and improved soil–structure contact. QA measures include pre- and post-CPT or SCPTu, permeability testing, grout-take mapping, and chemical durability verification [82].

8.2 Compaction grouting

Primarily used to densify loose granular soils and stabilise subsurface voids or sinkholes, this method involves injecting a stiff, low-slump grout to laterally displace and densify soils such as collapsible fills or loose sands, thereby increasing their density and bearing capacity. Injection should start at the base and progress upwards with strict pressure and volume control to minimise surface heave. Applications include settlement correction,

underpinning, liquefaction mitigation, and void stabilisation. Quality assurance (QA) involves heave monitoring, grout injection logs, refusal identification, and post-treatment CPT and visual inspection (VI) [83].

8.3 Jet grouting

A versatile technique, jet grouting stabilises various soils including loose sand, soft clays, and silts. It is particularly useful where other methods are constrained by site conditions, high water tables, or contamination. Single-, double-, or triple-phase systems erode and mix in-situ soils, forming concrete-like columns or panels without significantly altering natural permeability. Applications include cut-offs, anchor support, uplift resistance, and raft foundations. Design should define system type, rotation/lift rate, column geometry, overlap, UCS, and permeability. Quality assurance (QA) includes coring, sonic logging, UCS and K testing, and mitigation of brittleness and sulphate effects using GGBS-rich blends [84].

8.4 Stone columns

This technique is effective in soft compressive soils (clays or silts) and loose granular soils with high fines. Densely compacted gravel or crushed stone columns improve shear strength and provide drainage, thereby reducing settlement and cyclic pore pressure buildup. Design parameters include area-replacement ratio, column spacing and diameter, and load transfer platform design. Settlement and stability predictions are based on composite stiffness. QA involves backfill gradation control, electrical resistivity logging, integrity tests, and CPT validation [85].

8.5 Rigid inclusions and micropiles

These are used to improve stability in soft or compressible soils like organic clays or loose sands by either transferring loads to stronger substrata or increasing bearing capacity. Rigid inclusions are especially useful for immediate settlement control in deep deposits, offering high stiffness with minimal spoil and vibration. Load is distributed through a granular platform and basal support. Performance depends on composite stiffness, interface shear, replacement ratio, and drainage. Validation includes static load tests, platform response tests, and long-term deformation monitoring [86].

8.5 Cut-off and seepage control

Designed to stabilise soils prone to erosion or piping, particularly around earth dams or levees, this system prevents uncontrolled water flow. Methods

such as jet-grouted, DSM panels and microfine cement slurries achieve target hydraulic conductivity at vulnerable points (levee edges, shafts, basin walls). Success depends on continuity, layering, interface bonding, and must be validated using packer tests, piezometers, and tracer studies [87].

9 Bio-Electrochemical and Thermal Methods

9.1 Bio-Electrochemical

These methods combine electrochemical and biological processes and are mainly used for the dual purposes of soil stabilisation and remediation, particularly for contaminated fine-grained soils such as silts and clays, as well as expansive soils. They help remove or neutralise pollutants by converting them into less harmful substances, while also improving soil strength, stiffness, and hydraulic behavior.

9.1 Bio-Electrochemical

A notable bio-electrochemical technique is bioenzymatic treatment, which can increase UCS and reduce k [8]. For example, ureolysis raises the pH and promotes calcium carbonate ($CaCO_3$) precipitation, resulting in increased stiffness and improved strength and permeability. A $CaCO_3$ content of 1–3% yields significant stiffness improvement; 5–8% can generate unconfined compressive strength (UCS) values of several hundred kPa in clean sands. Effective application requires sufficient soil permeability and cyclic fluid injection to prevent blockage near injection points. Precautionary measures include capturing or neutralising ammonium by-products. Verification measures involve quantifying calcite content, conducting CPT and Vs measurements, testing hydraulic conductivity, and measuring UCS and triaxial strength. The durability under freeze–thaw and wet–dry cycles must also be assessed [88-89].

9.2 Thermal ground freezing

Thermal methods can be used to temporarily stabilise soils during excavation or tunneling, especially in saturated or loose conditions. Additional thermal approaches, such as microwave heating and electric resistance heating, can alter mineralogy and reduce volumetric instability in expansive soils. Design setups are pipe layout, soil thermal conductivity, groundwater flow, and required frozen thickness. Monitoring involves thermistors, thermal simulation, and core quality control. Ground heave is managed through sequenced freezing and load planning, while thaw settlement is addressed

using back-analysis and real-time monitoring. Energy efficiency and carbon reduction are optimized using duty-cycling strategies [90].

9.2 Sustainability considerations

Bio-cementation offers a lower carbon footprint compared to cement binders when ammonium by-products are effectively managed. Electrokinetic (EK) treatment avoids excavation and may be powered by renewable energy sources, although energy consumption depends on soil resistivity and treatment volume. While thermal freezing is energy-intensive, it may be more effective than deep dewatering in some contexts. All techniques require treatability studies, life cycle assessment (LCA), and performance-based acceptance criteria. These include Qc and Vs for MICP, Su and water content for EK, and temperature and frozen thickness for thermal methods, each supported by clear contingency plans and operational thresholds [91].

10 Decision Matrix: Problem–Solution Mapping

This decision matrix links commonly encountered problematic soil types with their corresponding improvement objectives, recommended first-line methods, expected outcomes of treated soils, key acceptance metrics, and critical implementation cautions. Apply this matrix after completing site reconnaissance and geotechnical investigation phases to confirm soil classification and behaviour (see Section 2), define quantitative improvement targets (see Section 3), and shortlist one to three stabilisation techniques for laboratory evaluation and field pilot trials. Acceptance criteria must be embedded in the method statement and documented within the inspection and testing plan (ITP) before full-scale implementation. The essential pillars of stabilisation include: accurate problem identification, precise definition of improvement targets, method selection, expected treated-soil performance, clear QA/QC criteria, and awareness of method-specific implementation risks.

Hybrid solutions are appropriate where no single method fully mitigates all geotechnical risks. Efficient systems may integrate columnar inclusions or DSM with basal reinforcement and sequential preloading in soft sands, vibro-compaction with stone columns in loose sands, or lime-treated soils with PVD preloading in embankments. Verification and control are essential, with tools tailored to the treatment type. Acceptance must be based on measurable, traceable evidence from trial to full implementation [92].

Begin by validating the soil type using historical records, index tests, and in situ measurements. Translate the project requirements into measurable objectives for ground improvement. Select two or three context-specific

techniques, based on functionality and site-specific limitations. Express the expected results in terms of clear performance metrics, for example: cone penetration resistance (Qc) ≥ 10 MPa at 5–10 m depth, degree of consolidation (U) ≥ 90% within 120 days, UCS ≥ 1.5 MPa at 28 days, and Sp ≤ 1% [93].

When multiple techniques satisfy the project's technical criteria, prioritise those with a lower embodied carbon footprint across the asset life cycle. Mechanical densification and inclusion systems generally result in lower carbon emissions than cement-based stabilisation. Where binders are necessary, opt for blended cements or geopolymers with optimised dosage. Consider also the potential for contaminant transport, leachate behaviour, remediation needs, and future maintenance burdens [94].

Finally, this section together with the soil diagnosis framework (Section 2) and the solution selection logic (Section 3), offers a structured, fast, and robust route from problematic ground conditions to reliable and sustainable ground improvement solutions. It ensures that improvement programmes are not only technically sound, but also verifiable, feasible, and implementation-ready.

11 Practical Checklists and Field Forms

The scope must be clearly defined, including the objectives, spatial limits, and performance criteria. A thorough desk study should be conducted on geology, hydrogeology, contamination, and burial services, followed by a site survey plan incorporating CPT, SCPT, or SPT, soil sampling and classification, and groundwater regime assessment. Laboratory testing should include Atterberg limits, LOI or TOC, oedometer or CRS, PI, swell, and UCS or mix design, alongside soil chemistry analysis (pH, EC, sulphate or pyrite, and chloride). Where stiffness or liquefaction is critical, Vs profiling should be applied. Instrumentation must include piezometers, inclinometers, and settlement plates, with strict health and safety measures and permits addressing contaminants, gas, traffic, and vibration. All narrative descriptions must remain concise to ensure clarity and field usability [95].

11.1 Mix method treatability form

Materials must be fully characterised, including soil classification, index properties, and geochemistry. For binders and grouts, record the type and dosage, water-to-binder ratio, and any additives. Curing conditions shall be documented in terms of ambient temperature, relative humidity, and testing ages at 7, 28, and 90 days. Parameters to be tested include: PI reduction, UCS, CBR, E, k, swell, wet–dry and freeze–thaw durability. Acceptance thresholds are PI ≤ 15, UCS ≥ 1.5 MPa at 28 days, k ≤ 1×10^{-8} m. s^{-1}, swell ≤ 1%, and

durability loss ≤ 20%. Field records should include core photos and anomaly logs. Investigation plans must specify CPT, SCPTu, or SPT. Use tick-boxes and numeric fields to ensure clarity, with minimal free-text reliance [96].

11.2 Field quality assurance

Grid or chainage references must clearly identify treated zones, supported by real-time process records such as energy input per point, vibrator current or amp draw, grouting pressure–volume data, and hammer blow counts. Hold points should include trial pad approvals, proof-rolling, and sampling protocols. Acceptance must be based on modulus envelopes, peak particle velocity thresholds, and defined heave or tilt limits. All non-conformance events must trigger corrective actions such as re-treatment, infill injection, or offset adjustment. Narrative diaries should be replaced with structured checklists and numeric forms to improve traceability and clarity [97].

11.3 Consolidation monitoring log

Loading logs must capture staging, elevation increments, and vacuum pressure (kPa). Pore pressure sensors should log readings by depth and radial spacing, and settlement data from plates or extensometers should be recorded daily or weekly. Analysis must determine degree of consolidation (U) using √t methods, with back-analysis of cv to confirm design assumptions. The factor of safety against instability must also be verified. Trigger events such as degree of consolidation (U) falling below target, seal leakage must initiate corrections like surcharge extension, seal repair, or PVD layout augmentation. Verification tools may include CPT, SCPTu, or SPT [98].

11.4 Daily report logs

Daily logs should include environmental and weather conditions, site location, personnel headcount, health and safety observations, progress against the testing plan, completed QA tests, non-conformities and corrective actions issued, notes of the stakeholders or supervisors, and photo logs with attachment references. Remove all duplicate form fields to avoid confusion. Authentication tools include CPT, SCPT, or SPT, as applicable.

11.5 Sign-off and handover checklist

The final documentation must verify compliance with all acceptance criteria, provide variance analysis, include full as-built drawings, and confirm post-construction monitoring plans. Also, it must further provide detail protocols for barrier systems and ground freezing, ensure regulatory approvals

are attached, include a voluntary carbon footprint summary, and verify all CPT, SCPT, or SPT results and field documentation.

12 Conclusion

This short practical guide will equip geotechnical engineers, site managers, postgraduates, and early-career professionals the clarity and confidence to successfully stabilise difficult soils. It offers hands-on tools for soil diagnostics, choice of stabilisation method and establishment of performance targets, ideal for exploratory studies, experimental tests, and field pilot experiments. Although not a substitute for standardised codes, it is a practical help in streamlining decision making in the field and in the soil mechanic laboratories, ensuring that results are measurable, feasible, and sustainable from the very beginning.

Abbreviations and Glossary

Symbols Acronyms	Meaning	Symbols Acronyms	Meaning
av	Coefficient of Compressibility	LCA	Life Cycle Assessment
ASTM	American Society for Testing and Materials	LCF	Lime–Cement–Fly Ash
BS	British Standards	LFA	Lime–Fly Ash
Cc	Compression Index	LOI	Loss on Ignition
Cp	Coefficient of Consolidation	LN_2	Liquid Nitrogen
Cr	Recompression Index	LWD	Light Weight Deflectometer
CBR	California Bearing Ratio	MICP	Microbially Induced Calcite Precipitation
CKD	Cement Kiln Dust	MDD	Maximum Dry Density
CPT	Cone Penetration Test	OMC	Optimum Moisture Content
CRS	Constant Rate of Strain test	PLT	Plate Load Test
C-S-H	Calcium Silicate Hydrate	PVD	Prefabricated Vertical Drain
DC	Dynamic Compaction / Direct Current	RSM	Response Surface Methodology
DDC	Dynamic Deep Compaction	S	Settlement
Dr	Relative Density	SF	Silica Fume
D	Degree of Improvement	S/S	Stabilisation / Solidification
D-GPS	Differential GPS	Su	Undrained Shear Strength
DoE	Design of Experiments	SAR	Sodium Adsorption Ratio
DSM	Deep Soil Mixing	SPT	Standard Penetration Test
E	Modulus of Elasticity	SPT (N)	Standard Penetration Test Blow Count
EC	Electrical Conductivity	SCPTu	Seismic Cone Penetration Test with Pore Pressure Measurement
EICP	Enzyme Induced Calcite Precipitation	SR	Sulphate-Resistant
EK	Electrokinetic	QA	Quality Assurance
EN 12457	European Leaching Test Standard	QC	Quality Control
E_{50}	Secant Modulus at 50% of Peak Strength	Qc	Cone Tip Resistance
FS	Factor of Safety or Free Swell	$\sigma'p$	Preconsolidation Pressure
FWD	Falling Weight Deflectometer	$\sigma'v$	Effective Stress
GGBS	Ground Granulated Blast Furnace Slag	RIC	Rapid Impact Compaction
ITP	Inspection and Test Plan	RHA	Rice Husk Ash
k	Coefficient of Permeability	U	Degree of Consolidation
Δ	Differential Settlement or Deformation	UCS	Unconfined Compressive Strength
Δu	Excess Pore Water Pressure	Vs	Shear Wave Velocity
PI	Plasticity Index	VST	Vane Shear Test

References

[1] Thampatti, K. M. (2022). Problem Soils: *Constraints and Management*. CRC Press.

[2] Dixit, M. (2016). Damage mechanism in problematic soils. *International Journal of Civil Engineering and Technology*, 7(5), 232-241.

[3] Puppala, A. J., & Pedarla, A. (2017). Innovative ground improvement techniques for expansive soils. *Innovative Infrastructure Solutions*, 2(1), 24.

[4] Bo, M. W., Arulrajah, A., Horpibulsuk, S., Leong, M., & Disfani, M. M. (2014). Densification of land reclamation *sands by deep vibratory compaction techniques. Journal* of Materials in Civil Engineering, 26(8), 06014016.

[5] Chu, J., Indraratna, B., Yan, S., & Rujikiatkamjorn, C. (2012, October). Soft soil improvement through consolidation: an overview. *In Proceedings of the international conference on ground improvement and ground control* (Vol. 2012, pp. 251-280).

[6] Verma, H., Ray, A., Rai, R., Gupta, T., & Mehta, N. (2021). Ground improvement using chemical methods: A review. *Heliyon*, *7*(7).

[7] Mahmoud, M. A., Radwan, A. M., Salaheldin, K. M., & Rashed, A. S. (2023). Utilizing a new columnar inclusion approach to treat loose and granular soils. *Alexandria Engineering Journal*, 84, 11-23.

[8] Li, J., Zhu, F., Wu, F., Chen, Y., Richards, J., Li, T., ... & Guo, Q. (2024). Impact of soil density on biomineralization using EICP and MICP techniques for earthen sites consolidation. *Journal of environmental management*, 363, 121410.

[9] Gaspar, T. A. V., Jacobsz, S. W., Heymann, G., Toll, D. G., Gens, A., & Osman, A. S. (2022). The mechanical properties of a high plasticity expansive clay. *Engineering Geology*, 303, 106647.

[10] Vipulanandan, C., & Mohammed, A. (2020). Characterizing the index properties, free swelling, stress–strain relationship, strength and compacted properties of polymer treated expansive ch clay soil using vipulanandan models. *Geotechnical and Geological Engineering*, 38(5), 5589-5602.

[11] Al-Gharbawi, A. S., Najemalden, A. M., & Fattah, M. Y. (2022). Expansive soil stabilization with lime, cement, and silica fume. *Applied Sciences*, 13(1), 436.

[12] Pandey, P. (2021). Effect of Modified Moisture Barrier in Mitigating Pavement Distresses Due to Expansive Subgrade. The University of Texas at Arlington.

[13] Ehwailat, K. I. A., Ismail, M. A. M., & Ezreig, A. M. A. (2022). Ettringite formation and stabilization methods of sulfate-bearing soil: a state-of-the-art review. *Indian Geotechnical Journal*, *52*(4), 927-941.

[14] Dafalla, M., & Al-Mahbashi, A. M. (2024). Identifying Problematic Soils Using Compressibility and Suction Characteristics. *Buildings*, *14*(2), 521.

[15] Ftouni, A. (2024). *Ground Improvement Techniques for Seabed Consolidation: An Evaluation of Stone Columns and Soil Mixing based on Settlement Performance* (Doctoral dissertation, Politecnico di Torino).

[16] Hwang, J., Humphrey, A., Bobet, A., & Santagata, M. C. (2005). Stabilization and improvement of organic soils.

[17] Kaniraj, S. R., & Yee, J. H. S. (2011). Electro-osmotic consolidation experiments on an organic soil. Geotechnical and Geological Engineering, 29(4), 505-518.

[18] Ghanbari, P. G., Momeni, M., Mousivand, M., & Bayat, M. (2022). Unconfined compressive strength characteristics of treated peat soil with cement and basalt fibre. *Int. J. Eng.*, *35*(5), 1089-1095.

[19] Opukumo, A. W., Davie, C. T., Glendinning, S., & Oborie, E. (2022). A review of the identification methods and types of collapsible soils. *Journal of Engineering and Applied Science*, *69*(1), 17.

[20] A. Abd El-Rahman et al. "Experimental Investigation on a Dispersive Soil and Treatment with Lime and Gypsum." Innovative Infrastructure Solutions, 2024.

[21] Lyu, Z., Shi, K., Goh, A. T. C., et al. (2024). Digital geotechnics for smarter ground improvement: from monitoring to acceptance. *International Journal of Geo-Engineering*, 15, 43. ResearchGate

[22] Yang, J. (2024). Towards a novel method for liquefaction evaluation of silty sands. *Japanese Geotechnical Society Special Publication*, 10(5), 96-107.

[23] Asadi, M. B. (2021). Geotechnical Characterisation of Pumiceous Soils for Liquefaction Assessment (Doctoral dissertation, University of Auckland).

[24] Czerewko, M. A., & Cripps, J. C. (2023). Implications of sulfur mineralogy and consequences of pyrite oxidation for ground engineering. *Journal of the geological society*, 180(4), jgs2022-101.

[25] Moradzadeh, M. Advancement In Oxidation Test For Sulphide-Bearing Aggregates In Concrete (Doctoral dissertation, Toronto Metropolitan University).

[26] Teng, J., He, H., Feng, X., Yan, H., & Zhang, S. (2024). A novel criterion for assessing frost heave susceptibility of soils. *Acta Geotechnica*, 19(4), 2233-2249.

[27] Jacob, S., Chavali, R. V. P., Saeidi, A., & Sadrekarimi, A. (2023). Remoulding energy as a criterion in assessing retrogressive landslides in sensitive clays: a review and its applicability to Eastern Canada. Natural Hazards, 118(3), 1833-1853.

[28] Salehi, Y. (2025). Application of Vertical Inclusions as Ground Improvement Techniques in Foundations of Transportation Infrastructure (Doctoral dissertation).

[29] Mines, A. E., Beckstrand, D. L., & Bunn, M. D. (2022). Landslide Monitoring Methods: Application of Existing Technologies to Long-Termand Real-time Monitoring of Slope Movements (No. cmr 23-002). Missouri. Department of Transportation. Construction and Materials Division.

[30] Petrillo, A., Fraternali, F., Acampora, A., Di Chiara, G., Colangelo, F., & Farina, I. (2025). Innovative solidification and stabilization techniques using industrial by-products for soil remediation. *Applied Sciences*, 15(7), 4002.

[31] Mulikat, S. O. (2022). Assessment of Heavy Metals, Persistent Organic Pollutants and Polycyclic Aromatic Hydrocarbons Contamination of Soil and Underground Water of Selected Abattoir Markets in North Central Nigeria (Master's thesis, Kwara State University (Nigeria).

[32] Wahab, N. A., Roshan, M. J., Rashid, A. S. A., Hezmi, M. A., Jusoh, S. N., Nik Norsyahariati, N. D., & Tamassoki, S. (2021). Strength and durability of cement-treated lateritic soil. *Sustainability*, 13(11), 6430.

[33] Worlu, B., Budu, E. D., & Erhiferhi, O. K. (2025). Evaluating the Unconfined Compressive Strength Retention of Corn Starch Stabilized Lateritic Soils. *Journal of Engineering Research and Reports*, 27(7), 347-362.

[34] Wang, F., Li, G., Alexander, F., Ma, W., Chen, D., Wu, G., ... & Zhang, Z. (2023). Applicability analysis of thermosyphon for thermally stabilizing pipeline foundation permafrost and its layout optimization. *Cold Regions Science and Technology*, 208, 103769.

[35] Liu, P., Zhu, R., Zhao, F., & Zhao, Y. (2024). Enhancing Dispersive Soil: An Experimental Study on the Efficacy of Microbial, Electrokinetics, and Chemical Approaches. *Sustainability*, 16(23), 10425.

[36] Evans, J., Ruffing, D., & Elton, D. (2021). Fundamentals of ground improvement engineering. CRC Press.

[37] Abiodun, A. A., Hassan, R. E. F., & Mohammed, A. M. A. (2024, June). Comprehensive soil investigation diagnostics: A paradigm shift in geotechnical engineering. *5th International Eurasian Conference on Science, Engineering and Technology (EurasianSciEnTech 2024), Turkey*.

[38] Raj, P. P. (1999). Ground improvement techniques (HB). *Firewall Media*.

[39] Hossain, M. U., Liu, J. C., Xuan, D., Ng, S. T., Ye, H., & Abdulla, S. J. (2022). Designing sustainable concrete mixes with potentially alternative binder systems: Multicriteria decision making process. Journal of Building Engineering, 45, 103587.

[40] Seco, A., del Castillo, J. M., Perlot, C., Marcelino-Sádaba, S., Prieto, E., & Espuelas, S. (2022). Experimental study of the valorization of sulfate soils for use as construction material. Sustainability, 14(11), 6609.

[41] Wehr, W., Topolnicki, M., & Sondermann, W. (2012, May). Design risks of ground improvement methods including rigid inclusions. In *Int. Symp. Ground Improv*.

[42] Townsend, F. C., & Anderson, J. B. (2004). *A compendium of ground modification techniques* (No. Final Report,).

[43] Sridhar, G. (2015). Studies on vacuum preloading of soft clay deposits. *Indian Institute of Technology Madras & National University of Singapore*.

[44] Salem, Z. B., Frikha, W., & Bouassida, M. (2017). Effects of densification and stiffening on liquefaction risk of reinforced soil by stone columns. *Journal of Geotechnical and Geoenvironmental Engineering*, *143*(10), 06017014.

[45] Wang, K., & Zhang, Y. (2025). Evaluation of the Service Performance of Soil–Bentonite Vertical Cut-Off Walls at Heavy Metal Contaminated Sites: A Review. *Applied Sciences*, *15*(9), 5215.

[46] Salih, S. R., & Shafiqu, Q. S. M. (2024). Effect of treating expansive soil with lime. *Al-Nahrain Journal for Engineering Sciences*, 27(2), 226-233.

[47] Mugambı, L. M., Toerı, J. R., Kınotı, I., Bedada, K. D., & Marangu, J. M. (2023). A comprehensive review on methods, agents and durability factors for stabilization of expansive soils. *Journal of Sustainable Construction Materials and Technologies*, *8*(4), 319-343.

[48] Jain, P. K. (2024). Enhancing the properties of swelling soils with lime, fly ash, and expanded polystyrene-A review. *Heliyon*, *10*(12).

[49] Milev, N. Y. (2024, December). Advanced soil improvement methods using DSM and stone columns for reducing settlement in logistics facilities considering construction stages. In *IOP Conference Series: Earth and Environmental Science* (Vol. 1427, No. 1, p. 012001). IOP Publishing.

[50] Fong-Martinez, B., Wheeless, J., Drimalas, T., & Folliard, K. J. (2021). *Evaluation of Chemical Solutions to Concrete Durability Problems* (No. FHWA/TX-20/0-6906-R1). University of Texas at Austin. Center for Transportation Research.

[51] Manual, C. (2004). Lime-Treated Soil Construction Manual Lime Stabilization & Lime Modification. *published by National Lime Association, USA, Bulletin*, *326*.

[52] Barman, D., & Dash, S. K. (2022). Stabilization of expansive soils using chemical additives: A review. *Journal of Rock Mechanics and Geotechnical Engineering*, *14*(4), 1319-1342.

[53] Horpibulsuk, S., Rachan, R., Chinkulkijniwat, A., Raksachon, Y., & Suddeepong, A. (2010). Analysis of strength development in cement-stabilized silty clay from microstructural considerations. Construction and building materials, 24(10), 2011-2021.

[54] Roshan, M. J., & Rashid, A. S. B. A. (2024). Geotechnical characteristics of cement stabilized soils from various aspects: A comprehensive review. *Arabian Journal of Geosciences*, 17(1), 1.

[55] Room, S. (2023). Comparison of the performance of class-C and class-F fly ash concrete mixtures produced with crushed stone sand. *Materials Today: Proceedings*.

[56] Moolchandani, K. (2025). Industrial byproducts in concrete: A state-of-the-art review. *Next Materials*, *8*, 100593.

[57] Mohammadi, E. L., Najafi, E. K., Ranjbar, P. Z., Payan, M., Chenari, R. J., & Fatahi, B. (2023). Recycling industrial alkaline solutions for soil stabilization by low-concentrated fly ash-based alkali cements. *Construction and Building Materials*, *393*, 132083.

[58] Fu, T., Saracho, A. C., & Haigh, S. K. (2023). Microbially induced carbonate precipitation (MICP) for soil strengthening: A comprehensive review. *Biogeotechnics*, *1*(1), 100002.

[59] Abiodun, A. A., & Nalbantoglu, Z. (2018, August). Sacrificial Anode Protection for Electrodes in Electrokinetic Treatment of Soils. In Proceedings of China-Europe Conference on Geotechnical Engineering: Volume 1 (pp. 773-777). Cham: Springer International Publishing.

[60] Yan, D., Lai, L., Xiao, X., Zhang, L., Zhao, Z., & Zhao, J. (2023). Water Consolidation Performance of Acrylic-Polymer-Modified Materials and Their Concrete Impermeability Repair Characteristics. Gels, 9(9), 764.

[61] Croce, P., Flora, A., & Modoni, G. (2014). *Jet grouting: technology, design and control*. Crc Press.

[62] Wang, S. L., Mu, M. G., Chen, D. W., & Ren, G. (2012). Field design of jet grouting parameters on soilcrete columns. *Applied Mechanics and Materials*, *170*, 3068-3071.

[63] Scott, B., Jaksa, M., & Mitchell, P. (2021). Depth of influence of rolling dynamic compaction. *Proceedings of the institution of civil engineers-ground improvement*, *174*(2), 85-94.

[64] Vlček, J., Gago, F., Mihálik, J., Malík, F., Bahleda, F., Prokop, J., & Štefánik, M. (2024). Investigation of dynamic effect of rapid impact compaction. *Scientific Reports*, *14*(1), 21364.

[65] Slocombe, B. C., Bell, A. L., & Baez, J. I. (2000). The densification of granular soils using vibro methods. *Géotechnique*, *50*(6), 715-725.

[66] Khalifa, M. B., Salem, Z. B., & Frikha, W. (2025). Soft Soil Consolidation Using Prefabricated Vertical Drains: Case Study of "Radès la Goulette" Bridge Project. *Transportation Infrastructure Geotechnology*, *12*(6), 1-25.

[67] Meng, X., Zheng, J., & Yang, B. (2024). A new method for predicting consolidation settlements of soft ground based on monitoring results. *Archives of Civil Engineering*, 403-416.

[68] Liu, K., He, H. T., Tan, D. Y., Feng, W. Q., Zhu, H. H., & Yin, J. H. (2024). A case study of performance comparison between vacuum preloading and fill surcharge for soft ground improvement. *International Journal of Geosynthetics and Ground Engineering*, *10*(1), 11.

[69] Indraratna, B. (2017). Recent advances in vertical drains and vacuum preloading for soft ground stabilisation. In *Proceedings of 19th International Conference on Soil Mechanics and Geotechnical Engineering, Seou,(London: International Society for Soil Mechanics and Geotechnical Engineering)* (pp. 145-170).

[70] Hammad, M. S., Fayed, A. L., & El-Mossallamy, Y. M. (2019). Application of prefabricated vertical drains in soft clay improvement. *International Journal of Engineering and Applied Sciences*, *6*(10), 68-77.

[71] Aparna, R. P., & Bindu, J. (2023). Utilization of waste materials as a substitute for the sand drain in clayey soil. *International Journal of Geo-Engineering*, *14*(1), 2.

[72] Cui, Y., Zhong, F., Qi, C., Yang, X., & Gao, X. (2023). A Vertical Electro-Osmosis Method to Improve the Bearing Capacity of Piles in Marine Soft Clay. *Journal of Marine Science and Engineering*, *11*(4), 790.

[73] Abiodun, A. A. (2013). *Improvement of clay soils using lime piles* (Master's thesis, Eastern Mediterranean University (EMU)-Doğu Akdeniz Üniversitesi (DAÜ)).

[74] Abiodun, A. A., & Nalbantoglu, Z. (2017). A Laboratory model study on the performance of lime pile application for marine soils. *Marine Georesources & Geotechnology*, *35*(3), 397-405.

[75] Iskandar, D., Putri, E. E., Hakam, A., & Fitri, A. (2023). Effectiveness of Portland cement type 1 In stabilizing soft clay soil as subgrade for road construction. *Jurnal Rekayasa Sipil*, *19*(1), 44-53.

[76] Bhattacharja, S. A. N. K. A. R., Bhatty, J. I., & Todres, H. A. (2003). Stabilization of clay soils by Portland cement or lime–a critical review of literature. *PCA R&D Serial*, *60*(1), 124-133.

[77] Elbaz, A. A., Aboulfotoh, A. M., Dohdoh, A. M., & Wahba, A. M. (2019). Review of beneficial uses of cement kiln dust (CKD), fly ash (FA) and their mixture. *J. Mater. Environ. Sci*, *10*(11), 1062-1073.

[78] Latifi, N., Horpibulsuk, S., Meehan, C. L., Abd Majid, M. Z., Tahir, M. M., & Mohamad, E. T. (2017). Improvement of problematic soils with biopolymer—an environmentally friendly soil stabilizer. *Journal of Materials in Civil Engineering*, *29*(2), 04016204.

[79] Alnunu, M. Z. (2023). *Deep Soil Mixing for Mitigation of Problematic Soils* (Doctoral dissertation, Eastern Mediterranean University).

[80] Villarroel-Ortega, J. (2022). *Characterisation of Stress-Strain Behaviour of a Chemically Stabilised Soft Soil Reinforced with Fibres Under Monotonic and Cyclic Loadings* (Doctoral dissertation, Universidade de Coimbra (Portugal)).

[81] Verma, H., Ray, A., Rai, R., Gupta, T., & Mehta, N. (2021). Ground improvement using chemical methods: A review. *Heliyon*, *7*(7).

[82] Xiang, Z., Zhang, N., Xie, Z., Tang, H., & Song, Z. (2025). Experimental Study on Permeation of Composite Grout with Multi-Particle-Size Distribution: Comparative Analysis with Nano-Silica Sol and Cement Grout. *Processes*, *13*(1).

[83] Bhuiyan, M. R., Masum, S. R., Parvej, M. T., & Sanuwar, S. M. (2024). An Overview of Soil Improvement through Ground Grouting. *Journal of Geoscience and Environment Protection*, *12*(1), 51-63.

[84] Shen, S. L., Wang, Z. F., Horpibulsuk, S., & Kim, Y. H. (2013). Jet grouting with a newly developed technology: The Twin-Jet method. *Engineering Geology*, *152*(1), 87-95.

[85] Farah, R. E. (2020). Behaviour of single and group of geotextile encased stone columns in single-layered and layered soil.

[86] Colorado-Urrea, G., Gonzalez, Y. D., Wang, H., Zapata-Medina, D., & Carranza-Argote, J. (2024, May). Rigid inclusions performance as ground improvement for lacustrine clays. In *IOP Conference Series: Earth and Environmental Science* (Vol. 1336, No. 1, p. 012008). IOP Publishing.

[87] Attia, M., Abdel Razek, M., & Salam, A. A. (2021). Seepage through earth dams with internal cut off. *Geotechnical and Geological Engineering*, *39*(8), 5767-5774.

[88] Wang, Y., Konstantinou, C., Tang, S., & Chen, H. (2023). Applications of microbial-induced carbonate precipitation: A state-of-the-art review. *Biogeotechnics*, *1*(1), 100008.

[89] Boruah, R. P., Mohanadhas, B., & K, J. (2025). Microbially Induced Calcite Precipitation for Soil Stabilization: A State-of-Art Review. *Geomicrobiology Journal*, 1-16.

[90] Alsabhan, A. H., & Hamid, W. (2025). Innovative thermal stabilization methods for expansive soils: mechanisms, applications, and sustainable solutions. *Processes*, *13*(3), 775.

[91] Omoregie, A. I., Muda, K., Ong, D. E. L., Ojuri, O. O., Bakri, M. K. B., Rahman, M. R., ... & Ling, Y. E. (2024). Soil bio-cementation treatment strategies: state-of-the-art review. *Geotechnical Research*, *11*(1), 3-27.

[92] Dixit, M. S., Jaiswal, S. S., Satyam, N., Singh, A. P., & Maji, V. B. (Eds.). (2025). *Proceedings of the Indian Geotechnical Conference (IGC 2024), Volume 1: Ground Improvement Techniques* (Vol. 626). Springer Nature.

[93] Okiye, S. E. (2021). Model for Advancing Quality Control Practices in Concrete and Soil Testing for Infrastructure Projects: Ensuring Structural Integrity.

[94] Ige, O. E., Moloi, K., & Kabeya, M. (2025). Sustainability Assessment of Cement Types via Integrated Life Cycle Assessment and Multi-Criteria Decision-Making Methods. *Sci*, *7*(3), 85.

[95] Cambridge, M., Monroy, R., Diaz, M., & Molloy, C. (2018). Material Characterisation. In *The Hydraulic Transport and Storage of Extractive Waste: Guidelines to European Practice* (pp. 33-82). Cham: Springer International Publishing.

[96] Briaud, J. L. (2023). *Geotechnical engineering: unsaturated and saturated soils*. John Wiley & Sons.

[97] Ziajahromi, S., & Leusch, F. D. (2022). Systematic assessment of data quality and quality assurance/quality control (QA/QC) of current research on microplastics in biosolids and agricultural soils. *Environmental Pollution*, *294*, 118629.

[98] Karstunen, M., & Leoni, M. (Eds.). (2008). *Geotechnics of Soft Soils: Focus on Ground Improvement: Proceedings of the 2nd International Workshop held in Glasgow, Scotland, 3-5 September 2008*. CRC Press.